

Copyright

by

Andrew James Weldon

2014

**The Thesis Committee for Andrew James Weldon
Certifies that this is the approved version of the following thesis:**

Construction and Validation of a Hot Torsion Testing Instrument

**APPROVED BY
SUPERVISING COMMITTEE:**

Supervisor:

Eric M. Taleff

Carolyn Conner Seepersad

Construction and Validation of a Hot Torsion Testing Instrument

by

Andrew James Weldon, B.S.M.E.

Thesis

Presented to the Faculty of the Graduate School of

The University of Texas at Austin

in Partial Fulfillment

of the Requirements

for the Degree of

Master of Science in Engineering

The University of Texas at Austin

May 2014

Dedication

To my grandfather,

Dr. Henry Grady Rylander, Jr.,

and my father,

James M. Weldon,

for inspiring me to pursue a career in mechanical engineering

Acknowledgements

First and foremost, I would like to thank my advisor Dr. Eric Taleff for his help over the course of this study. Dr. Taleff has patiently taught me many things over my academic career (such as the meaning of a floating ground). He has always taken the time to explain material clearly and effectively, no matter how busy he is. His positive outlook on life has is an encouragement to everyone he works with. I am truly blessed to have him as my advisor and friend.

I would also like to thank Dr. Trevor Watt for his assistance throughout my graduate career. Dr. Watt has always provided helpful advice when needed most. His selfless attitude is shown in his continuous service for others.

My deepest gratitude goes out to Danny Jares for his machining expertise and assistance with this investigation. His machining abilities never cease to amaze me.

Finally, I would like to thank my fellow researcher and friend, Thomas Ivanoff. Thomas has selflessly spent many long days assisting me with this investigation. My completion of this study could not have been accomplished without his support.

Abstract

Construction and Validation of a Hot Torsion Testing Instrument

Andrew James Weldon, M.S.E.

The University of Texas at Austin, 2014

Supervisor: Eric M. Taleff

The need to increase vehicle performance, particularly fuel efficiency, has led to an increased interest in using lightweight metals for vehicle structural components. Lightweight aluminum alloys offer the potential to significantly reduce vehicle mass when structural components that use steel are replaced. Mass reduction is a very efficient route to increase vehicle performance. In vehicles with traditional powertrains, mass reduction can increase fuel efficiency. In vehicles with electrical powertrains, mass reduction can increase driving range. Regardless of the specific structural application, the best performance of any aluminum alloy is only obtained by achieving a microstructure that produces the best material properties. For wrought aluminum alloys, hot and cold deformation steps are critical to obtaining a desirable microstructure prior to the forming of a final component. For sheet material, the first step in controlling the final microstructure is microstructure evolution during hot rolling the cast ingot material. Hot rolling precedes cold rolling of the sheet to final thickness in most commercial sheet manufacturing operations. Microstructure during hot rolling is difficult to study because it requires a combination of high temperatures, fast strain rates

and large strains to do so. Furthermore, specimens for microstructural examination must be extracted from these conditions while retaining the characteristics of the specific conditions that are to be studied. Hot torsion testing is the traditional approach to meeting these experimental requirements. In this investigation, a new hot torsion testing instrument is designed, fabricated and validated to enable future experiments that will elucidate microstructure evolution under conditions pertinent to hot rolling. This new instrument is integrated with computerized control and data acquisition systems. Validation experiments were conducted to characterize its capabilities. It is concluded that the completed instrument meets the requirements necessary to study plastic deformation and microstructure evolution in aluminum alloys under conditions relevant to hot rolling.

Table of Contents

List of Tables	xii
List of Figures	xiii
I. INTRODUCTION	1
1.1. Purpose of Study	1
1.2. Introduction to Recrystallization.....	2
1.3. Literature Review.....	4
1.3.1. Static Recrystallization and Its Mechanisms	4
1.3.1.1. Particle Stimulated Nucleation	4
1.3.1.2. Shear Banding.....	5
1.3.1.3. Strain Induced Grain Boundary Migration	5
1.3.2. Critical Strain Annealing	6
1.3.3. Dynamic Recrystallization.....	7
1.3.4. Geometric Dynamic Recrystallization	7
1.4. Problem Statement	9
II. EXPERIMENTAL INSTRUMENTATION DESIGN	11
2.1. Design Requirements	11
2.2. Deliverables	11
2.3. Instrument Design and Relevant Calculations.....	12
2.3.1. Static Recrystallization and Its Mechanisms	12
2.3.1.1. Body Design.....	12
2.3.1.2. Shearing Strian Rate	14
2.3.1.3. Mounting Rails.....	15
2.3.1.4. Shaft Selection	15
2.3.1.5. Spline Shaft Assembly	17
2.3.1.6. Flywheel.....	18
2.3.2. Data Acquisition and Controls Equipment	19
2.3.2.1. Clutch Brake	19

2.3.2.2. Reaction Torque Sensor and Signal Conditioner	19
2.3.2.3. Tachometer	21
2.3.1.4. Rotary Encoder	21
2.3.1.2. Data Acquisition Software	22
2.3.3. Temperature Control	23
2.3.3.1. Furnace Specifications	23
2.3.3.2. Temperature Profile	23
2.3.4. Torsion Grip Design	25
2.3.5. Specimen Design	28
2.4. Final Instrument Design	29
III. EXPERIMENTAL PROCEDURE	32
3.1. Initial Instrument Calibration	32
3.1.1. Torque Cell Calibration	32
3.1.2. Tachometer Calibration	34
3.2. Test Preparation	35
3.2.1. Cooling Water	35
3.2.2. Cooling Fan and Clutch Power	35
3.2.3. Specimen Loading	36
3.2.4. Furnace Controls	38
3.2.5. Lathe Controls	39
3.2.6. Acquisition Setup	40
3.2.7. Program Initiation	41
3.2.7.1. Setting the Experiment Time	41
3.2.7.2. Selecting the File Path and Testing	41
3.3. Air Quenching	42
IV. EXPERIMENTAL RESULTS AND DISCUSSION	44
4.1. Instrument Characterization	44
4.1.1. Speed Verification	44
4.1.2. Timing Synchronization	45
4.2. Testing Parameters	46

4.2.1. Material Selection	46
4.2.2. Strain Rate and Test Temperature.....	50
4.3. Data Analysis	51
4.3.1. Torque vs. Rotational Displacement.....	51
4.3.2. Shear Stress vs. Shear Strain.....	52
4.3.2.1. Experiment Repeatability.....	54
4.3.2.2. Literature Comparison	55
4.4. Metallography.....	56
4.4.1. Specimen Mounting.....	58
4.4.1.1. Compression Specimens	58
4.4.1.2. Torsion Specimen	58
4.4.2. Polishing Procedure	60
4.4.3. Imaging	60
4.4.3.1. Compression Specimens	61
4.4.3.2. Torsion Specimen	63
4.4.4. Heat Treating the Compression Specimens	64
V. CONCLUSIONS AND FUTURE WORK	67
5.1. Concluding Remarks.....	67
5.2. Future Work.....	68
5.2.1. Data Acquisition	68
5.2.1. Gas Quenching.....	69
5.2.1. Instrument Modifications.....	69

Appendix A: Technical Drawings	70
Appendix B: Warner Electric UM-100 Clutch/Brake	83
Appendix C: Omega TQ202 Torque Cell.....	92
Appendix D: ElectroSensors TR400 Tachometer.....	94
Appendix E: Encoder Products 25T Encoder	97
Appendix F: Thermal Analysis on Hollow Shaft	100
Bibliography	102

List of Tables

Table 2.1:	Typical conditions for hot rolling aluminum alloys. Table is from Ref. [4].	11
Table 2.2:	Alloy Specimen Compositions	17
Table 2.3:	Torsion specimen dimensions in inches	28
Table 4.1:	Chemical composition comparison of aluminum alloys in wt. pct. Data taken from Ref. [23].	47
Table 4.2:	Specimen geometry comparison between the FSA alloy and AA5083 alloy.	49
Table 4.3:	Specimen preparation procedure for the Al-4.5Mg torsion and compression specimens.	60
Table 4.4:	Comparing mean grain sizes between Al-4.5Mg compression specimens and Al-4.5Mg torsion specimens.	65

List of Figures

Figure 1.1: Effect of cold working on recrystallized grain size. Figure is from Ref. [9].	6
Figure 1.2: Effect of hot working on grain boundary spacing. Figure is from Ref. [5].	8
Figure 1.3: Subgrain A with low angle boundary at B being pinched off to form nucleation sites for recrystallization. Figure is from Ref. [10].	9
Figure 2.1: Torsion testing instrument designed by Bressan. Figure is from Ref. [7].	13
Figure 2.2: Rockwell 12-inch wood lathe. Figure is from Ref. [11].	13
Figure 2.3: T-shaped rail mounting assembly.	15
Figure 2.4: Spline shaft and torque coupling.	18
Figure 2.5: Flywheel for storing kinetic energy.	18
Figure 2.6: Warner Electric clutch/brake. Image is from Ref. [14].	19
Figure 2.7: (a) Omega TQ202 torque cell (Image is from Ref. [15]), (b) Vishay 2120B signal conditioner.	20
Figure 2.8: (a) ElectroSensors TR400 tachometer (Image is from Ref. [17]), (b) through-bore pulser disk (Image is from Ref. [18]).	21
Figure 2.9: Encoder Products 25T rotary encoder. Image is from Ref. [19].	22
Figure 2.10: Quad-elliptical infrared radiation furnace.	23
Figure 2.11: A 1-Dimensional analysis of shaft temperature.	24
Figure 2.12: Annular fins with forced convection provided by a computer fan.	25
Figure 2.13: Torsion instrument grip design variants. Figure is from Ref. [22].	26
Figure 2.14: Final torsion instrument grip design.	27

Figure 2.15: (a) Images show the left grip fixed and the right grip off, (b) both grips fixed, (c) isometric view with the left grip fixed and the right grip off, and (d) isometric view of both grips fixed.....	27
Figure 2.16: Torsion specimens with scale marker in inches.....	28
Figure 2.17: Isometric view of the torsion testing instrument.....	29
Figure 2.18: Labeled SolidWorks™ model of the torsion instrument....	30
Figure 2.19: Torsion testing apparatus.....	31
Figure 3.1: The Vishay signal conditioning unit.....	32
Figure 3.2: Calibration curve for the TQ202 torque cell.....	33
Figure 3.3: Calibration curve for the TR400 tachometer.....	34
Figure 3.4: (a) Flow meters mounted on the front of the instrument, (b) red arrows indicate valve turning direction for cooling water.....	35
Figure 3.5: Power unit for the cooling fan and clutch brake.....	36
Figure 3.6: (a) Thermocouples protruding from the left grip, (b) positioning the outer thermocouple to contact the specimen surface. The quartz tube surrounds the assembly.....	37
Figure 3.7: Thermocouple display, furnace controller, and tachometer.....	37
Figure 3.8: (a) Left Eurotherm model 818 controller used to adjust and set the temperature, (b) right Eurotherm model 832 power supply used to adjust the current output.....	39
Figure 3.9: Lathe controls.....	39
Figure 3.10: Data acquisition setup using two computers.....	40
Figure 3.11: Computer 1 program front panel.....	41
Figure 3.12: Computer 2 program front panel.....	42
Figure 3.13: Compressed air valve and regulator for gas quenching.....	43

Figure 4.1: Rotational speed is shown versus time.....	45
Figure 4.2: Timing synchronization between the torque cell and rotary encoder.....	46
Figure 4.3: Alloying effect of manganese on tensile properties of wrought 99.95% Al at room temperature. Figure is taken from Ref. [24].....	48
Figure 4.4: The logarithm of diffusivity-compensated strain rate versus the logarithm of modulus-compensated stress. Figure from Ref [25].....	49
Figure 4.5: Shear stress versus shear strain for AA5083. Figure is from Ref. [23].....	50
Figure 4.6: Shear stress versus shear strain for AA5083. Figure is from Ref. [23].....	52
Figure 4.7: A plot of shear stress versus shear strain for the Al-4.5Mg material where $T = 460^{\circ}\text{C}$ and $\dot{\gamma} = 15\text{s}^{-1}$	54
Figure 4.8: (a) Shear stress vs. shear strain for Al-4.5Mg (this study, where $\dot{\gamma} = 15\text{s}^{-1}$), (b) Mean shear stress vs. mean shear strain for Al-4.5Mg (this study, where $\dot{\gamma} = 15\text{s}^{-1}$) compared with AA5083 (literature, where $\dot{\gamma} = 10\text{s}^{-1}$). Literature data taken from Ref. [23]......	56
Figure 4.9: (a) Sectioning the Al-4.5Mg compression specimen, (b) Mounting the Al-4.5Mg compression specimen.....	58
Figure 4.10: An Al-4.5Mg torsion specimen where buckling is observed. The specimen was tested at a temperature of 450°C and a strain rate of 3.5 s^{-1} to a final strain of 0.45.....	59
Figure 4.11: (a) Sectioning the extracted torsion specimen piece, (b) mounting the sectioned torsion specimen pieces.....	59

Figure 4.12: Al-4.5Mg material tested in compression at a temperature of 500°C, strain rate of 1 s^{-1} , to a final strain of 0.5. (a) Grain morphology at the middle-center of the specimen; (b) Grain morphology at the bottom-center of the specimen.....61

Figure 4.13: Al-4.5Mg material tested in compression at a temperature of 400°C, strain rate of 1 s^{-1} , to a final strain of 0.5. (a) Grain morphology at the middle-center of the specimen; (b) Grain morphology at the bottom-center of the specimen.....62

Figure 4.14: Al-4.5Mg material tested in compression at a temperature of 400°C, strain rate of 1 s^{-1} , to a final strain of 0.5. The figure shows a magnified middle center view showing small equiaxed grains marked with arrows.....62

Figure 4.15: Mosaic images of the Al-4.5Mg torsion specimen cross sections. This specimen was tested in torsion at 450°C, a strain rate of 1 s^{-1} , to a final strain of 0.45.....63

Figure 4.16: Al-4.5Mg compression specimen microstructures following a 10 minute heat treatment. The left image indicates the specimen originally tested in compression at a temperature of 500°C, strain rate of 1 s^{-1} , to a final strain of 0.5. The right image indicates the specimen originally tested in compression at a temperature of 400°C, strain rate of 1 s^{-1} , to a final strain of 0.5.....64

I. INTRODUCTION

1.1. PURPOSE OF STUDY

The U.S. Energy Information Administration's (EIA) Monthly Energy Review for December 2013 states that over 65% of total U.S. oil is consumed by personal vehicles [1]. This daunting statistic places a heavy emphasis on finding solutions to increase vehicle fuel efficiency in the near future. One way of increasing fuel efficiency is to reduce vehicle weight. It was estimated by the U.S. Department of Energy (DOE) that a 10% reduction in vehicle weight produces fuel savings of roughly 7% [2]. Statistics like these led to increased interest in the use of lightweight metals for vehicle manufacturing. Light alloys of aluminum are commonly used for interior and exterior vehicle parts. Because of their high strength and good formability, aluminum alloys are an important asset to the automotive industry. Sheets of aluminum are formed into side panels, trunk closures, and hoods for vehicle bodies [3]. However, before the sheet material is formed into a desired shape, it must first be rolled to a desired thickness. Ingots of aluminum are typically annealed in a furnace prior to rolling. Annealing allows alloy constituents to diffuse, giving the material a more homogeneous composition. The ingots are then rolled at elevated temperatures between 300°C and 500°C. This process is known as hot rolling. Once hot rolling is complete, the material is cold rolled to give it additional strength and further reduce its thickness. Subsequent annealing treatments may follow to ensure the desired microstructure is attained [4].

During the hot rolling process, microstructure changes dramatically with each rolling pass. Highly deformed microstructures can recover and recrystallize during and between rolling steps. If the aluminum manufacturing process is to be improved, a better understanding of microstructure evolution during hot deformation is necessary. Improvements made in the hot rolling process could lead to better microstructure refinement and potentially reduce the amount of cold work needed after hot rolling, thus reducing cost. Before addressing ways to better attain microstructure refinement, it is crucial to understand the recovery and recrystallization processes.

1.2. INTRODUCTON TO RECRYSTALLIZAITON

When a metal (in our case aluminum) is deformed, dislocations are generated within the material and begin to cluster and tangle together. These dislocation clusters store energy and provide additional strength to the material. Heating the material for annealing increases atomic activity and leads to dislocation movement. Dislocation movement during annealing reduces stored energy by two primary means: the annihilation of dislocations and the reordering of dislocations into subgrains. In these ways, dislocation movements attempt to “recover” the material to the prior “softer” state that existed before deformation [5]. Aluminum alloys are known for having a high level of recovery in hot working, largely a result of their high stacking fault energies [6].

While recovery is fairly homogeneous in that it occurs similarly throughout a microstructure, recrystallization is a more complex process. Recrystallization is the formation and growth of new strain-free grains within a deformed microstructure. This

phenomenon may occur under static (post deformation) or dynamic (during deformation) conditions and usually occurs in two stages: nucleation and grain growth. It is important to note that the term “nucleation” used when discussing recrystallization does not refer to an embryonic nucleation. There is typically a small preexisting nucleus within the deformed microstructure where the grain initiates growth. Although “initiation site” is a more accurate description of this phenomenon, the historically accepted term nucleation will be used throughout this document [5].

In order to study microstructure evolution during the hot rolling process, a means for experimentally simulating the process is necessary. However, one important question arises: how can hot rolling be simulated? Rolling processes can reach large strain rates of up to 100 s^{-1} . These strain rates are much faster than those typically achieved in tensile tests, which rarely exceed 10^{-2} s^{-1} [7]. Thus, an alternative to tensile testing must be sought out. For the past 50 years, torsion test machines have been used to physically simulate commercial rolling [6]. Torsion test machines use rotational motion to test materials in shear. Although there is a wide variety of make-ups and designs, most torsion machines are capable of producing large strains similar to those produced during rolling. Design, construction, and validation of a torsion testing apparatus are the primary goals of this study.

1.3. LITERATURE REVIEW

1.3.1. Static Recrystallization and Its Mechanisms

Static recrystallization occurs during static annealing following cold deformation. Deformed material holding strain energy is annealed at elevated temperatures to initiate recrystallization. Prior research has advanced the understanding of mechanisms responsible for recrystallization in metals. This section outlines some of the important mechanisms that lead to static recrystallization in aluminum and its alloys.

1.3.1.1. Particle Stimulated Nucleation

Particle stimulated nucleation (PSN) of recrystallization (RX) arises from hard particles, typically greater than 1 μm , trapped within a deformed material. During deformation, there is incompatibility of plastic flow between the hard particles and the softer matrix. This incompatibility causes intense strain fields to develop in the matrix around the particle. The dislocation cells produced in heavily deformed material near particles have boundaries with high dislocation densities and relatively high misorientations, making them good nucleation sites for RX. Examples of the PSN mechanism include Al-Mg-Mn alloys with Al_6Mn particles and Al-Si alloys with Si particles [6]. Similar particles from impurities may also give rise to PSN of RX in commercially pure aluminum. PSN of RX produces a fairly randomly oriented crystallographic texture [5].

1.3.1.2. Shear Banding

Another mechanism responsible for recrystallization in aluminum alloys is shear banding. Instabilities during cold rolling can produce regions of intense strain oriented at approximately 35° to the rolling plane. These regions, called shear bands, are commonly found in Al-Mg alloys. Shear bands in Al-Mg alloys are promoted by magnesium in solid solution, which also reduces the amount of recovery during and after deformation by decreasing the stacking fault energy. Reducing the amount of recovery increases the likelihood of recrystallization at elevated temperatures. Nucleation sites are thought to occur at the intersections of shear bands because these regions have high strain energy. The crystallographic texture of the recrystallized grains depends heavily on the amount of deformation. For small amounts of reduction (< 90%), the characteristic cube texture from cold rolling remains after recrystallization. However, as the amount of deformation increases, recrystallized grains at shear bands become more randomly oriented [5].

1.3.1.3. Strain Induced Grain Boundary Migration

Strain induced grain boundary migration (SIBM) is another mechanism responsible for recrystallization of aluminum alloys under smaller amounts of deformation. In SIBM, preexisting grain boundaries bulge into grains with greater dislocation densities. This produces new strain-free grains having orientations similar to old grains from which the boundaries migrated. Because the new orientation is analogous to that of the old grain, SIBM creates a texture similar to that of the deformed material.

SIBM can be the dominant mechanism for recrystallization in hot rolled aluminum for reductions less than 20% [5].

1.3.2. Critical Strain Annealing

Recrystallization can be studied through critical strain annealing. After deformation to a controlled plastic strain, a material is statically annealed at elevated temperatures to initiate recrystallization. In critical strain annealing, recrystallization does not occur unless a minimum critical strain is imposed during deformation prior to annealing. Figure 1.1 shows that below the critical strain there is not enough strain energy for the material to recrystallize. Once the critical strain is reached, new grains will begin to nucleate and grow to a coarse size by one or more of the possible mechanisms of recrystallization. Increasing the strain increases the number of initiation sites, which leads to a smaller spacing between grains. After large rolling reductions, initiation sites become so frequent during annealing that grain boundaries quickly meet. This creates a fine, stable grain structure in the newly recrystallized material [8].

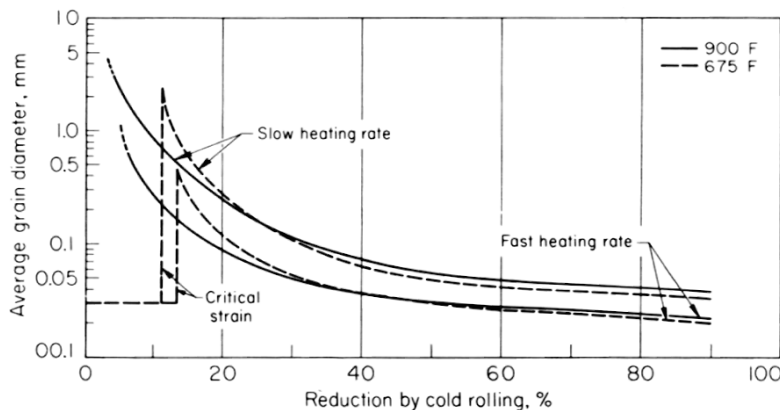


Figure. 1.1: Effect of cold working on recrystallized grain size. Figure is from Ref. [9].

1.3.3. Dynamic Recrystallization

Dynamic recrystallization occurs at elevated temperatures during the deformation process. In addition to strain, dynamic recrystallization requires thermal energy. While the material is deformed, new grains nucleate and grow. Sometimes new grains form at old grain boundaries. This is a type of discontinuous recrystallization process and often produces a “pearl necklace” type microstructure. Grains nucleate and grow when a critical strain for recrystallization is reached, just as in static recrystallization. Studying dynamic recrystallization is extremely difficult. Nevertheless, by creating experiments to isolate specific effects, dynamic recrystallization can be studied in a controlled manner [5].

1.3.4. Geometric Dynamic Recrystallization

Geometric dynamic recrystallization (GDRX) is a continuous recrystallization process that occurs at elevated temperatures and large strains. Unlike discontinuous recrystallization, GDRX has no distinct nucleation or growth stages. As strain increases during deformation, the spacing between high angle grain boundaries (HAGB) decreases. Figure 1.2 shows the spacing between HAGB decreasing at a rate faster than the spacing between low angle grain boundaries (LAGB) in the substructure [5]. With increasing deformation, the HAGB width will reach a size comparable to the subgrain size.

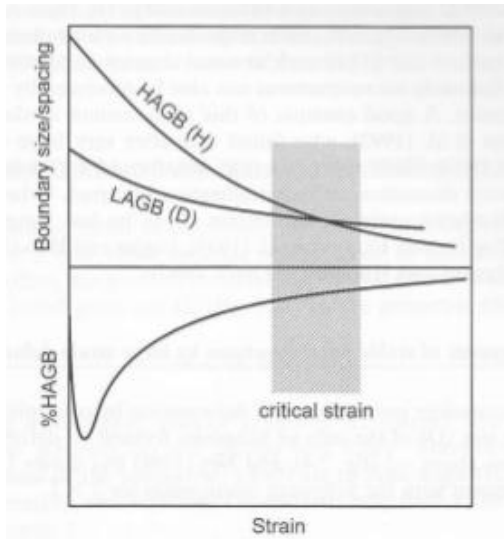


Figure 1.2: Effect of hot working on grain boundary spacing. Figure is from Ref. [5].

The GDRX phenomenon was investigated by Chang *et al.* while attempting to identify the cause for abnormal grain growth in AA5182 (Al-Mg alloy) sheet material during hot deformation. In those experiments, GDRX was determined to produce nuclei responsible for the growth of abnormal grains. Although abnormal grain growth is not a major concern in the present investigation, there exists the possibility of using GDRX for microstructure refinement. This possibility would reduce the amount of cold work required after hot rolling, thus reducing the cost of the rolling process.

In his investigation, Chang determined that at a plastic strain of $\epsilon=1.45$, subgrains begin to pinch off and form new grains with a size similar to the prior subgrains, as shown in Figure 1.3. These new grains have HAGBs produced by polygonization of grain boundaries during deformation. It is hypothesized that these detached subgrains are nucleation sites for recrystallization during static annealing after deformation. If

deformation were to continue to $\epsilon=1.8$, the GDRX mechanism is expected to produce a fully recrystallized microstructure. This strain is known as the critical strain for GDRX (ϵ_{GDRX}).

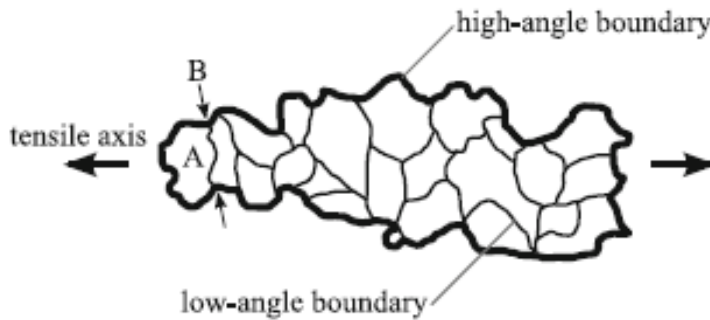


Figure 1.3: Subgrain A with low angle boundary at B being pinched off to form nucleation sites for recrystallization. Figure is from Ref. [10].

Chang's discoveries offer insight into controlling the recrystallized grain size using both dynamic and static mechanisms. The GDRX mechanism can produce nucleation sites for static recrystallization. By deforming the material to strains less than ϵ_{GDRX} , nucleation sites for the material can then be statically annealed to obtain a desired microstructure. Thus, there exists the possibility of obtaining a desired microstructure by utilizing GDRX mechanisms prior to static annealing.

1.3.5. Problem Statement

The primary focus of this study is to design and construct a hot torsion testing instrument. This device will simulate the hot rolling process by testing materials at fast strain rates to large strains. Data collected from this instrument will help answer

questions regarding the mechanisms responsible for recrystallization in aluminum alloys. By isolating controlling parameters, such as temperature, strain rate, and alloy content, a better understanding of the dynamic recrystallization process may be gained.

II. EXPERIMENTAL INSTRUMENTATION DESIGN

2.1. DESIGN REQUIREMENTS

The torsion testing instrument must be capable of producing strains and strain rates similar to those in commercial rolling operations for aluminum. Such typical values are displayed in Table 2.1. This will require a sufficient rotational speed from the instrument in addition to a compatible specimen geometry. To experimentally simulate hot rolling, specimens will be tested at elevated temperatures similar to those presented in Table 2.1. Furthermore, a method of quenching is needed to preserve the specimen's microstructure after completing a test.

Table 2.1: Typical conditions for hot rolling aluminum alloys. Table is from Ref. [4].

	Reversible	Tandem	Cold rolling
Start temperature [°C]	500–600	400–500	20
Finish temperature [°C]	400–500	250–350	100
Number of passes	9–25	2–5	2–10
Initial thickness [mm]	400–600	45–15	2–6
Final thickness [mm]	45–15	2–9	0.01–1
Strain per pass	0.1–0.5	0.7	0.3–0.7
Total strain	3.5	3	<5
Strain rates [sec ⁻¹]	1–10	10–100	>50
Inter-stand times [sec]	10–300	<5	

2.2. DELIVERABLES

The main goals of this study are to design and fabricate a hot torsion testing device. The computer program interface used for instrument control and data acquisition

should be user friendly and output useful information, such as torque, rotational displacement, and angular frequency. Because rotating machinery will be used in this study, a barrier between the instrument and the user is required to ensure user safety. Deliverables also include qualitative and quantitative data analysis validated by previous literature. The instrument will be used in future studies to help better understand microstructure evolution, such as dynamic recrystallization, during hot deformation.

2.3. INSTRUMENT DESIGN AND RELEVANT CALCULATIONS

2.3.1. Mechanical Design

2.3.1.1. Body Design

Torsion machines are available in a variety of shapes and sizes. While each design may differ slightly from the other, most torsion machines share similar design layouts. For example, each machine requires rotational motion that is typically provided by an electric or hydraulic motor. Torsion machines also require an electromagnetic clutch to transfer rotational motion to the test specimen once it is at temperature. A flywheel is often used to ensure a constant speed when the specimen is engaged. Most machines use a reaction load cell to measure torque at the fixed end [6]. This design layout is schematically illustrated in Figure 2.1. Specimen grip designs are where torsion machines vary the most. Grip designs will be discussed to greater depth in a latter section.

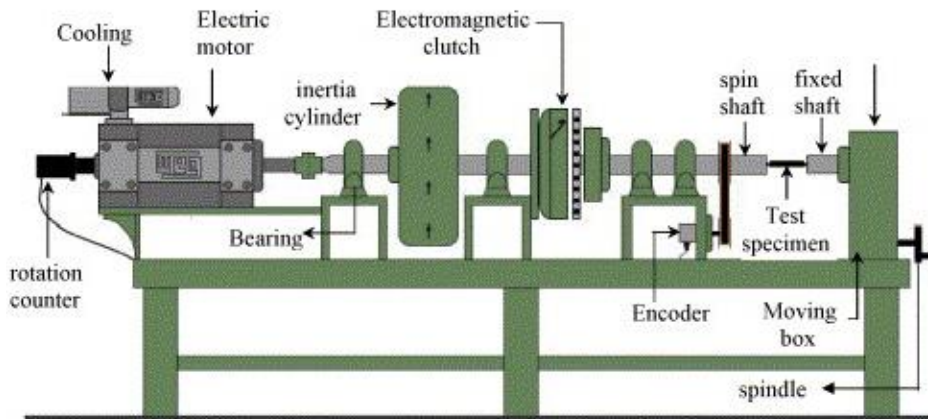


Figure 2.1: Torsion testing instrument designed by Bressan. Figure is from Ref. [7].

A torsion machine can essentially be thought of as lathe. In this analogy, the tailstock is replaced with a reaction torque transducer [6]. Lathes are capable of operating at high rotational speeds and can be used to experimentally simulate rolling. Lathe rails offer superb alignment for mounting devices. Therefore, a lathe will make an excellent starting point for the design of a torsion machine. In this investigation, a Rockwell 12-inch wood lathe was selected as a starting point. The lathe contains a 1 hp motor with a variable-speed belt drive capable of producing rotational speeds in the range of 265 to 3200 RPM. Figure 2.2 presents the lathe in its original state prior to design modifications.

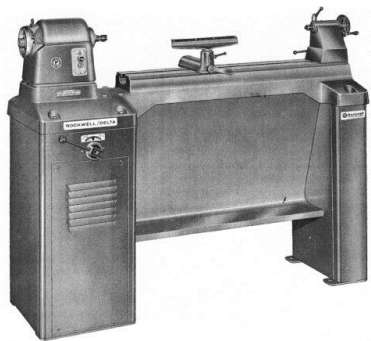


Figure 2.2: Rockwell 12-inch wood lathe. Figure is from Ref. [11].

2.3.1.2. Shearing Strain Rate

The shearing strain rate is determined by rotational speed and gauge section geometry. Hot rolling strain rates range from 1 to 100 s^{-1} , as shown in Table 2.1. Typical torsion test specimens have gauge diameters of 0.25 to 0.50 inches and gauge lengths ranging from 0.1 to 2.0 inches [12]. Based on this information, the shearing strain rate is calculated using Equation 1,

$$\dot{\gamma} = \frac{r\dot{\theta}}{L} \quad (1)$$

where $\dot{\gamma}$ is the shearing strain rate, r is the radius within the gauge length, $\dot{\theta}$ is the rotational frequency in radians* s^{-1} , and L is the length of the gauge section. Using the minimum lathe speed of 265 RPM, the rotational frequency in radians* s^{-1} is calculated using Equation 2.

$$\dot{\theta} = 265 \frac{rev}{min} \times 2\pi \frac{rad}{rev} \div 60 \frac{sec}{min} = 27.75 \frac{rad}{sec} \quad (2)$$

Assuming a specimen geometry that has an outer gauge diameter of 0.25 inches and a gauge length of 1 inch, the shearing strain rate is approximately $3.5s^{-1}$. This is close to the minimum strain rates expected in hot rolling. However, modifications to decrease the lathe speed can be made in the future. Thus, the Rockwell wood lathe was selected for this investigation.

2.3.1.3. Mounting Rails

Extruded aluminum alloy “80/20” beams were attached to the lathe rails using a T-shaped mounting assembly shown in Figure 2.3. These beams provide an easy way to safely and securely attach equipment to the lathe without the risk of damaging the lathe rails. The rail mounts also serve the purpose of aligning the aluminum beams with the lathe rails. Detailed CAD drawings of all custom parts are provided in Appendix A.

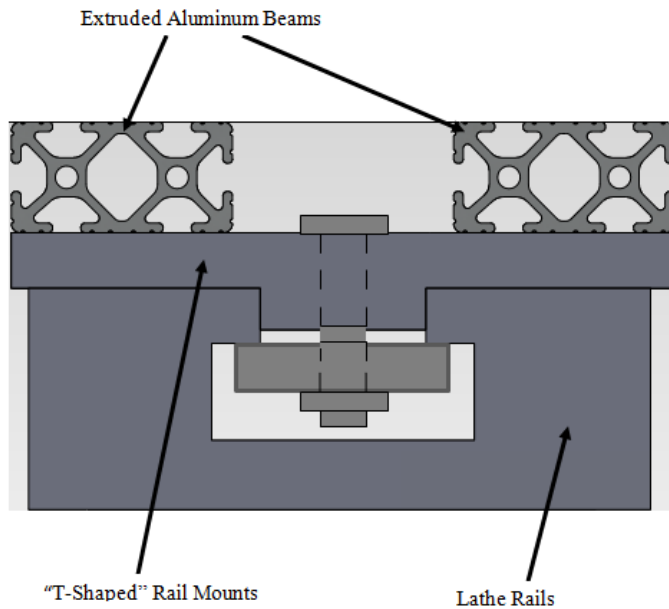


Figure 2.3: T-shaped rail mounting assembly.

2.3.1.4. Shaft Selection

For the purpose of this investigation a 5/8 inch hollow shaft with a 1/4 inch inner diameter made of 4130 steel was selected. Alloy 4130 steel has fair machinability and a carbon content (0.27 to 0.34%) low enough to avoid the formation of martensite. The material has a high yield strength of 70,000 psi. The shaft is hollow to reduce heat conduction along its length. The inside of the shaft also serves as a pathway to the

specimen for quenching gas. The maximum allowable torque for the shaft is calculated using Equation 3,

$$\tau_{max} = \frac{Tr}{J} \quad (3)$$

where τ is the materials maximum shear strength, T is the torque necessary to shear the shaft, r is the radius of the shaft, and J is the shaft polar moment of inertia. Because the shaft is fully keyed, a correction factor was used from Jadon and Verma's *Analysis and Design of Machine Elements* [13] and is presented below in Equation 4,

$$\tau_{keyway} = k_e \tau_{max} \quad (4)$$

where τ_{keyway} is the corrected shear strength and k_e is the correction factor. This correction factor is expanded in the following equation:

$$k_e = 1 - \frac{0.2b}{d} - \frac{1.1h}{d} \quad (5)$$

where b and h represent the width and depth of the keyway, respectively, and d represents the outer diameter of the shaft. A standard keyway size with a width of 0.188 inches and a depth of 0.079 inches was selected, yielding a correction factor of 0.8. Tresca's yield criterion is used to calculate the materials shear strength.

$$\tau_{max} = \frac{S_y}{2} \quad (6)$$

Equation 6 predicts a shear strength of 35,000 psi for the shaft. Accounting for the keyway correction factor using Equation 4 results in a maximum shear strength of 28,000 psi. Using Equation 3, the maximum allowable torque on the shaft is 1,300 in-lbs.

The shaft is expected to withstand stresses capable of deforming the aluminum alloys being investigated in this study. These alloys are described below in Table 2.2. To ensure shaft reliability, a worst-case scenario is examined by selecting the strongest material (Al-4.5Mg) deformed at room temperature.

Table 2.2: Alloy Specimen Compositions.

Specimen	Designation	Composition (wt.%)
Al 1xxx	Al	0.004Cu-0.09Si-0.11Fe-0.05Mn-0.00Mg-0.016Zn-0.05Cr-0.01Ti
Al 5xxx	Al-0.5Mg	0.002Cu-0.10Si-0.11Fe-0.05Mn-0.50Mg-0.006Zn-0.05Cr-0.01Ti
Al 5xxx	Al-4.5Mg	0.004Cu-0.11Si-0.11Fe-0.05Mn-4.39Mg-0.004Zn-0.05Cr-0.01Ti
Al 6xxx	Al-0.5Mg-1.0Si	0.003Cu-1.05Si-0.09Fe-0.05Mn-0.53Mg-0.009Zn-0.05Cr-0.01Ti

The Al-4.5Mg alloy has a shear strength of approximately 20,000 psi at room temperature [22]. Assuming a 0.25 inch gauge diameter for the specimen geometry, the torque required to yield the specimen is 61 in-lbs (Equation 3). These results confirm that the 4130 steel shaft selected for this investigation has sufficient strength to shear the aluminum specimens.

2.3.1.5. Spline Shaft Assembly

It is desired to test specimens in pure shear without the presence of axial loads. Therefore, a spline shaft is used at the fixed end of the of the torsion machine. The shaft is set inside a linear bearing that allows it to slide freely in the axial direction, but prevents the shaft from rotating. The shaft couples directly to the torque cell. This assembly is presented in Figure 2.4. The bearing is fixed between two aluminum blocks

allowing for easy alignment. The torque capacity of the spline shaft bearings are 734 in*lbs [27].

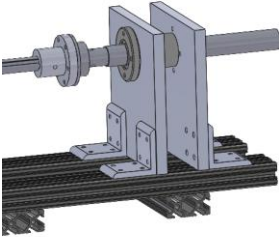


Figure 2.4: Spline shaft and torque coupling.

2.3.1.6. Flywheel

Flywheels are used to store kinetic energy. A cast iron flywheel with a 10 inch diameter is fixed to the rotating shaft on the torsion machine, as shown in Figure 2.5. When a specimen is engaged while testing, the energy stored in the flywheel is used to maintain a consistent shaft speed, thus giving a more consistent strain rate.

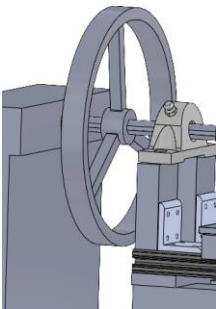


Figure 2.5: Flywheel for storing kinetic energy.

2.3.2. Data Acquisition and Controls Equipment

2.3.2.1. Clutch Brake

In order for the hot-torsion device to accurately apply rotation for a controlled time and angle of deflection, a clutch/brake is needed to rapidly engage and transfer power to a test specimen at a desired rotational speed. Furthermore, the clutch brake is responsible for disengaging and stopping the drive train by braking once the test is finished. Without a clutch/brake in the system the lathe would be turned on and instantly twist the specimen, producing uncontrolled torsion and possibly damaging equipment. The clutch/brake purchased for this project was Warner Electric's UM-100 1020 configuration, shown in Figure 2.6. The UM-100 is capable of withstanding torques up to 360 in-lbs. Detailed specifications for the UM-100 are provided in Appendix B.



Figure 2.6: Warner Electric clutch/brake. Image is from Ref. [14].

2.3.2.2. Reaction Torque Sensor and Signal Conditioner

Most torsion testing machines use reaction torque sensors to measure loads. A torque cell uses strain gauges to produce small electrical signals that are converted to torque readings. These signals are often too small to read directly from the torque cell itself, thus requiring amplification. A signal-conditioning device serves the purpose of

amplifying this signal before it is sent to the data acquisition software. An Omega TQ202 series reaction torque sensor was selected as the load cell for this investigation (see Appendix C for detailed TQ202 specifications). The TQ202 torque sensor has a standard operating range of 0 to 250 in-lb with a resolution of $\pm 0.2\%$ of the full scale range. It is also capable of supporting a safe overload of 150% of its maximum capacity, yielding a maximum operating torque of 375 in-lb. Vishay's 2120B model was selected for signal conditioning. The 2120B model provides built in excitation to the load cell and outputs the amplified load cell signal to the data acquisition board. The Vishay unit is capable of providing a 50 kHz response. This rapid response time allows for high sampling rates and time synchronization with other devices. Both the load cell and the signal conditioner are displayed in Figure 2.7.



(a)



(b)

Figure 2.7: (a) Omega TQ202 torque cell (Image is from Ref. [15]), (b) Vishay 2120B signal conditioner.

2.3.2.3. Tachometer

Before the clutch is engaged, the rotational frequency of the shaft must be known. For this reason, an ElectroSensors TR400 series tachometer was selected (see Appendix D for detailed TR400 specifications). The tachometer is equipped with a digital display that outputs a 4-20mA analog signal. The TR400 has 0.1% accuracy of the full scale analog output range. The device uses a Hall-effect sensor that communicates with a magnetic pulser wrap attached to the shaft. As the shaft spins, the Hall-effect sensor scans the collar and sends a signal to the tachometer. Once the shaft reaches the desired rotational frequency, the clutch may be engaged.

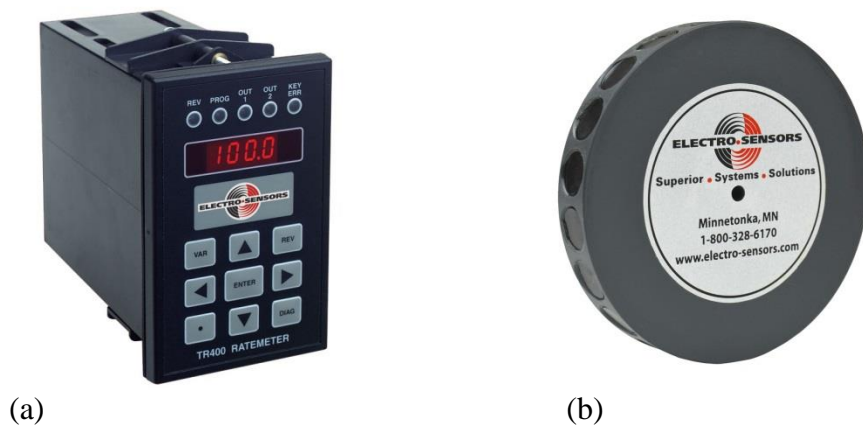


Figure 2.8: (a) ElectroSensors TR400 tachometer (Image is from Ref. [16]), (b) through-bore pulser disk (Image is from Ref. [17]).

2.3.2.4. Rotary Encoder

The rotational displacement of the shaft is measured using a through-bore rotary encoder. A 25T model from Encoder Products Company was selected to fulfill this purpose. The encoder uses differential square wave forms to “count” the shaft’s rotational position as the instrument torques the specimen. Rotational displacement data are used to

calculate strains and strain rates. The encoder has a resolution of 1000 counts per revolution. The 25T model is presented below in Figure 2.9. Detailed encoder specifications are provided in Appendix E.



Figure 2.9: Encoder Products 25T rotary encoder. Image is from Ref. [18].

2.3.2.5. Data Acquisition Software

The torque cell, tachometer, and rotary encoder relay data to a USB-6210 data acquisition board (DAQ board) made by National Instruments. The board accepts both analog and digital inputs and is compatible with each component selected for the project. The board communicates with the user through LabView's graphical programming language.

2.3.3. Temperature Control

2.3.3.1. Furnace Specifications

A quad-elliptical infrared radiative furnace is used to rapidly heat the test specimen. The furnace is easily capable of operating in the temperature ranges used for hot rolling of aluminum alloys. Research Incorporated recommends this E4 model for heating smaller diameter objects of approximately ¼ inch, thus making it a perfect choice for this investigation. The furnace, shown in Figure 2.10, is hinged and opens like a clamshell for easy access [19]. The furnace is controlled by a Eurotherm model 818 controller and powered by a Eurotherm model 832 power supply.

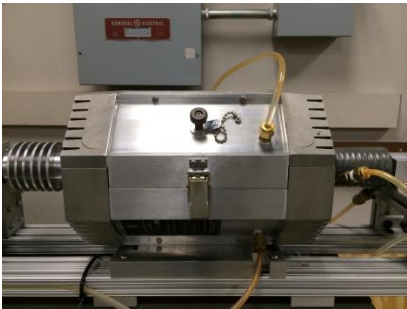


Figure 2.10: Quad-elliptical infrared radiation furnace.

2.3.3.2. Temperature Profile

A 12-inch shaft section protrudes from the radiant furnace and couples with the clutch break. The rotary encoder is fixed at a set distance of 8 inches from the furnace. The operating temperature range for the rotary encoder is -20°C to 85°C. Heat conduction through the shaft is therefore a concern. A one-dimensional, steady-state heat analysis was performed using equations from *The Fundamentals of Heat and Mass Transfer* [20].

Results of the analysis are presented in Figure 2.11. At a distance of 8 inches from the furnace the rotary encoder is expected to reach a steady-state temperature of 100°C.

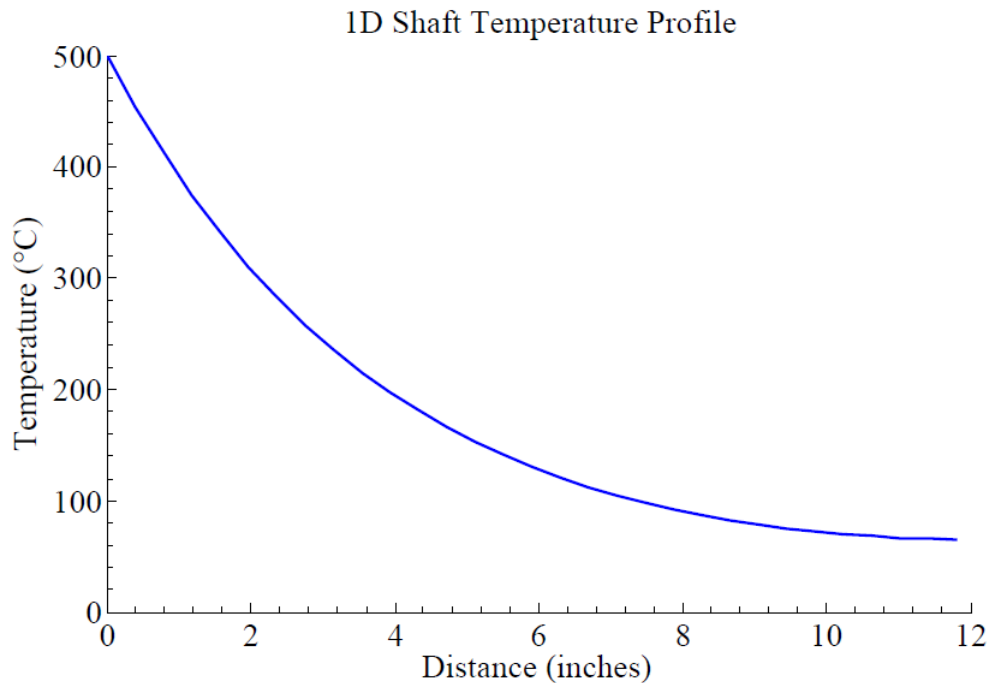


Figure 2.11: A 1-Dimensional analysis of shaft temperature.

To prevent the temperature from exceeding 85°C, annular fins of 6061 aluminum were fixed to the shaft. A cooling fan is mounted below the fins to enhance heat dissipation from the fins. This setup is shown below in Figure 2.12. It is important to note that the one-dimensional heat transfer analysis performed for Figure 2.11 assumes steady-state temperatures. The radiative furnace will heat the test specimen to the desired temperature well before steady-state heat conduction is reached in the shaft. Therefore, the annular fins with forced convection are merely a precaution. The program used to generate the prediction of the steady-state temperature profile is provided in Appendix F.

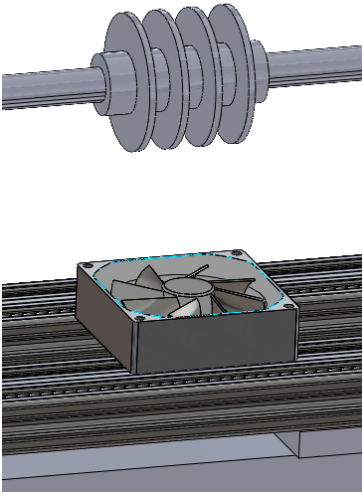


Figure 2.12: Annular fins with forced convection provided by a computer fan.

2.3.4. Torsion Grip Design

The torsion grip design depends on the geometry of the test specimen. There are two common types of torsion specimen designs: (1) the specimen ends are threaded or (2) the specimen ends are squared. Threaded specimens tighten as the shaft rotates. Specimens with square ends fit into square slots in the grips. As the shaft rotates, the square ends are constrained by the slots as the specimen is deformed. Both specimen designs have a gauge length with a reduced diameter and a circular cross section. The design variants for these grips are shown below in Figure 2.13.

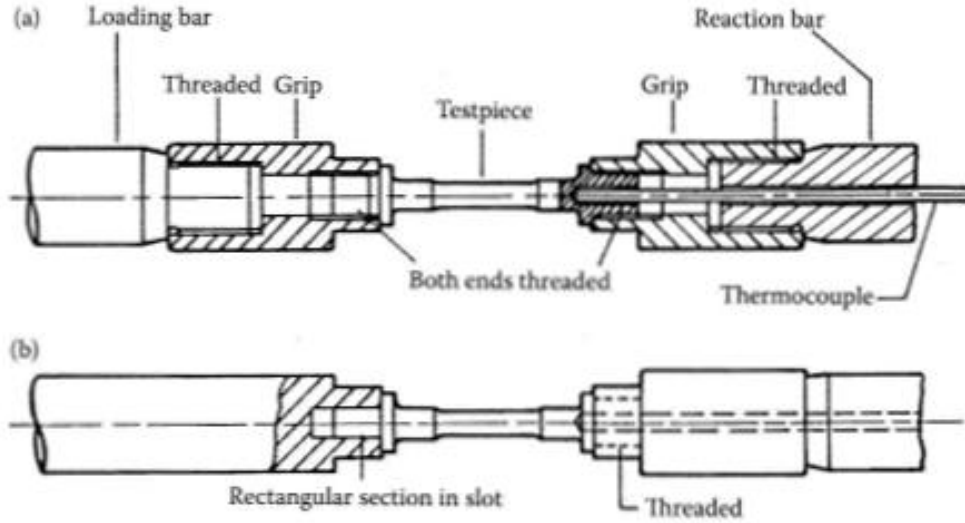


Figure 2.13: Torsion instrument grip design variants. Figure is from Ref. [21].

The torsion machine in the present investigation uses square slotted grips. The instrument grips were designed by Joseph Bass, an undergraduate research assistant working on the project. The grips are threaded onto the 4130 shaft. Both sides of the shaft have left handed threads so the grips tighten when a specimen is engaged. The grips are made of 316L stainless steel and are depicted in Figures 2.14 and 2.15. A detailed grip design is provided in Appendix A.

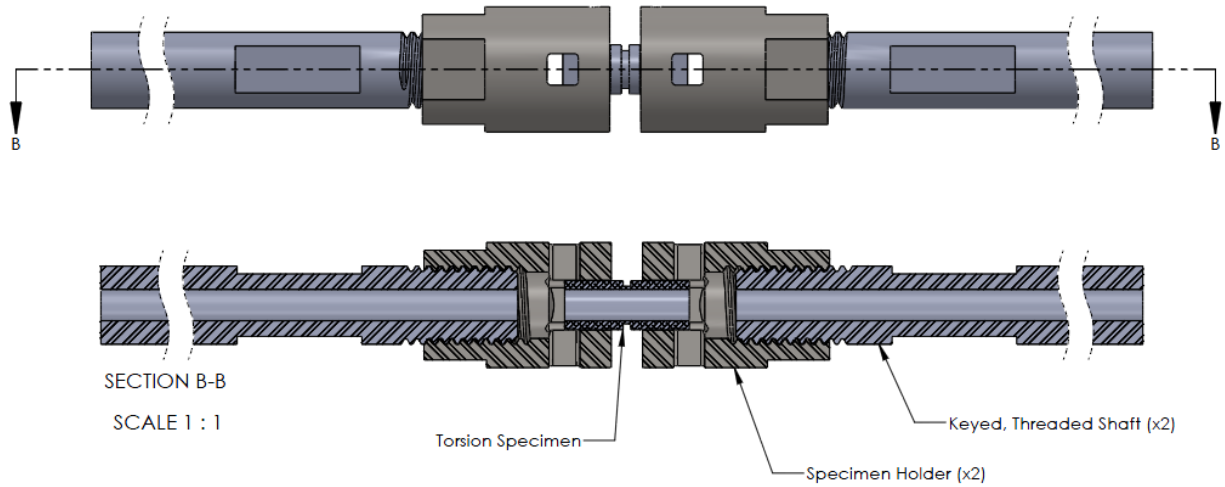


Figure 2.14: Final torsion instrument grip design.

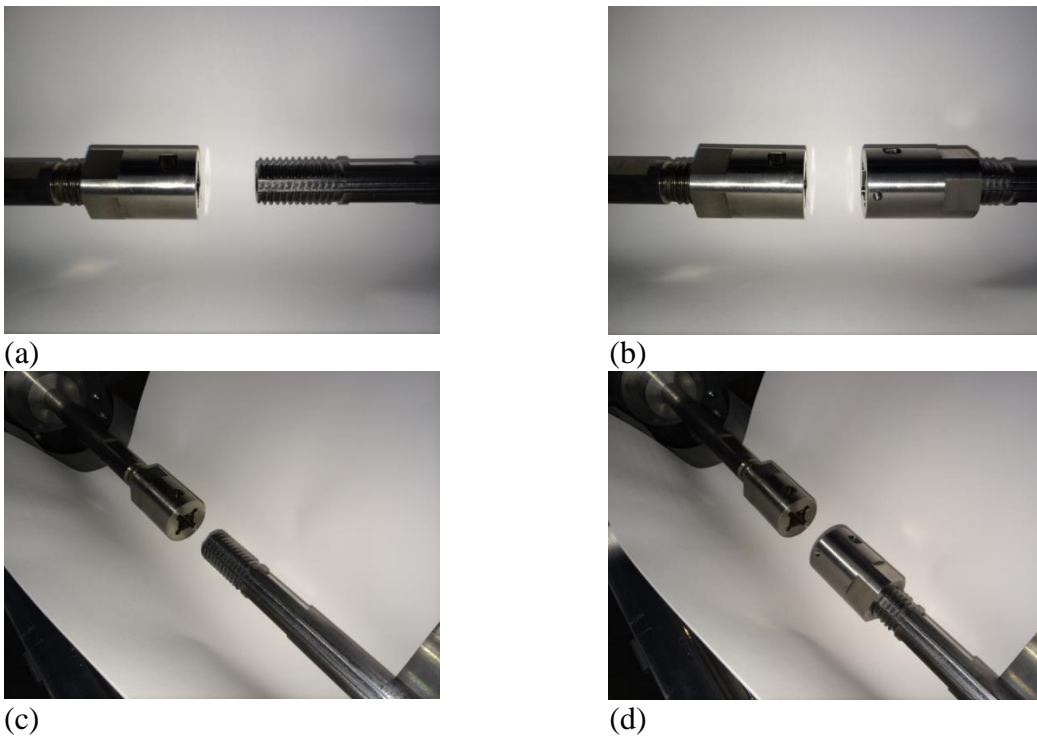


Figure 2.15: (a) Images show the left grip fixed and the right grip off, (b) both grips fixed, (c) isometric view with the left grip fixed and the right grip off, and (d) isometric view of both grips fixed.

2.3.5. Specimen Design

As mentioned previously, typical torsion test specimens have gauge diameters of 0.25 to 0.50 inches and gauge lengths of approximately 1 inch [12]. The two specimen designs used in this investigation have gauge lengths of 1 inch and 0.5 inches with an outer gauge diameter slightly larger than $\frac{1}{4}$ inch. Table 2.3 shows relevant specimen dimensions. Both specimens are shown below in Figure 2.16. With the longest (1 in.) specimen geometry, tests may be performed at strain rates as low as $3.5s^{-1}$. Each specimen is a hollow tube to reduce strain and strain rate gradients within the specimen. Furthermore, air may be injected through the axial hole in the specimen to allow for faster quenching [6]. Detailed specimen designs are provided in Appendix A.

Table 2.3: Torsion specimen dimensions in inches.

Specimen Number	OD	ID	Gauge Length	Fillet Radius
1	0.265	0.125	1.00	1/32
2	0.328	0.250	0.50	1/16

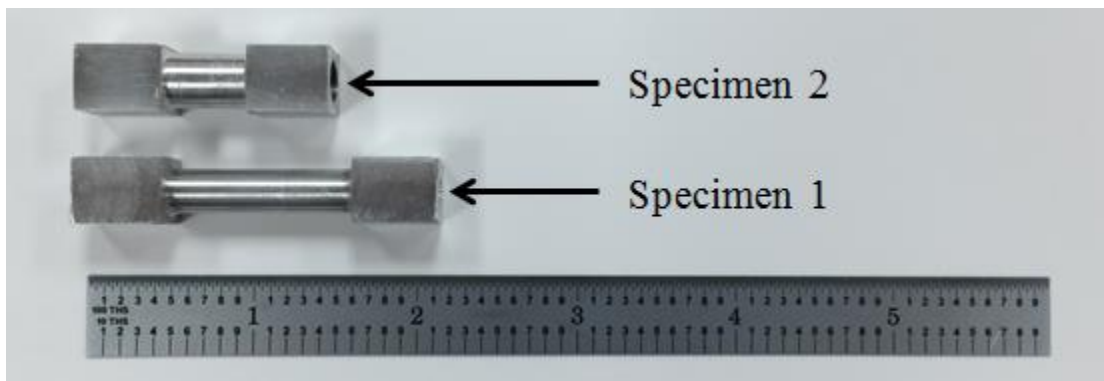


Figure 2.16: Torsion specimens with scale marker in inches.

2.4. FINAL INSTRUMENT DESIGN

The torsion machine was fabricated following the instrument design. Figure 2.17 displays an isometric view of the torsion machine. Figure 2.18 presents a labeled side view of the instrument. Figure 2.19 shows the actual instrument with water- and air-cooling lines.

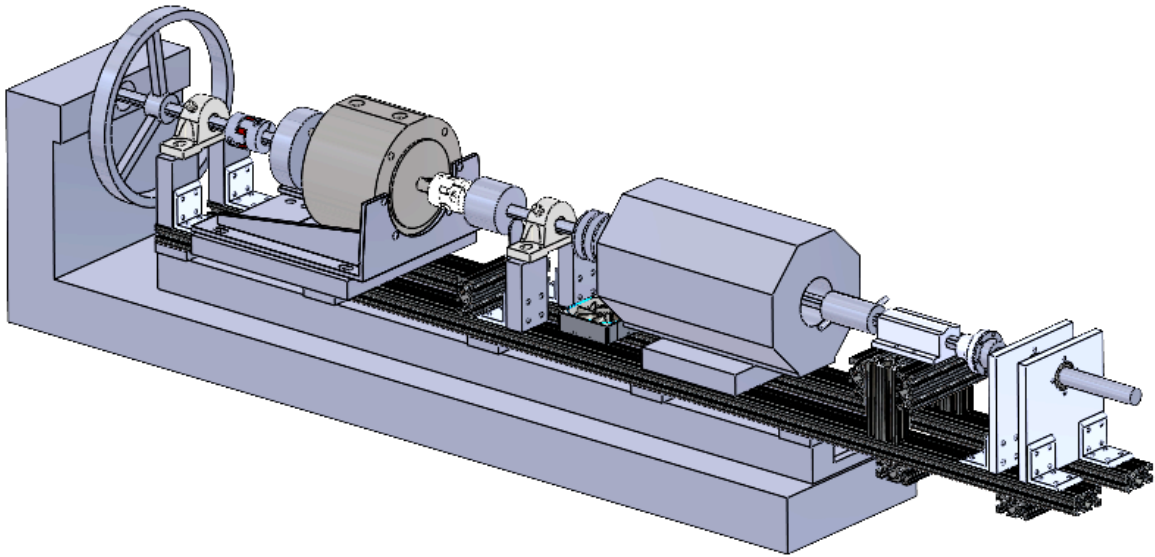


Figure 2.17: Isometric view of the torsion testing instrument.

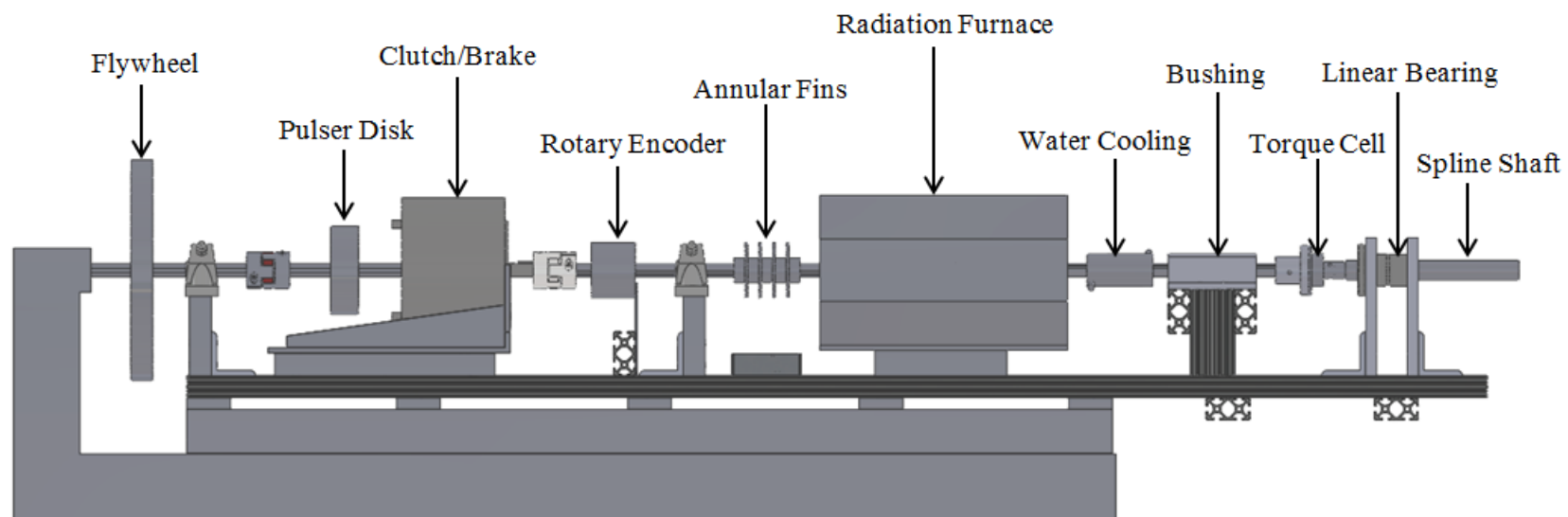


Figure 2.18: Labeled SolidWorks™ model of the torsion instrument.

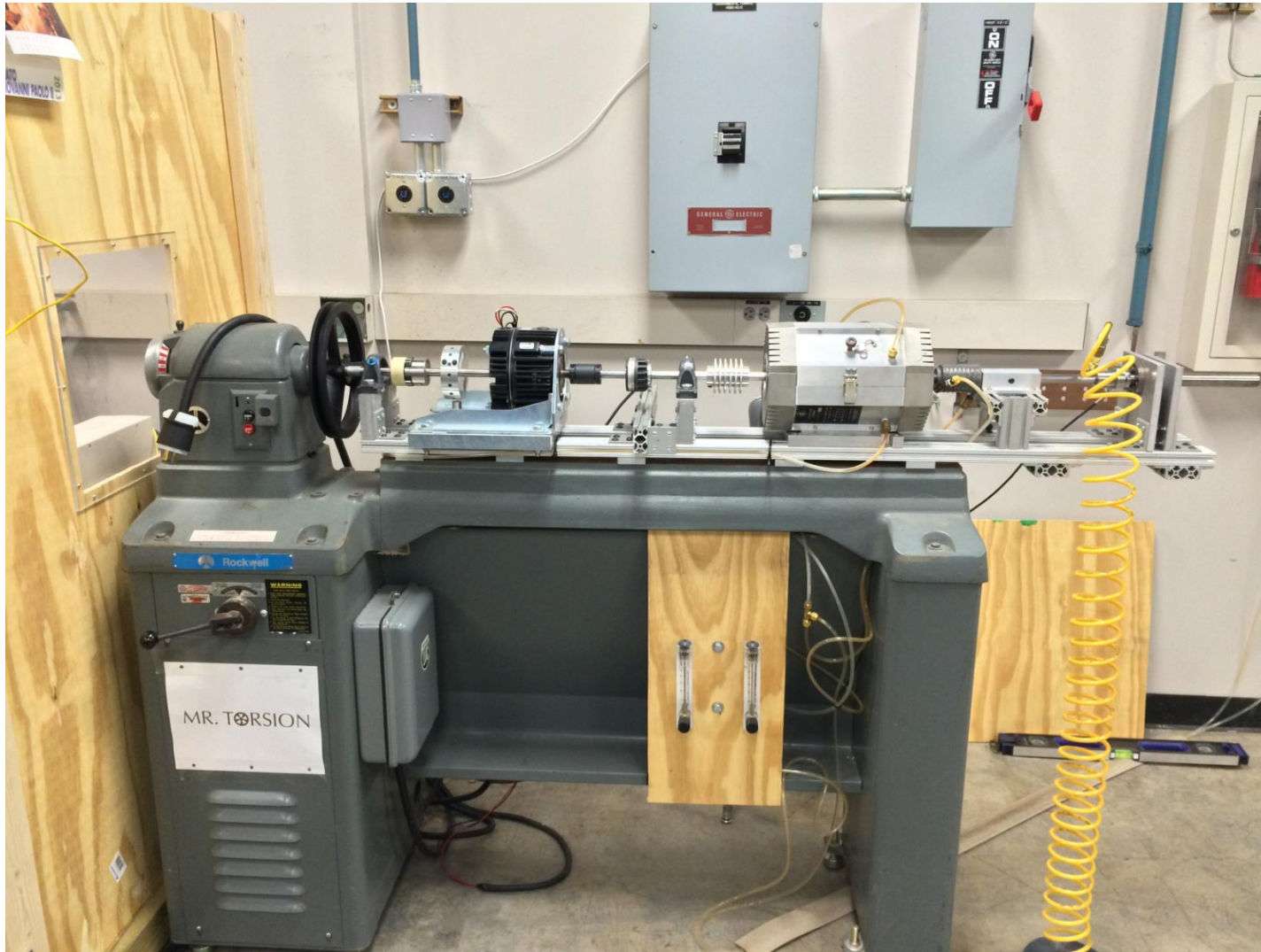


Figure 2.19: Torsion testing apparatus.

III. EXPERIMENTAL PROCEDURE

3.1. INITIAL INSTRUMENT CALIBRATION

3.1.1. Torque Cell Calibration

The torque cell was calibrated using a Vishay 2120B signal conditioner and an ACDelco digital torque wrench. The TQ202 torque cell requires 10 volt DC excitation across its bridge. Adjust the bridge excitation screw till the excitation volt meter reads 10 volts, as presented in Figure 3.1. Zero the signal output from the Vishay unit by adjusting the balance knob until the balance LEDs dim. It is important that no torque is acting on the torque cell while adjusting the balance knob. The DAQ board receiving the output signal accepts 0 to 10 volts. The TQ202 torque cell operates in a 0 to 20 millivolt range. The Vishay unit should amplify the signal from the torque cell to match the 0 to 10 volt range of the analog input on the DAQ board.

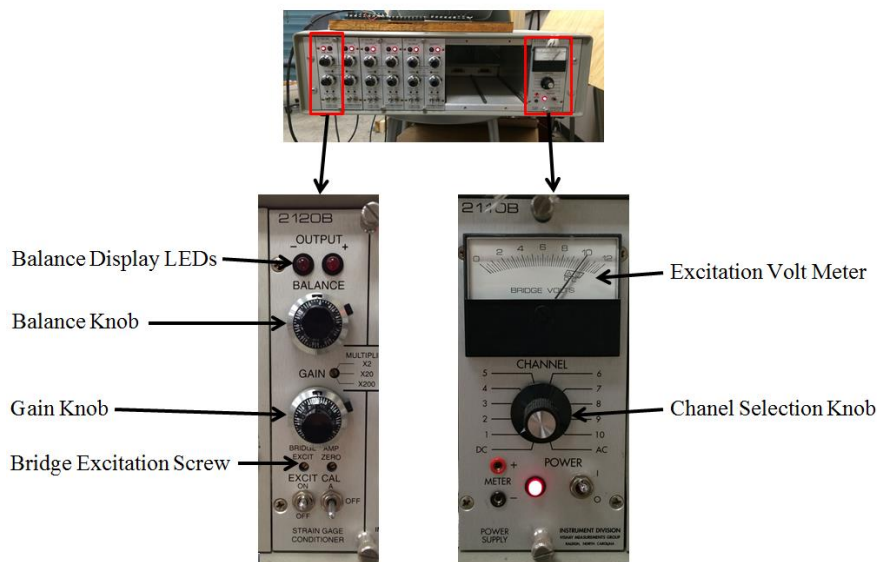


Figure 3.1: The Vishay signal conditioning unit.

Proper signal amplification is achieved by adjusting the gain knob, as shown in Figure 3.1. It is desired to set the 10 volt output signal to match the maximum torque from the torque cell (250 in-lbs). Adjust the gain knob until the output reads 1 volt for every 25 in-lbs displayed on the digital torque wrench. Repeat these measurements in 25 in-lb increments while recording both output voltage and torque. These data are used to plot a calibration curve. The torque cell calibration is presented below in Figure 3.2.

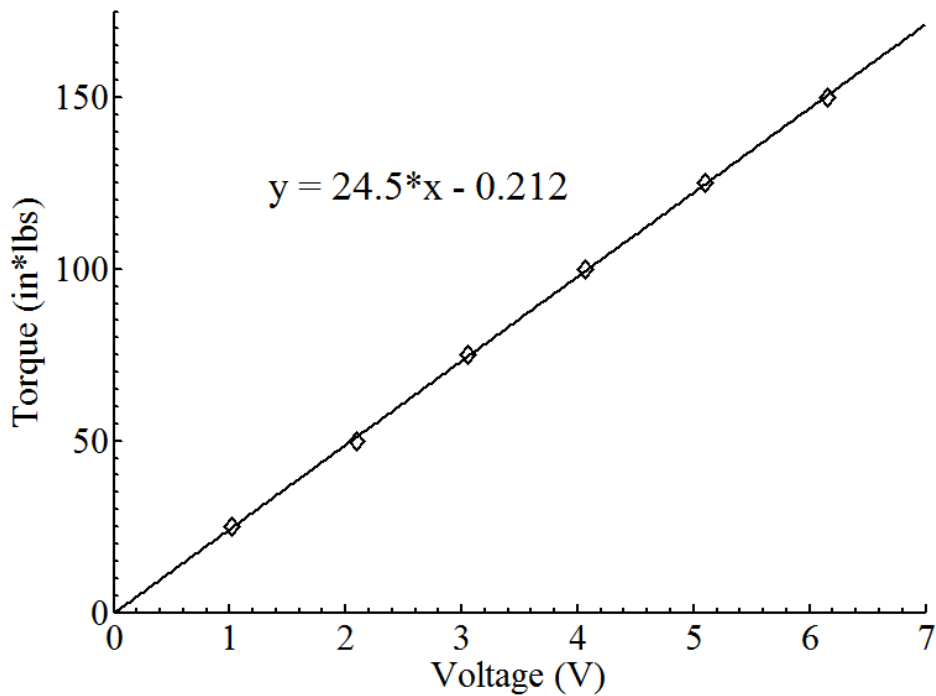


Figure 3.2: Calibration curve for the TQ202 torque cell.

3.1.2. Tachometer Calibration

Calibration of the tachometer was accomplished by using a hand-held, digital tachometer. Reliability DIRECT's TC811B tachometer provides shaft speed measurements to match the output current signal from the TR400 tachometer. Place a piece of reflective tape at any location along the torsion instrument shaft. Set the TC811B to the rpm_{photo} setting. Holding the TC811B approximately 1 inch from the reflective tape, measure the shaft speed while reading the digital display. The TR400 tachometer has a linear correlation between speed and current. Therefore, a calibration curve is easily made by recording the shaft speed and current output from the tachometer. A calibration curve for the tachometer is shown in Figure 3.3.

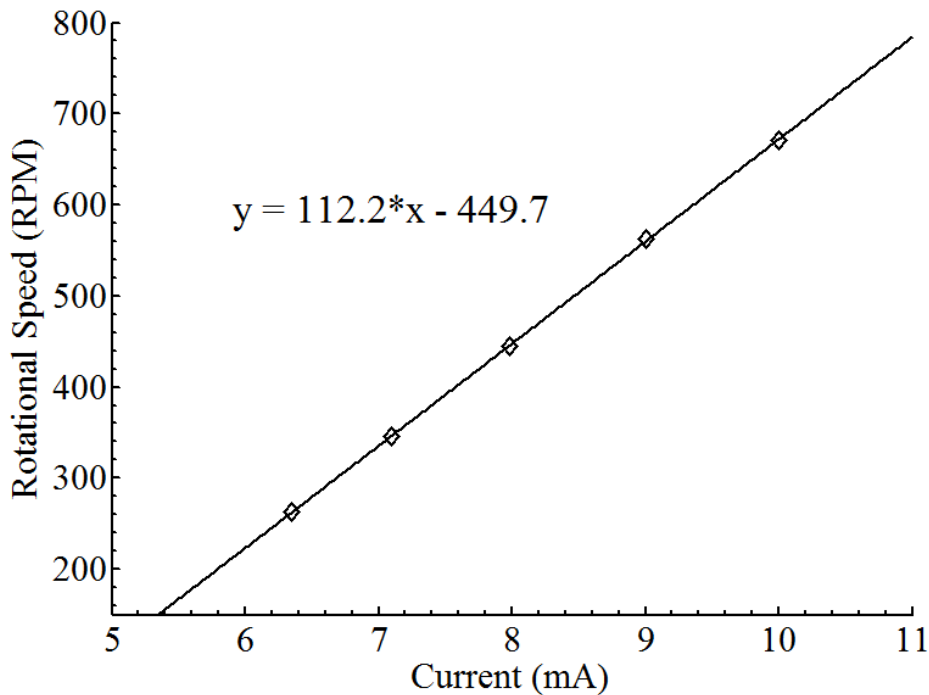


Figure 3.3: Calibration curve for the TR400 tachometer.

3.2. TEST PREPARATION

3.2.1. Cooling Water

Cooling water is supplied from the building facilities to the radiant furnace and ridged shaft section on the right of the furnace. The flow is controlled by two meters mounted on the front of the lathe as shown in Figure 3.4 (a). The left flow meter is set to 0.6 gpm and the right flow meter is set to 0.4 gpm. If testing at elevated temperatures, turn both water valves to the vertical position, as shown in Figure 3.4 (b). The flow indicators display flow rates in gallons per minute.

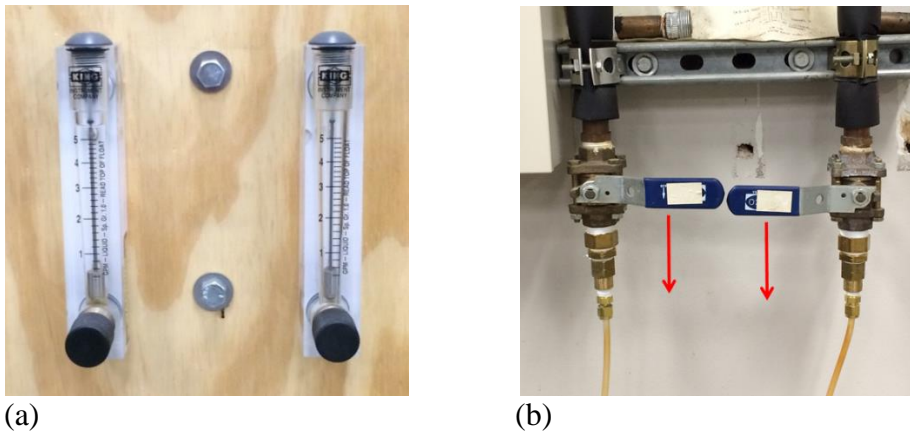


Figure 3.4: (a) Flow meters mounted on the front of the instrument, (b) red arrows indicate valve turning direction for cooling water.

3.2.2. Cooling Fan and Clutch Power

The cooling fan and electric clutch are both wired into the same power unit, as presented in Figure 3.5. Flip both switches to the “on” position. The electric clutch will automatically engage in the “brake” position. A red LED light below the switches will confirm the clutch is locked in the brake position.



Figure 3.5: Power unit for the cooling fan and clutch brake.

3.2.3. Specimen Loading

A 1.5 inch diameter quartz tube surrounds the grip assembly to protect the furnace heating elements and provide uniform heating while testing. Before loading a specimen, carefully slide the tube towards the annular fins on the left side of the furnace. Wear latex or neoprene gloves while moving the tube to avoid getting oils on the outer surface. When the tube has made contact with the annular fins, slide the spline shaft away from the furnace. This provides enough space to fit the specimen into the grip on the right side. Two thermocouples protrude from the grip on the right side, as shown in Figure 3.6 (a). One of the thermocouples acts as a reference for the furnace controller during testing, and the other is connected to the thermocouple display shown in Figure 3.7. These thermocouples measure the inside wall temperature of the specimen during testing. Gently guide the thermocouples into the hollow specimen while sliding the specimen into the grip. Next, slide the shaft towards the opposite grip. Align the specimen with the grip slot by rotating the shaft on the left side of the furnace. Once the specimen is aligned,

gently push the spline shaft until the specimen end enters the left grip. If any misalignment is observed, remove the specimen from the grips and realign the instrument. Slide the quartz tube over the entire assembly. Lastly, position the third thermocouple to lightly contact the outer surface of the specimen gauge section, as shown in Figure 3.6 (b). The thermocouple end must be in contact with the surface of the specimen to ensure accurate temperature readings. Cover the ends of the tube with quartz wool to enclose the heating area.

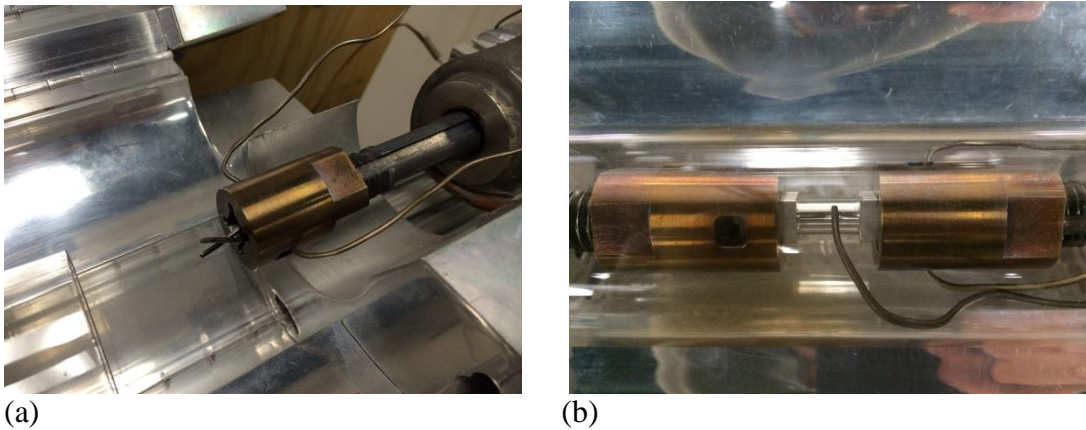


Figure 3.6: (a) Thermocouples protruding from the left grip, (b) positioning the outer thermocouple to contact the specimen surface. The quartz tube surrounds the assembly.

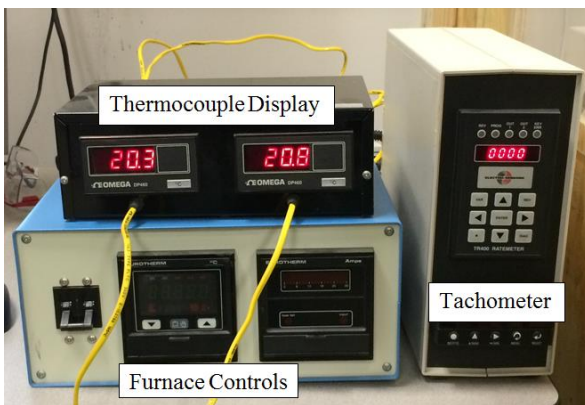


Figure 3.7: Thermocouple display, furnace controller, and tachometer.

3.2.4. Furnace Controls

The radiant furnace is controlled by a Eurotherm model 818 controller, shown in Figure 3.8 (a). The furnace is powered by a Eurotherm model 832 power supply, presented in Figure 3.8 (b). Before powering the furnace, set the current output on the power supply to the desired setting. The current output is the white knob located at the bottom of the right controller shown in Figure 3.8 (b). The current knob was set to the half-way point (approximately 50% power) during testing. Flip the power switch to the “on” position and select the desired test temperature using the “up” and “down” arrows on the left display. Once the temperature is selected, press the hold button on the left panel shown in Figure 3.8 (a). This creates a “set point” temperature. The furnace responds quickly to the controller. It is important to note that the furnace has a tendency to overshoot the selected temperature (near 450°C) value under the tuning parameters used (PID controller was set to the self-tune method). Thus, a temperature slightly below the desired temperature should be selected if these same parameters are used to achieve similar temperatures. Use the thermocouple display in Figure 3.7 to determine if the furnace requires more or less power. The thermocouple display shows two readings: one for the thermocouple on the outer surface (left reading) and one for the thermocouple located inside the specimen (right reading). The thermocouple inside the specimen is taken as the more accurate test temperature because it is not exposed directly to the infrared heating elements.



(a)



(b)

Figure 3.8: (a) Left Eurotherm model 818 controller used to adjust and set the temperature, (b) right Eurotherm model 832 power supply used to adjust the current output.

3.2.5. Lathe Controls

While the specimen is heating to the test temperature, push the start button of the lathe. The lathe speed is adjusted using the control lever shown in Figure 3.9. Turn the lever counter-clockwise to reduce the speed and clockwise to increase the speed. The minimum possible speed is 265 RPM.



Figure 3.9: Lathe controls.

3.2.6. Acquisition Setup

Two computers are currently used in the data acquisition and control system. This is primarily because of timing synchronization limitations in the NI USB 6210 DAQ boards. It is a future goal to acquire a DAQ board that has internal timing synchronization between analog and digital channels. Figure 3.10 graphically presents the current system. Computer 1 and DAQ 1 are used to generate a digital pulse (clock signal) and trigger the clutch/brake. The clock signal is passed to DAQ 2, where the encoder, tachometer, and torque cell acquire data at the clock signal.

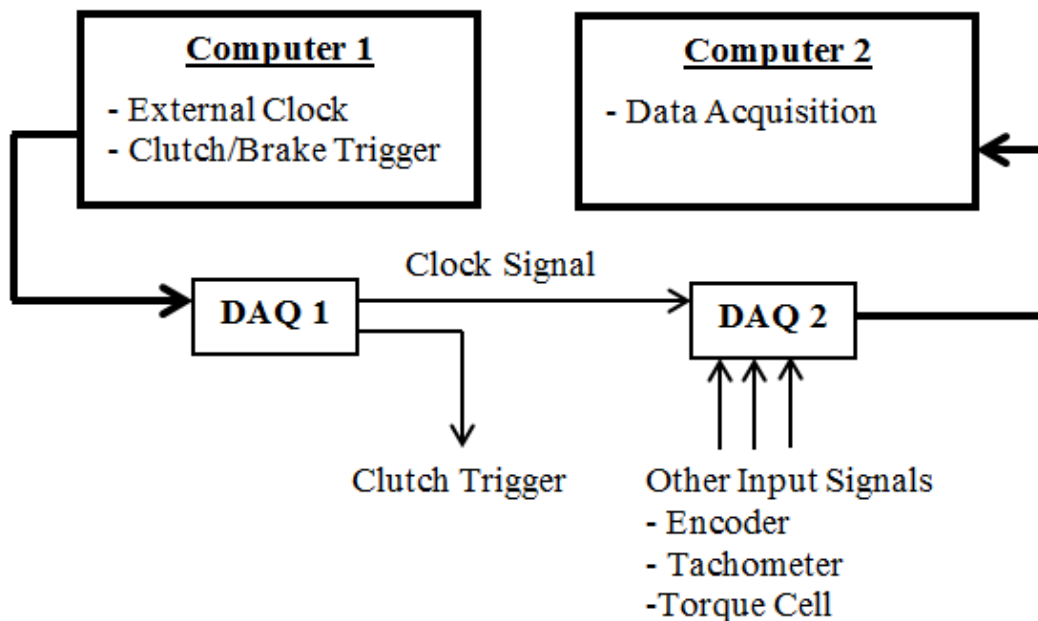


Figure 3.10: Data acquisition setup using two computers.

3.2.7. Program Initiation

3.2.7.1. *Setting the Experiment Time*

Select the desired total test time by adjusting the “Time Target” indicator located on the front panel of computer 1. The test time and rotational speed determine the total shear strain imposed during a test. The front panel for computer 1 is shown in Figure 3.11. Start the program to generate the external clock signal at 1000 Hz or other desired frequency of data acquisition. The clutch will not engage until the “Start Test” icon is clicked.

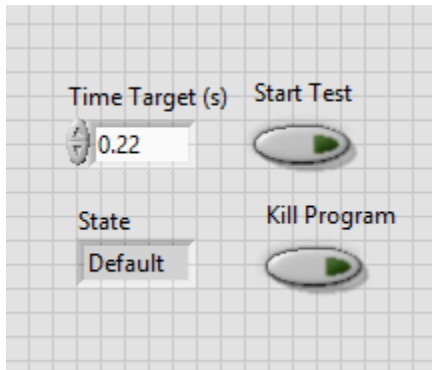


Figure 3.11: Computer 1 program front panel.

3.2.7.2. *Selecting the File Path and Testing*

Start the program on computer 2 before the furnace reaches the test temperature. The front panel for the user interface on computer 2 is presented in Figure 3.12. The panel displays crucial information, such as the drive shaft speed, torque, and total degrees rotated. Before running a test, the user is prompted to select a file path for saving the data. The program records all raw data to a text file format and exports it to the selected

file path. Once the file path is selected, the instrument automatically begins acquiring data. Click the “Start Test” icon to run an experiment. The program code for this experiment is provided in Appendix G.

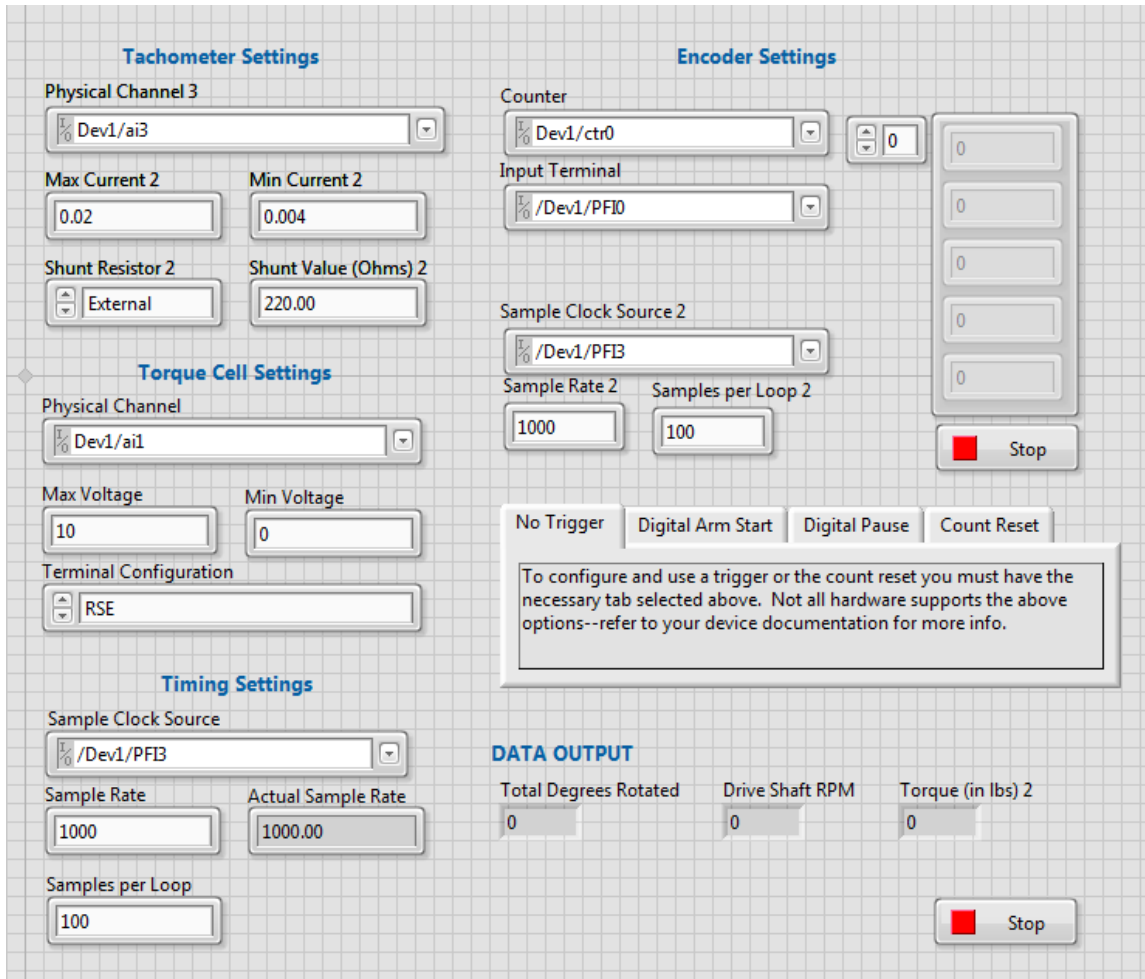


Figure 3.12: Computer 2 program front panel.

3.3. Air Quenching

Immediately after running a test, it is desired to quench the specimen to preserve its microstructure. Compressed air is injected into the hollow shaft and through the specimen

to ensure rapid cooling. The air valve is located on the wall next to the torsion instrument and is shown in Figure 3.13.



Figure 3.13: Compressed air valve and regulator for gas quenching.

IV. EXPERIMENTAL RESULTS AND DISCUSSION

4.1. INSTRUMENT CHARACTERIZATION

The torsion testing apparatus fabricated in this study is a fairly complex instrument. Each device on the instrument must work properly to obtain meaningful data. The following addresses verification of the instrument functionality.

4.1.1. Speed Verification

A graph of rotational speed versus time is presented in Figure 4.1. In this figure, the rotational speed measured from the rotary encoder and the tachometer are compared for a test performed at 460°C. The tachometer outputs data in RPM, which is easily converted to degrees per second. The rotary encoder provides data for angle at a specific time, and rotational speed must be calculated as the first derivative of these data. The rotational speed was calculated from the rotary encoder data using linear regression within a moving window of five (5) data points. The algorithm used in this calculation takes a window of five data points and determines their slope, the first derivative of the data, which is assigned to the average window time. Since the time increment between measurements is constant at 1 millisecond, the average window time is easily computed. The window shifts up one data point after each calculation, and then the calculation is repeated for the new window. This algorithm produces some smoothing of the rotational speed curve from the rotary encoder data. Figure 4.1 confirms that the tachometer speed and the speed calculated using the rotary encoder match at approximately 2600 degrees

per second (or 433 RPM) during testing. The calculated encoder velocity ramps up at the start of the test and levels out after 20 milliseconds, which is consistent with clutch engagement. The spike in the encoder speed at 0.1 seconds indicates specimen failure.

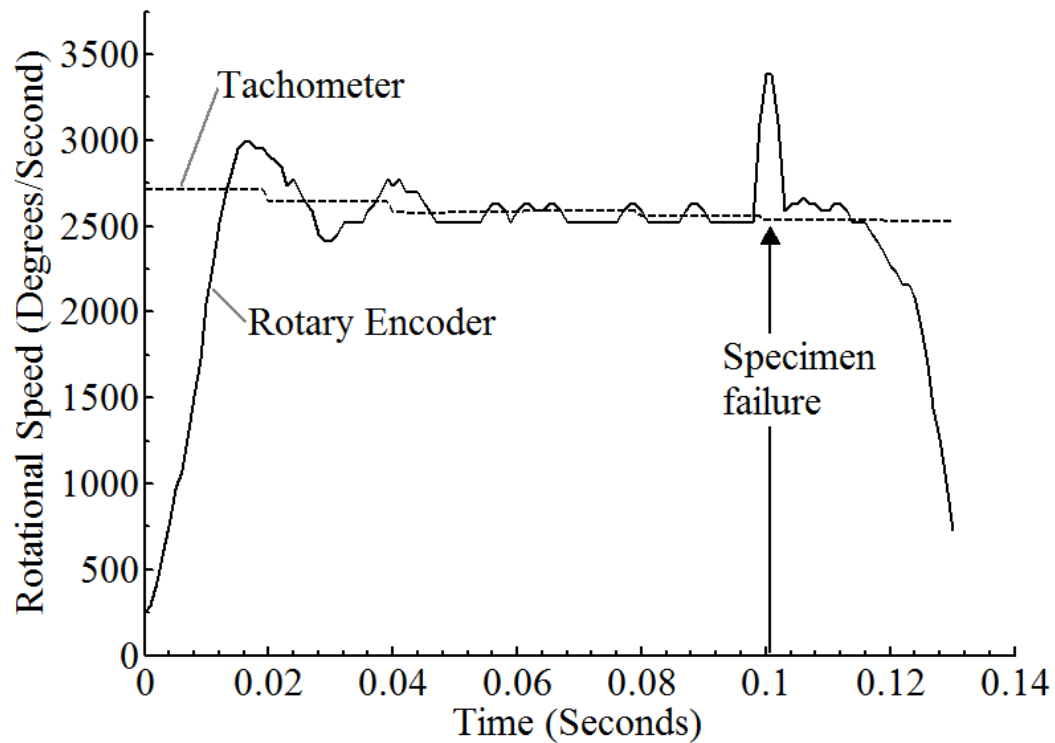


Figure 4.1: Rotational speed is shown versus time.

4.1.2. Timing Synchronization

Timing synchronization between the rotary encoder and the torque cell is crucial to obtaining meaningful stress-strain data. Figure 4.2 compares two plots: torque versus time and rotational displacement versus time. The time scale is identical in both plots. The dashed line at 0.01 seconds marks the start of the test, when the clutch is engaged. As the encoder begins to rotate, the torque rises. This confirms that the torque cell and rotary

encoder are synchronized. It is important to note that the tachometer is not synchronized with the torque cell and rotary encoder. The tachometer signal conditioning has a response time of approximately 30 milliseconds. The delayed signal from the tachometer does not affect the final stress-strain data because the tachometer is used only to adjust motor speed prior to testing.

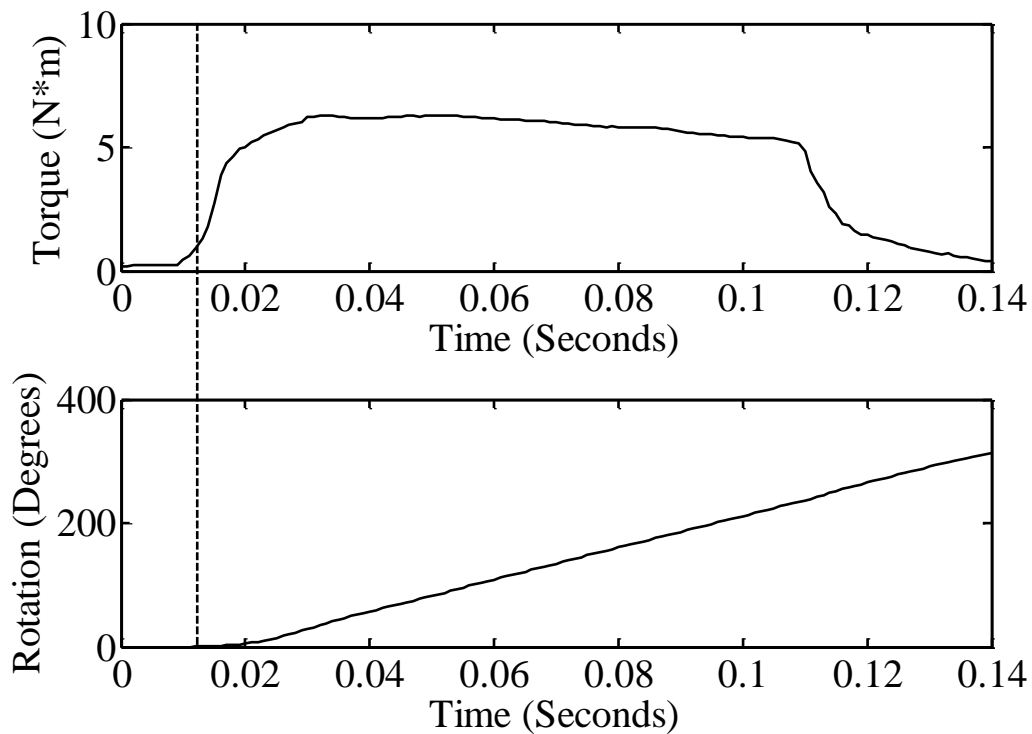


Figure 4.2: Timing synchronization between the torque cell and rotary encoder.

4.2. TESTING PARAMETERS

4.2.1. Material Selection

All experiments in this study were performed at elevated temperatures using the Al-4.5Mg material. The specimen material was provided by Furukawa-Sky Aluminum

Corp. (FSA). Strain rates and testing temperatures were selected based on a previous investigation of a similar material conducted by Ueki *et al* [23]. In their investigation, Ueki used hot torsion testing to experimentally simulate hot rolling of aluminum alloy AA5083. A comparison between the chemical compositions of the AA5083 alloy used in Ueki’s investigation and the FSA alloy used in this investigation is presented in Table 4.1. The data of Ueki *et al.* are compared to results produced in this study because their material is the most similar for which torsion data are available in the literature.

Table 4.1: Chemical composition comparison of aluminum alloys in wt. pct. Data taken from Ref. [23].

	Cu	Si	Fe	Mn	Mg	Zn	Cr	Ti
FSA Alloy	0.004	0.11	0.11	0.05	4.39	0.004	0.05	0.01
AA5083 Alloy	0.01	0.09	0.17	0.61	4.24	NA	0.2	0.04

The largest difference in chemical composition between the two alloys is the amount of manganese (Mn). The AA5083 alloy contains twelve (12) times more manganese than the FSA alloy. Figure 4.3 illustrates the effect of manganese on commercially pure aluminum at room temperature. Increasing the amount of manganese from 0.05% to 0.61% approximately doubles the yield strength at room temperature.

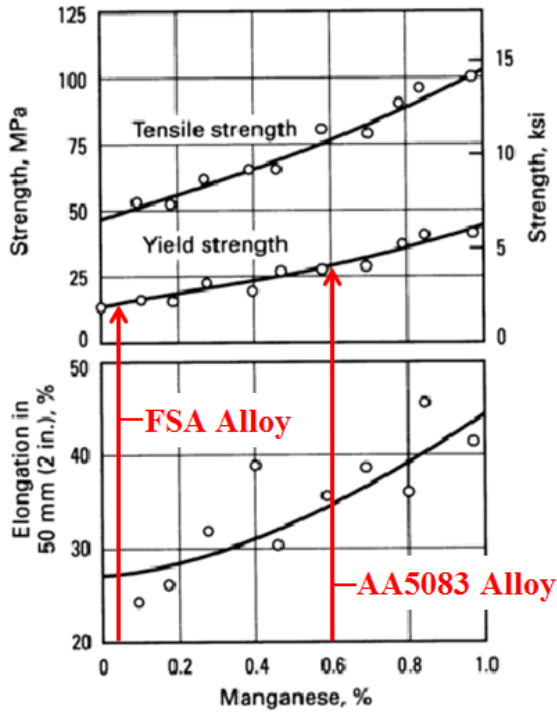


Figure 4.3: Alloying effect of manganese on tensile properties of wrought 99.95% Al at room temperature. Figure is taken from Ref. [24].

However, at high temperatures manganese addition has much less effect on alloy strength [25]. Figure 4.4 presents the logarithm of diffusivity-compensated strain rate versus the logarithm of modulus-compensated stress for aluminum-magnesium alloys containing various amounts of manganese [25]. In this figure, $\dot{\epsilon}$ is the true-strain rate and D is the appropriate diffusivity. D is calculated using Equation 7,

$$D = D_o \exp\left(\frac{-Q_{sol}}{RT}\right) \quad (7)$$

where D_o is the Mg solute diffusivity constant ($D_o = 5 \times 10^{-5} \text{ m}^2/\text{s}$), Q_{sol} is the activation energy of Mg diffusion in Al ($Q_{sol} = 136 \text{ kJ/mol}$), R is the universal gas

constant, and T is the temperature. Testing at 460°C with a shearing strain rate of 15s^{-1} gives a diffusivity-compensated strain rate $\left(\frac{\dot{\epsilon}}{D}\right)$ of $8.5 \times 10^{14} \text{ m}^{-2}$. Under this condition, the data of Figure 4.4 suggest that the AA5083 alloy is not likely to be much stronger than the FSA alloy. Nonetheless, it should be noted that these are two different materials, and as such, they are expected to behave differently during testing.

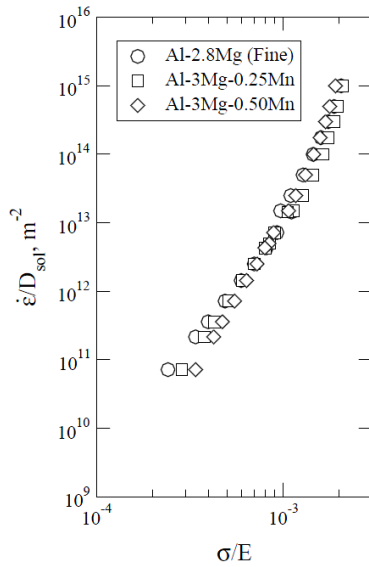


Figure 4.4: The logarithm of diffusivity-compensated strain rate versus the logarithm of modulus-compensated stress. Figure from Ref [25].

The specimen geometry from the present investigation is compared to the specimen geometry used in Ueki’s investigation in Table 4.2. The AA5083 alloy used in Ueki’s investigation has a larger OD and a similar gauge length to the FSA samples.

Table 4.2: Specimen geometry comparison between the FSA alloy and AA5083 alloy.

	OD (mm)	ID (mm)	Gauge Length (mm)	ID/OD
FSA Alloy	8.33	6.35	12.7	0.762
AA5083 Alloy	18	10	15	0.556

4.2.2. Strain Rate and Test Temperature

Shear stress versus shear strain data from Ueki's investigation of AA5083 are presented in Figure 4.5. In his experiments, the shearing strain rate was held constant at 10 s^{-1} for tests at temperatures of 400°C , 450°C , and 500°C .

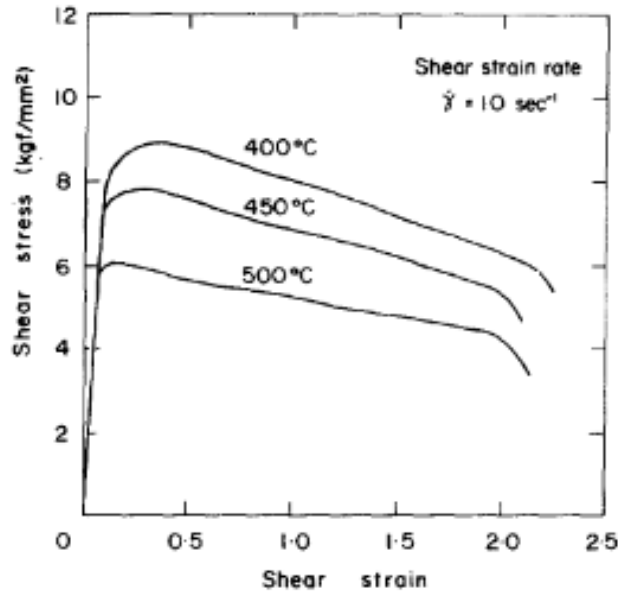


Figure 4.5: Shear stress versus shear strain for AA5083. Figure is from Ref. [23].

To replicate as closely as possible the shearing strain rates used in Ueki's investigation, Equation 8 is used,

$$\dot{\theta} = \frac{L\dot{\gamma}}{r} \quad (8)$$

where $\dot{\theta}$ is the rotational speed in $\text{radians}\cdot\text{s}^{-1}$, L is the length of the gauge section, $\dot{\gamma}$ is the shearing strain rate, and r is the radius within the gauge length. Using the specimen geometry in the present investigation and setting $\dot{\gamma}$ to be 10s^{-1} , the equivalent rotational

speed ($\dot{\theta}$) is calculated to be 30.5 radians*s⁻¹(or 300 RPM). The rotational speed decreases slightly when the clutch is engaged. For this reason, a speed of 500 RPM was selected for testing. It was later discovered that this slight increase in speed is unnecessary.

4.3. DATA ANALYSIS

4.3.1. Torque vs. Rotational Displacement

Two tests were performed at elevated temperatures using Al-4.5Mg specimens. Figure 4.6 presents raw data from tests performed at 460°C and 475°C. These tests were conducted at a constant shear strain rate of 15 s⁻¹ using specimen design 2 (the specimen design with the 0.5 inch gauge length). As the temperature is increased, the torque required to deform the specimen is decreased. This relationship is confirmed by Equation 9,

$$\sigma_f = C \left[\dot{\epsilon} \exp\left(\frac{Q}{RT}\right) \right]^{\frac{1}{n}} \quad (9)$$

where σ_f is the flow stress, C is a material-dependent constant, $\dot{\epsilon}$ is the effective strain rate, Q is the activation energy for plastic flow, R is the universal gas constant, T is the temperature, and n is the stress exponent. Temperature is directly related to the flow stress. As the temperature increases, the stress to deform the material at a constant strain rate decreases. The torque required to deform the specimen peaks initially and decreases as further deformation takes place.

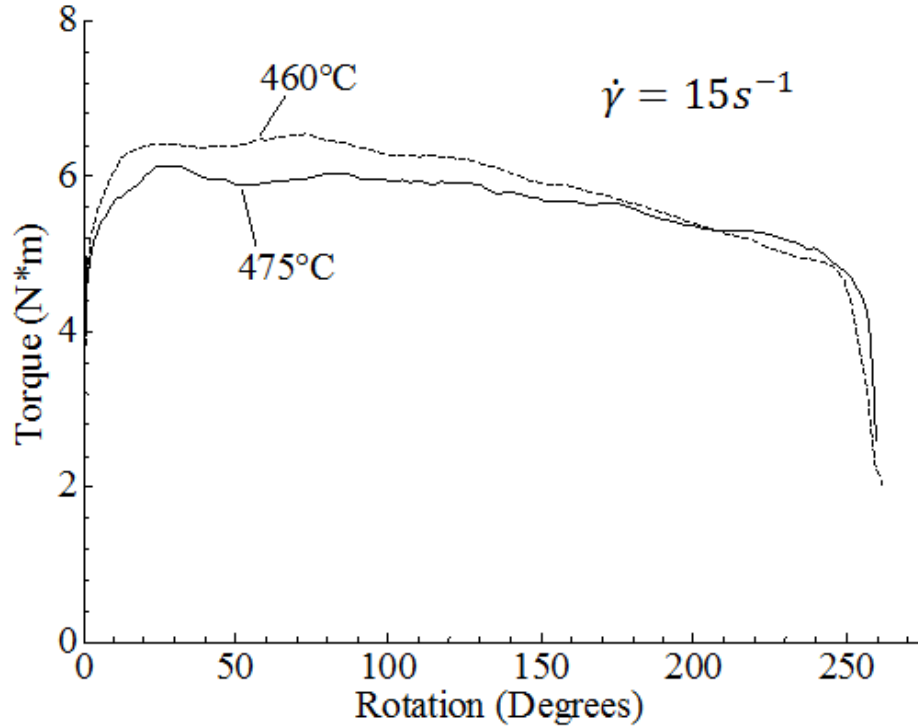


Figure 4.6: Torque versus rotational displacement at elevated temperature for the Al-4.5Mg material.

4.3.2. Shear Stress vs. Shear Strain

The data from each test were saved in a text file that includes torque (in*lbs) and rotational displacement (degrees) as functions of time. The torque was converted to a shear stress using Equation 10,

$$\tau = \frac{Tr}{J} \quad (10)$$

where τ is the shear stress, T is the torque, r is the outer radius of the specimen gauge section, and J is the polar moment of inertia. Shear stress values are typically taken at the outer surface of the specimen [12]. This standard was implemented in the current

investigation. The rotational displacement is converted to a shear strain by using Equation 11,

$$\gamma = \frac{r\theta}{L} \quad (11)$$

where γ is the shear strain, r is the outer radius of the specimen gauge section, θ is the rotational displacement in radians, and L is the gauge length. Similarly to shear stress measurements, the shear strain measurements were taken at the outer surface of the specimen. Taking stress-strain measurements at a specimen's surface is the most commonly used method and is the ASM handbook recommendation [12].

Shear stress and shear strain data taken from Ueki's investigation of AA5083 use mean stress-strain measurements [23]. It is important to note that mean stress-strain measurements are not commonly used in torsion testing investigations. The mean shear stress in Ueki's investigation was calculated using Equation 12,

$$\tau = \frac{12}{\pi(D_1^3 - D_2^3)} T \quad (12)$$

where τ is the mean shear stress, D_1 is the outer diameter, D_2 is the inner diameter, and T is the torque. The mean shear strain in Ueki's investigation was calculated using Equation 13,

$$\gamma = \frac{D_1 + D_2}{4L} \varphi \quad (13)$$

where γ is the mean shear strain, D_1 is the outer diameter, D_2 is the inner diameter, L is the gauge length, and φ is the twist angle in radians.

4.3.2.1. Experiment Repeatability

Two tests were conducted on the Al-4.5Mg material at a temperature of 460°C and a strain rate of 15s^{-1} to test for experiment repeatability. The 0.5-inch specimen geometry was used. Figure 4.7 presents the results of these two tests on a plot of shear stress versus shear strain. As expected, the data demonstrate good repeatability. This proves that the torsion testing instrument is capable of accurately repeating experiments with constant test variables.

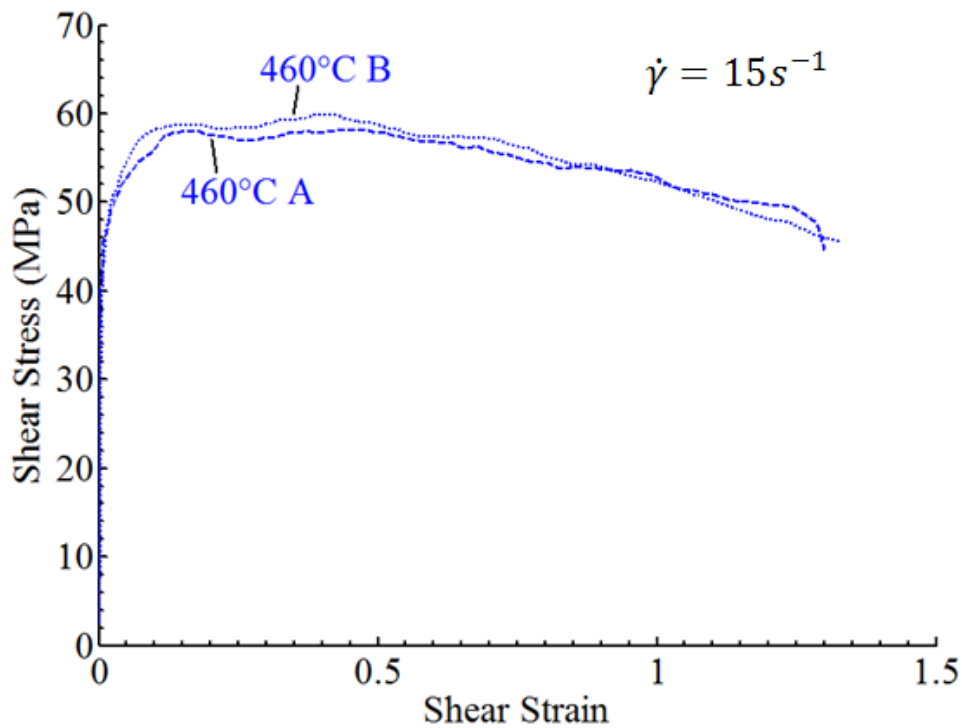


Figure 4.7: A plot of shear stress versus shear strain for the Al-4.5Mg material where $T = 460^\circ\text{C}$ and $\dot{\gamma} = 15\text{s}^{-1}$.

4.3.2.2. Literature Comparison

Figure 4.8 (a) shows the shear stress vs. shear strain results from three independent torsion experiments. Figure 4.8 (b) compares these same data from the torsion machine fabricated in this study with data taken from Ueki's investigation (marked Lit.). The torsion data were calculated for Figure 4.8 (b) using Ueki's mean stress and mean strain calculations in order to fairly compare these different data sets. Figure 4.8 (b) is the only plot where the stress-strain data are calculated as such mean values. As a result of this calculation, the flow stress is lowered by approximately 20%. The shape of the stress-strain data collected in this study is similar to the data found in the literature. In both cases, there is a rapid increase in the stress at the beginning of the test. The stress peaks at strains between 0.1 and 0.3, with the exception of one test from this study. After the peak stress is reached, the stress continues to decrease slightly as the specimen deforms plastically. The results of this study agree with this general trend found in the literature, proving the torsion instrument is capable of producing data similar to those in the literature.

However, the experimental data collected for the Al-4.5Mg material are slightly different in flow stress from the literature data, as is shown in Figure 4.8 (b). The tests conducted in this investigation show stress values approximately 35% lower than the available literature data. This may be attributed to the different materials used. Although the AA5038 alloy is similar to the Al-4.5Mg FSA alloy, it is still a different material. Small differences in chemical composition could be responsible for the higher strength exhibited by the AA5038 alloy. It is also important to note that the strain rates are slightly different between the experimental and literature data. A shearing strain rate of $15s^{-1}$

was used for experiments in this study while a shearing strain rate of $10s^{-1}$ was used in the literature tests. A higher strain rate should produce a higher shear strength. Despite the difference in material strength, this comparison with the data of Ueki *et al.* verifies that the torsion instrument produces data similar to those available in the literature.

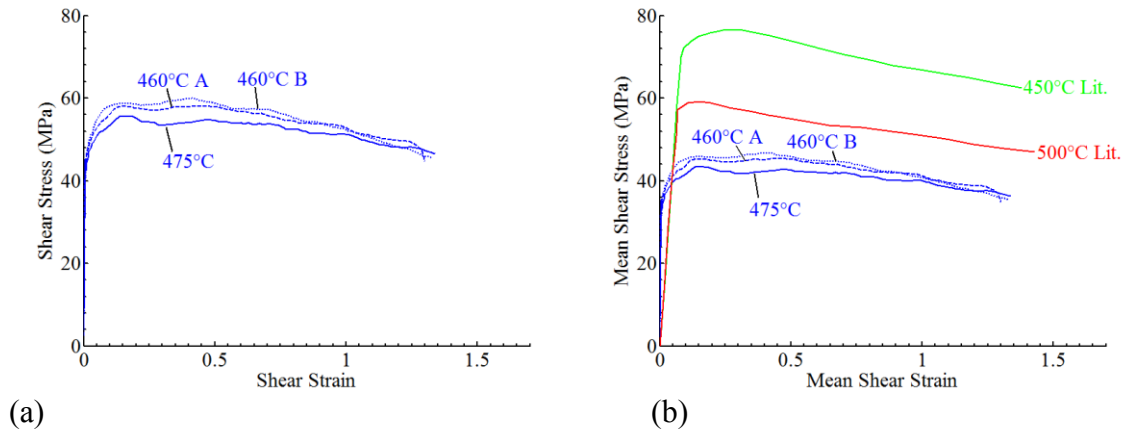


Figure 4.8: (a) Shear stress vs. shear strain for Al-4.5Mg (this study, where $\dot{\gamma} = 15s^{-1}$), (b) Mean shear stress vs. mean shear strain for Al-4.5Mg (this study, where $\dot{\gamma} = 15s^{-1}$) compared with AA5083 (literature, where $\dot{\gamma} = 10s^{-1}$). Literature data taken from Ref. [23].

4.4. Metallography

A primary goal of this task was to compare the microstructures of torsion specimens with microstructures from compression specimens tested under similar conditions (i.e. similar temperature, strain, and strain rate). The microstructures of the torsion specimens and compression specimens were generally expected to be similar, with the exception that compression specimens exhibit barrel distortion with very non-uniform strain distribution. Barrel distortion is created by friction between the dies and the specimen surfaces in contact with the dies. This creates “dead zone” areas, where

little deformation is observed, on the top and bottom of the specimen. As a result, deformation is greatest in the middle of the specimen. Microstructural comparisons between torsion specimens and compression specimens might give insight into the torsion instrument's capability to produce more uniform microstructures.

Prior to this investigation, compression tests were performed by Nippon Steel Corp. (now Nippon Steel & Sumitomo Metals Corp.) on Al-4.5Mg cylinders that were manufactured by Furukawa-Sky Aluminum Corp. (FSA). The cylinders used in those experiments had an initial diameter of 8 mm and an initial height of 12 mm. The specimens were compressed to a final height of 6 mm, producing a final engineering strain of -0.5. Tests were conducted at various temperatures and strain rates to observe the effects on microstructure. Two of these test cylinders are examined in the present investigation: (1) an Al-4.5Mg cylinder tested at 500°C at a strain rate of 1 s^{-1} and (2) an Al-4.5Mg cylinder tested at 400°C at a strain rate of 1 s^{-1} . Both specimens were quenched with helium at a rate of 20°C/second immediately after testing to preserve their microstructures.

An Al-4.5Mg specimen with a 1-inch gauge length was tested in torsion at a temperature of 450°C and a strain rate of 3.5 s^{-1} . This test was conducted to a final effective strain of 0.45, and the specimen was air quenched after deformation. The three specimens (two compression specimens, one torsion specimen) were prepared for microstructural examination. The compression specimens were also examined after annealing to allow for static recrystallization.

4.4.1. Specimen Mounting

4.4.1.1. Compression Specimens

Compression specimens were sectioned in half with a diamond abrasive saw. The specimens were mounted in transparent epoxy with their cross sections exposed. Figure 4.9 presents the sectioning and mounting process for the Al-4.5Mg compression specimens.

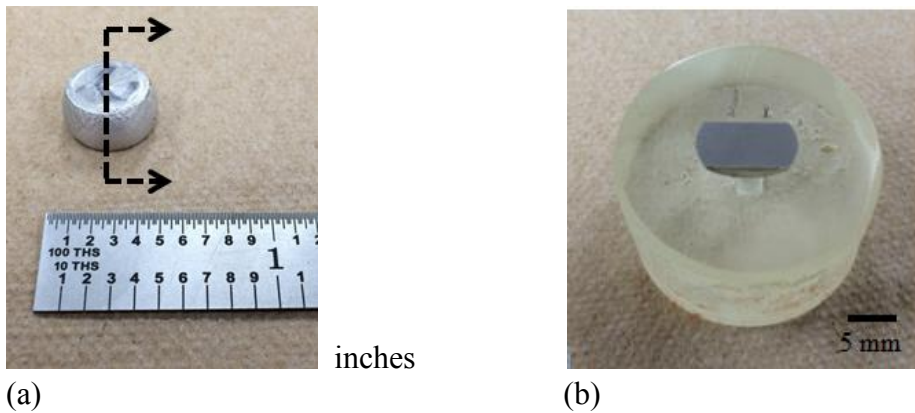


Figure 4.9: (a) Sectioning the Al-4.5Mg compression specimen, (b) Mounting the Al-4.5Mg compression specimen.

4.4.1.2. Torsion Specimen

The specimen tested in torsion is shown in Figure 4.10. A slight bend along the specimen's gauge section indicates some buckling during testing. This is common with long tubular specimens tested in torsion. Buckling can be prevented by decreasing the gauge length and increasing the gauge diameter. A section for metallography was taken from a region where buckling was not observed. This section is indicated by the dashed lines shown in Figure 4.10.

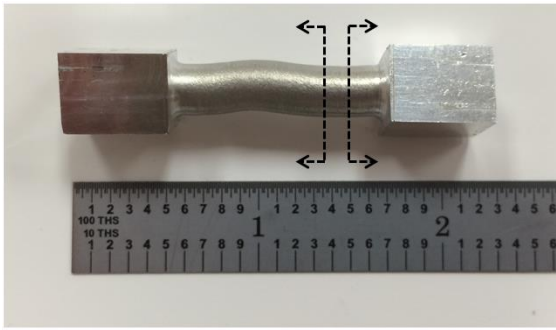
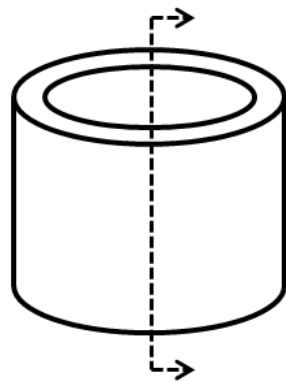
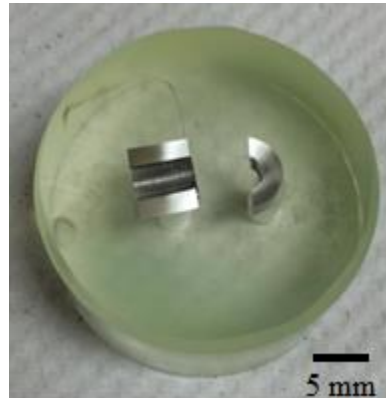


Figure 4.10: An Al-4.5Mg torsion specimen where buckling is observed. The specimen was tested at a temperature of 450°C and a strain rate of 3.5 s^{-1} to a final strain of 0.45.

After sectioning the tubular specimen, the extracted section was cut into two pieces, as indicated in Figure 4.11 (a). The two pieces were then mounted in a transparent epoxy and positioned to show the radial and axial cross sections, as presented in Figure 4.11 (b).



(a)



(b)

Figure 4.11: (a) Sectioning the extracted torsion specimen piece, (b) mounting the sectioned torsion specimen pieces.

4.4.2. Polishing Procedure

The specimen preparation procedure for metallographic examination is detailed in Table 4.3. All polishing steps up to the final polishing step used water-free suspensions with alcohol-based lubricant. Specimens were cleaned in an ultrasonic bath of ethanol between polishing steps to avoid contamination. The final polishing step used colloidal silica. Polishing during the final step was kept under 15 minutes to avoid undesired etching by the silica solution.

Table 4.3: Specimen preparation procedure for the Al-4.5Mg torsion and compression specimens.

Sectioning	Cut with diamond abrasive saw
Mounting	24-hour transparent epoxy (LECO)
Course Grinding	400 grit SiC paper + water, 300 RPM, 5 minutes 1200 grit SiC paper + water, 300 RPM, 3-5 minutes 15 μm diamond suspension, 200 RPM, 5 minutes 9 μm diamond suspension, 200 RPM, 5 minutes
Fine Grinding	3 μm diamond suspension, 150 RPM, 5 minutes 1 μm diamond suspension, 150 RPM, 5 minutes
Final Polishing	0.04 μm colloidal silica, 150 RPM, 5 minutes
Etching	Barker's reagent (1.8% HBF_4 in H_2O), 25 VDC, 2-3 minutes

4.4.3. Imaging

Multiple images were taken of each specimen using an optical polarizing microscope under 50x magnification. These images were stitched together using GIMP [26] to form full mosaics of each specimen cross section. A sensitive tint (λ plate) was used to reveal the microstructure in color.

4.4.3.1. Compression Specimens

The center of the compression specimen tested at a temperature of 500°C and strain rate of 1 s^{-1} is shown in Figure 4.12 (a). A highly deformed microstructure is observed at the center of the specimen with small (20 to 40 μm) equiaxed grains appearing at grain boundaries. This suggests partial recrystallization either during or after testing. The bottom edge of the specimen is shown in Figure 4.12 (b). In this figure, large equiaxed grains are observed. This region is known as the “dead zone”, where die friction impeded deformation from occurring at the top center and bottom center of the specimen.

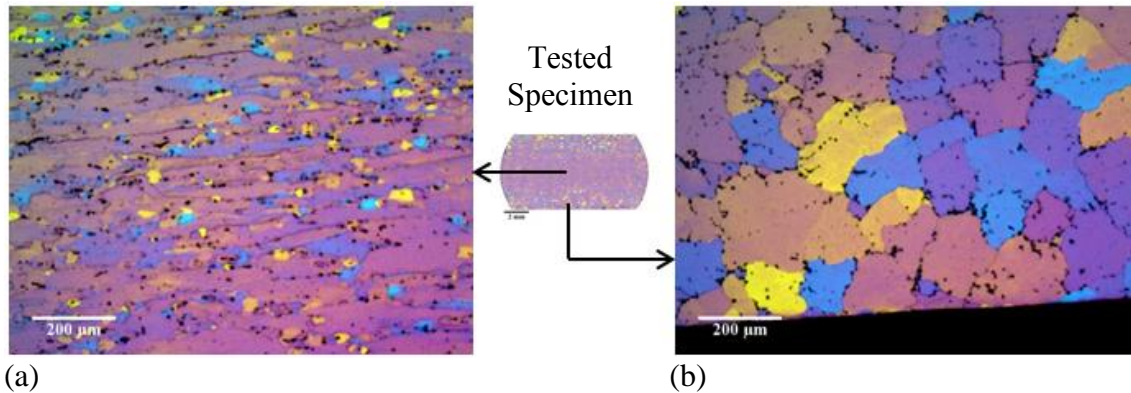


Figure 4.12: Al-4.5Mg material tested in compression at a temperature of 500°C, strain rate of 1 s^{-1} , to a final strain of 0.5. (a) Grain morphology at the middle-center of the specimen; (b) Grain morphology at the bottom-center of the specimen.

Microstructure images of the specimen tested at a temperature of 400°C and strain rate of 1 s^{-1} are presented in Figure 4.13. The specimen’s center, shown in Figure 4.13 (a), has a highly deformed microstructure with no signs of recrystallization when observed at low magnification. However, upon closer examination, small (4 to 10 μm) equiaxed grains are observed in the deformed microstructure. These grains are shown in Figure

4.14 and are marked with arrows. This suggests partial recrystallization in the specimen tested at a temperature of 400°C. Figure 4.13 (b) shows the bottom of the specimen with large, equiaxed grains.

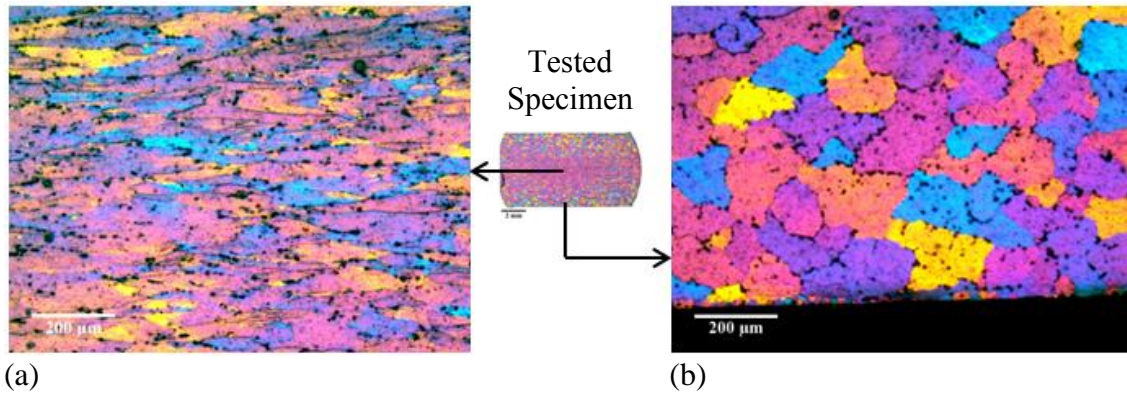


Figure 4.13: Al-4.5Mg material tested in compression at a temperature of 400°C, strain rate of 1 s^{-1} , to a final strain of 0.5. (a) Grain morphology at the middle-center of the specimen; (b) Grain morphology at the bottom-center of the specimen.

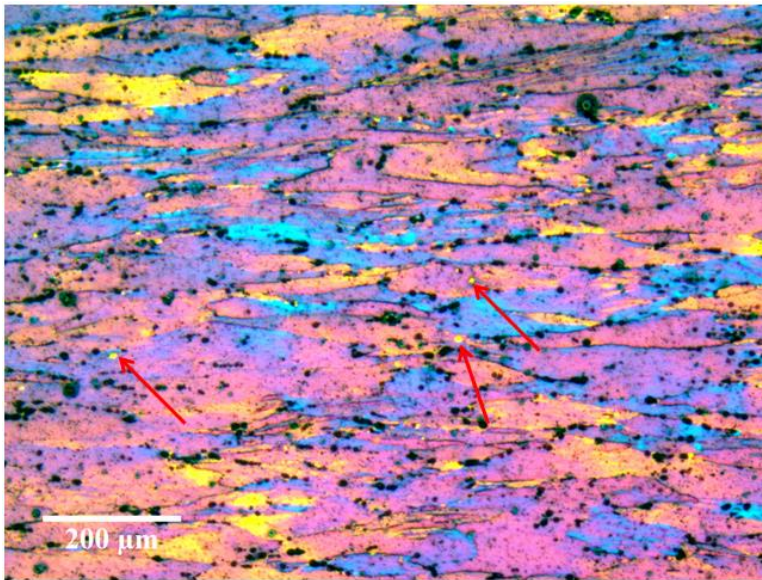


Figure 4.14: Al-4.5Mg material tested in compression at a temperature of 400°C, strain rate of 1 s^{-1} , to a final strain of 0.5. The figure shows a magnified middle center view showing small equiaxed grains marked with arrows.

4.4.3.2. Torsion Specimen

Figure 4.15 presents the microstructures of both section views for the Al-4.5Mg torsion specimen. The test was conducted at a temperature of 450°C, at a strain rate of 3.5 s^{-1} , and to a final strain of 0.45. Both views of the torsion specimen show equiaxed grains with no visible signs of deformation. This indicates that the material recrystallized. Importantly, the microstructure produced by torsion testing is quite uniform. The only exception is at the exterior surface of the specimen, shallow surface deformation during machining likely reduced the recrystallized grain size. To obtain a better understanding of the recrystallization process in the torsion specimen, both compression specimens were subjected to a 10 minute heat treatment at their respective test temperatures to induce recrystallization.

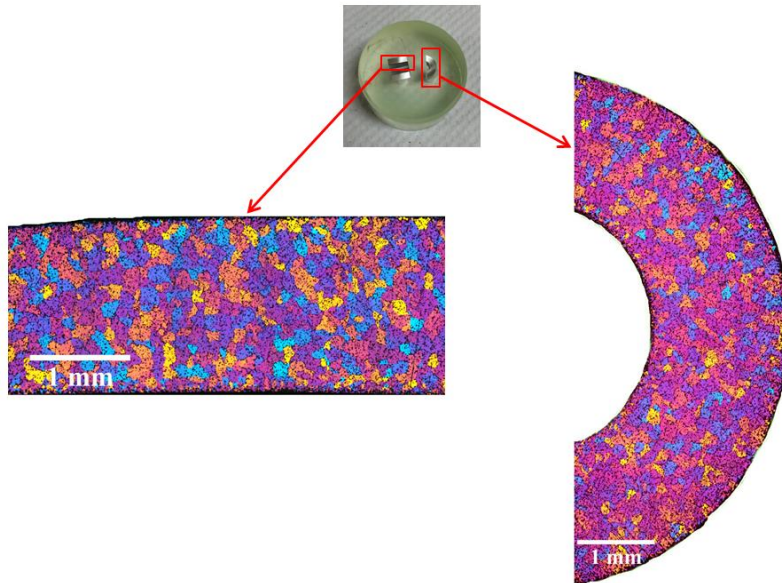


Figure 4.15: Mosaic images of the Al-4.5Mg torsion specimen cross sections. This specimen was tested in torsion at 450°C, a strain rate of 1 s^{-1} , to a final strain of 0.45.

4.4.4. Heat Treating the Compression Specimens

The two Al-4.5Mg compression specimens underwent a 10 minute heat treatment at their respective test temperatures. The compression specimen tested at 500°C was annealed for 10 minutes at 500°C, while the compression specimen tested at 400°C was annealed for 10 minutes at 400°C. Heat treatments were performed using a salt bath. The resulting microstructures are presented in Figure 16. A fully recrystallized microstructure is observed in both compression specimens.

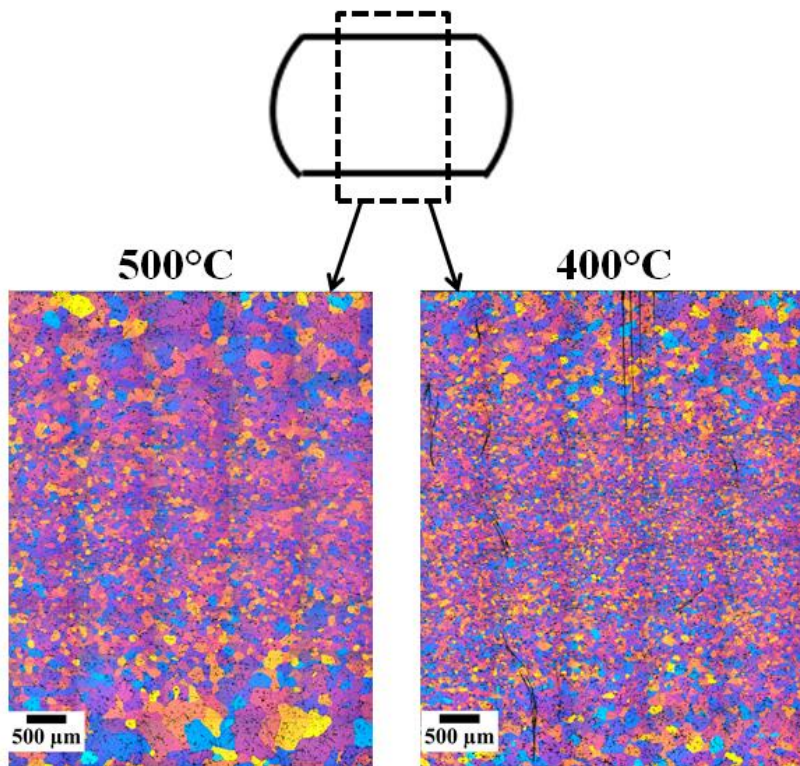


Figure 4.16: Al-4.5Mg compression specimen microstructures following a 10 minute heat treatment. The left image indicates the specimen originally tested in compression at a temperature of 500°C, strain rate of 1 s^{-1} , to a final strain of 0.5. The right image indicates the specimen originally tested in compression at a temperature of 400°C, strain rate of 1 s^{-1} , to a final strain of 0.5.

Table 4.4 compares the average grain size of the torsion specimen with the average grain size at the center of the compression specimens after a 10 minute heat treatment. The grains in the torsion experiment are approximately twice the size of the grains observed at the center of the compression specimen tested at 500°C, and approximately four times the size of the grains observed at the center of the compression specimen tested at 400°C. The larger grain size observed in the torsion specimen may be partially attributed to less accurate temperature control during the torsion test. Testing at a higher temperature will produce larger grains. If the temperature recorded during the torsion test was lower than the actual test temperature, a larger grain size is expected.

Table 4.4: Comparing mean grain sizes between Al-4.5Mg compression specimens and Al-4.5Mg torsion specimens.

Deformation Mode	Temp (°C)	Stain Rate (s⁻¹)	Annealing Time (min)	Annealing Temp (°C)	Mean Grain Size (µm)	Grain Size Error (µm)	Aspect Ratio
Compression	500	1	10 min	500	67	4	1.06
Compression	400	1	10 min	400	46	5	1.03
Torsion	450	3.5	N/A	N/A	168	18	1.01

The cooling time for the torsion specimen was also somewhat slow in comparison to the fast helium quench of the compression specimens. A slower cooling rate gives more time for static recrystallization and grain growth, thus producing a microstructure with larger grains. A means for faster quenching is needed before a more meaningful comparison can be made between specimens tested in torsion and specimens tested in compression.

There is one more possible reason for the larger recrystallized grain size in the torsion specimen compared to the center of the compression specimens. A result of the large “dead zones” produced by the compression geometry is localization of much plastic flow to the specimen center. Thus, the centers of the compression specimens likely have significantly larger effective strains than the torsion specimen. A larger plastic strain generally produces a finer recrystallized grain size. This is another possible reason for the finer recrystallized grain sizes at the center of the compression specimen than in the torsion specimen. Nevertheless, the uniform microstructure produced by the torsion testing demonstrates a clear advantage over the nonuniform microstructures produced by compression testing.

V. CONCLUSIONS AND FUTURE WORK

5.1. CONCLUDING REMARKS

The research investigation presented in this study began by discussing the potential benefits of improving the hot rolling process for aluminum and its alloys. This prompted the design and fabrication of a hot torsion testing instrument. A series of tests was conducted in this investigation to confirm the functionality of the instrument. The instrument will be used in future investigations to aid in the understanding of microstructure evolution during hot deformation.

After the instrument was constructed, its functionality was evaluated. The rotary encoder and tachometer were used to confirm the rotational speed during testing. Results showed a consistent speed reading from both devices and confirmed the accuracy of the measured rotational speed while testing. Another test was conducted to confirm the timing synchronization between the torque cell and rotary encoder. It is crucial that these devices be synchronized so that meaningful stress-strain data are generated. The test results confirmed the synchronization between these two devices. Two experiments were conducted at identical strain rates and temperatures to check experiment repeatability. The tests confirmed that the instrument is capable of accurately repeating experiments conducted with similar testing conditions.

A test was performed to compare data from the torsion testing apparatus with data available from literature. The torsion instrument generated data similar to the data from the literature source, further proving the instrument's reliability.

Microstructures of torsion specimens were compared with microstructures from compression specimens tested under similar conditions. A fully recrystallized microstructure was observed in the Al-4.5Mg torsion specimen tested at a temperature of 450°C and a strain rate of 3.5 s⁻¹. The torsion test produced a generally uniform microstructure through the thickness of the cylindrical specimen, as was desired. This microstructure was compared to compression specimens of the same material tested under similar conditions. The compression specimens were annealed for 10 minutes to produce fully recrystallized microstructures at their centers, where deformation was localized. Results showed a larger recrystallized grain size for the torsion specimen in comparison to the compression specimens. It was concluded that a faster quenching rate is necessary in torsion tests to avoid static recrystallization.

5.2. FUTURE WORK

5.2.1. Data Acquisition

The current data acquisition setup uses two computers: one computer is used to generate a clock signal while a second computer is used to acquire data from the instrument. This is primarily because of timing synchronization limitations in the NI USB 6210 DAQ boards currently being used. It is a future goal to have both the clock signal and data acquisition on one DAQ board and use only one computer.

One potential solution involves purchasing a more robust DAQ board. National Instrument's NI USB 6225 DAQ board is capable of performing on-board timing for both

digital and analog inputs. This allows for timing synchronization between all digital and analog inputs active while testing, thus eliminating the need for two computers.

5.2.2. Gas Quenching

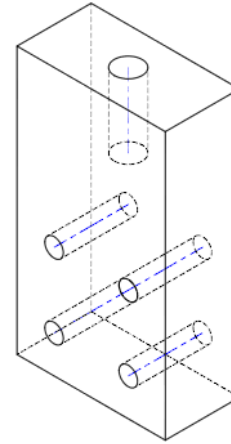
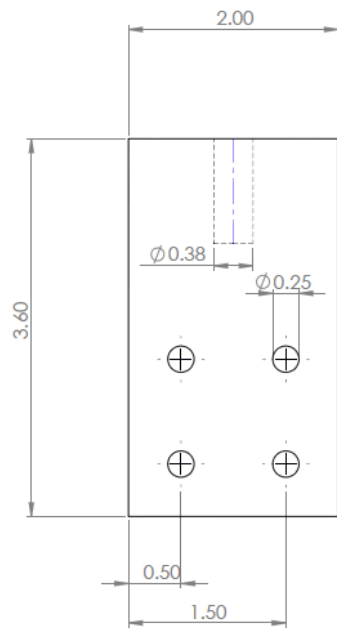
A means for more rapid quenching is needed to better preserve the unrecrystallized specimen microstructure after testing. In the current setup, compressed air is injected into the hollow shaft and through the specimen. To achieve more rapid cooling, an additional compressed air line should be added to the assembly. The air lines should be computer controlled through a solenoid valve, instead of manually controlled, to better provide cooling immediately at the end of the test, when the brake on the clutch/brake is applied. The outer air line should be directed at the specimen's gauge section to provide cooling to its outer surface. Another option for increasing the specimen cooling rate involves the use of helium gas for quenching. Helium is an inert gas with a high thermal conductivity, making it an excellent option for quenching.

5.2.3. Instrument Modifications

The addition of a second bearing is recommended in the middle section (the section with the annular fins and rotary encoder) of the torsion machine. A second bearing will help prevent unwanted shaft whirl during testing and improve instrument alignment. A high-temperature bearing is recommended as this bearing would be close to the radiant furnace.

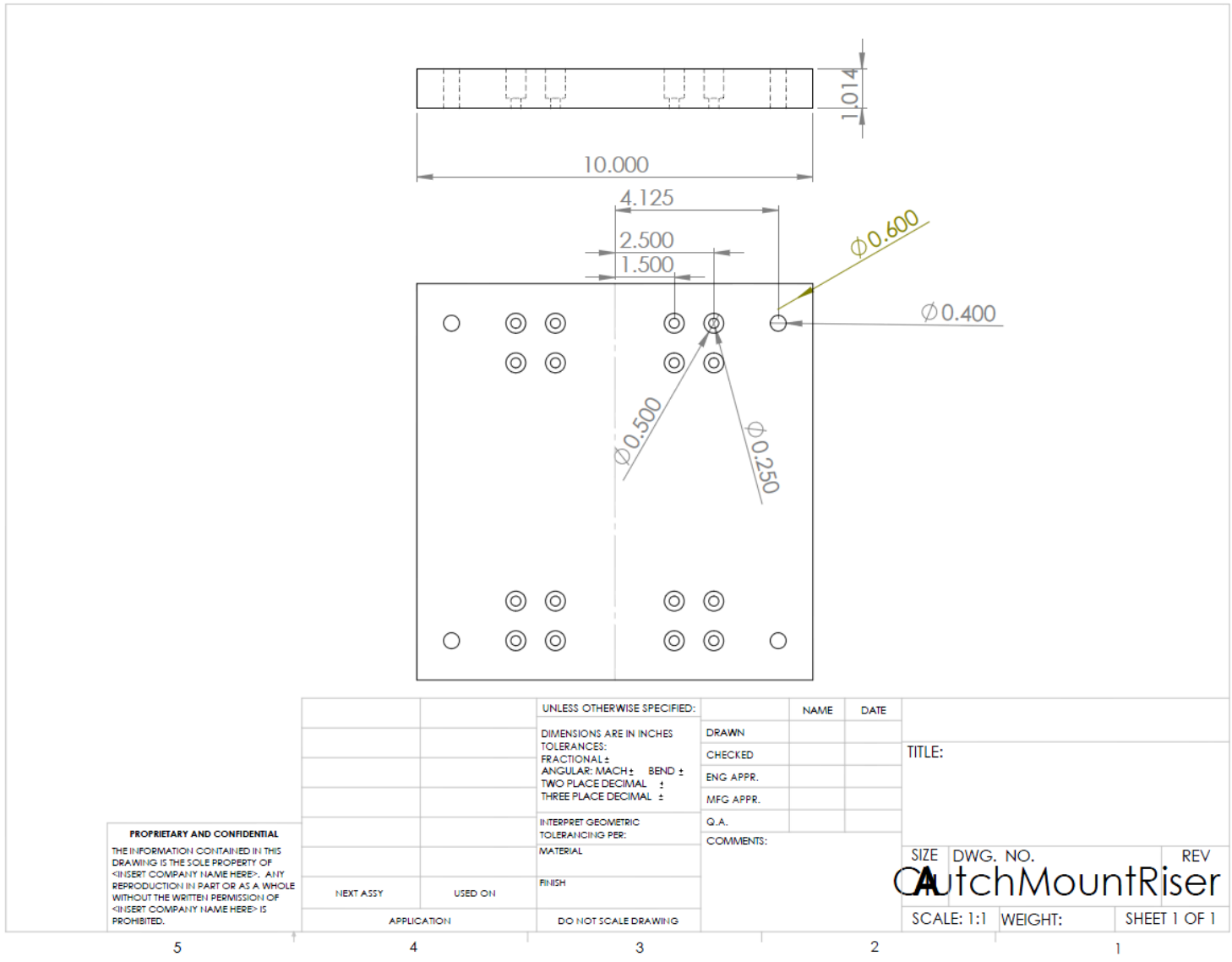
Appendix A: Technical Drawings

Bearing Support Block



UNLESS OTHERWISE SPECIFIED: DIMENSIONS ARE IN MILLIMETERS SURFACE FINISH: TOLERANCES: LINEAR: ANGULAR:				FINISH:	DEBUR AND BREAK SHARP EDGES	DO NOT SCALE DRAWING	REVISION
DRAWN	NAME	SIGNATURE	DATE			TITLE:	
CHK'D							
APP'VD							
MFG							
Q.A.					MATERIAL:	DWG NO:	Bearingsupport
							A3
					WEIGHT:	SCALE:1:1	SHEET 1 OF 1

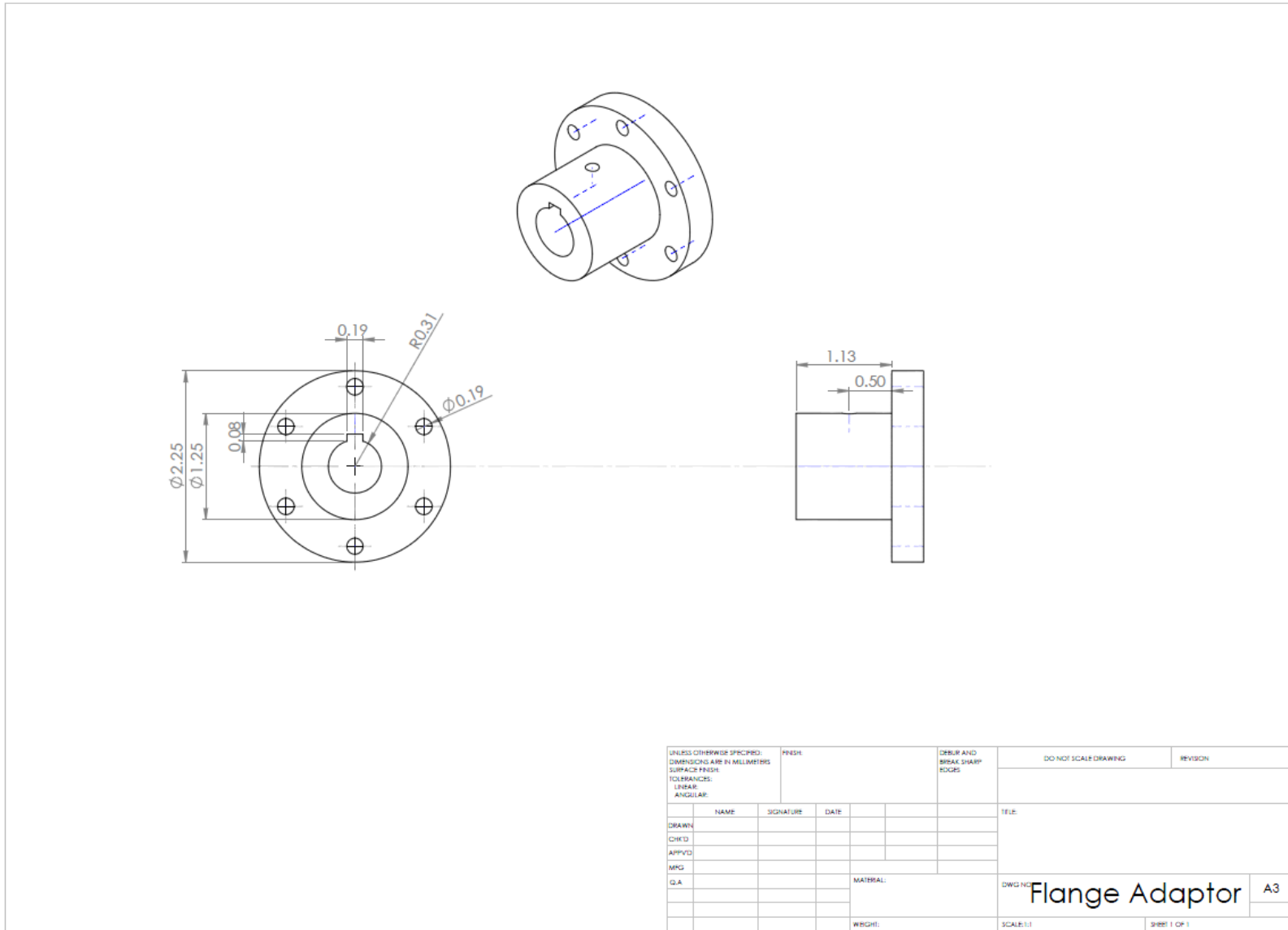
Clutch Riser Plate



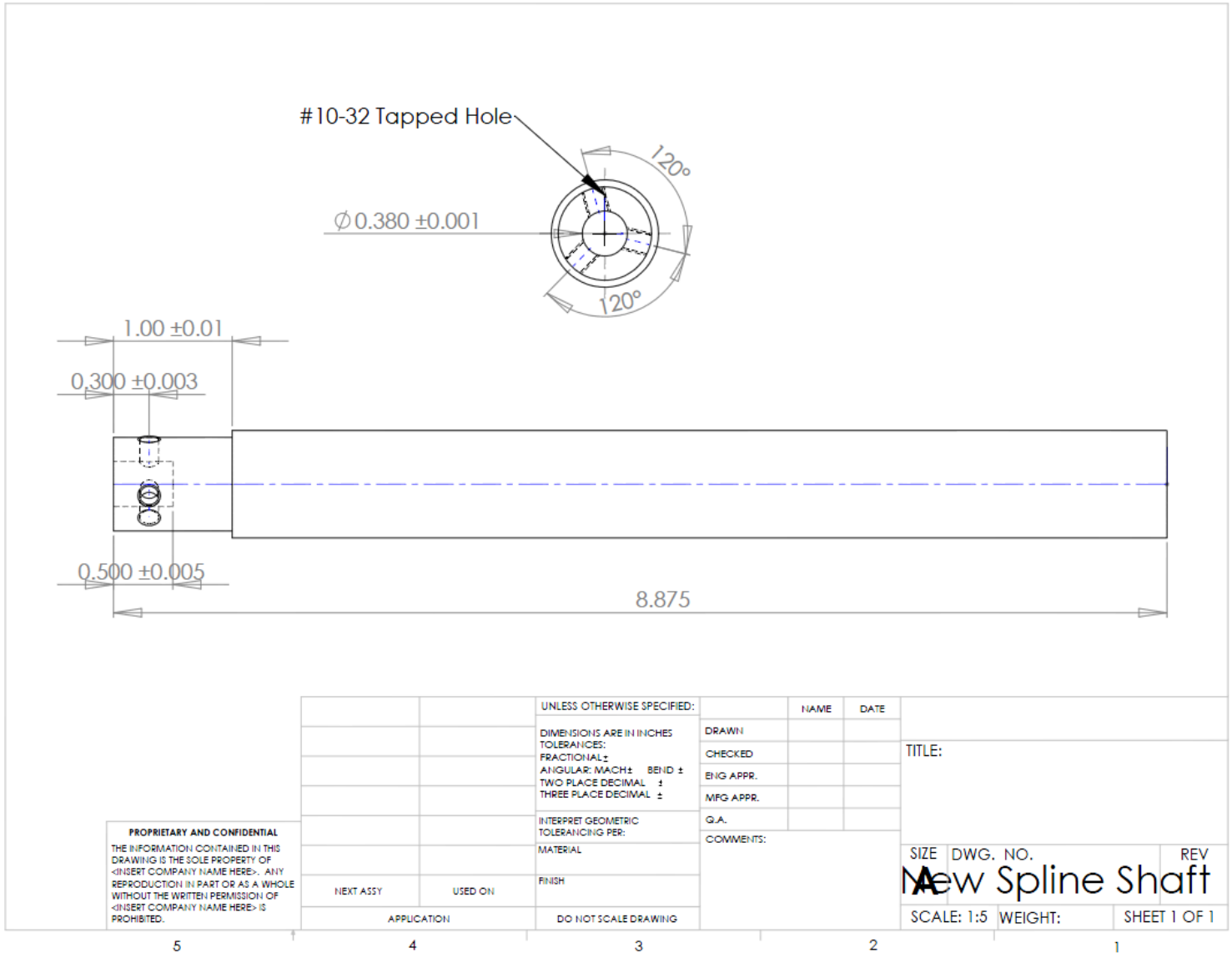
PROPRIETARY AND CONFIDENTIAL
 THE INFORMATION CONTAINED IN THIS DRAWING IS THE SOLE PROPERTY OF <INSERT COMPANY NAME HERE>. ANY REPRODUCTION IN PART OR AS A WHOLE WITHOUT THE WRITTEN PERMISSION OF <INSERT COMPANY NAME HERE> IS PROHIBITED.

		UNLESS OTHERWISE SPECIFIED:		NAME	DATE		
		DIMENSIONS ARE IN INCHES	DRAWN			TITLE:	
		TOLERANCES:	CHECKED				
		FRACTIONAL ±	ENG APPR.				
		ANGULAR: MACH ± BEND ±	MFG APPR.				
		TWO PLACE DECIMAL ±	Q.A.				
		THREE PLACE DECIMAL ±	COMMENTS:			SIZE	
		INTERPRET GEOMETRIC				DWG. NO.	
		TOLERANCING PER:				REV	
		MATERIAL				ClutchMountRiser	
		FINISH				SCALE: 1:1	
		APPLICATION	DO NOT SCALE DRAWING			WEIGHT:	
						SHEET 1 OF 1	

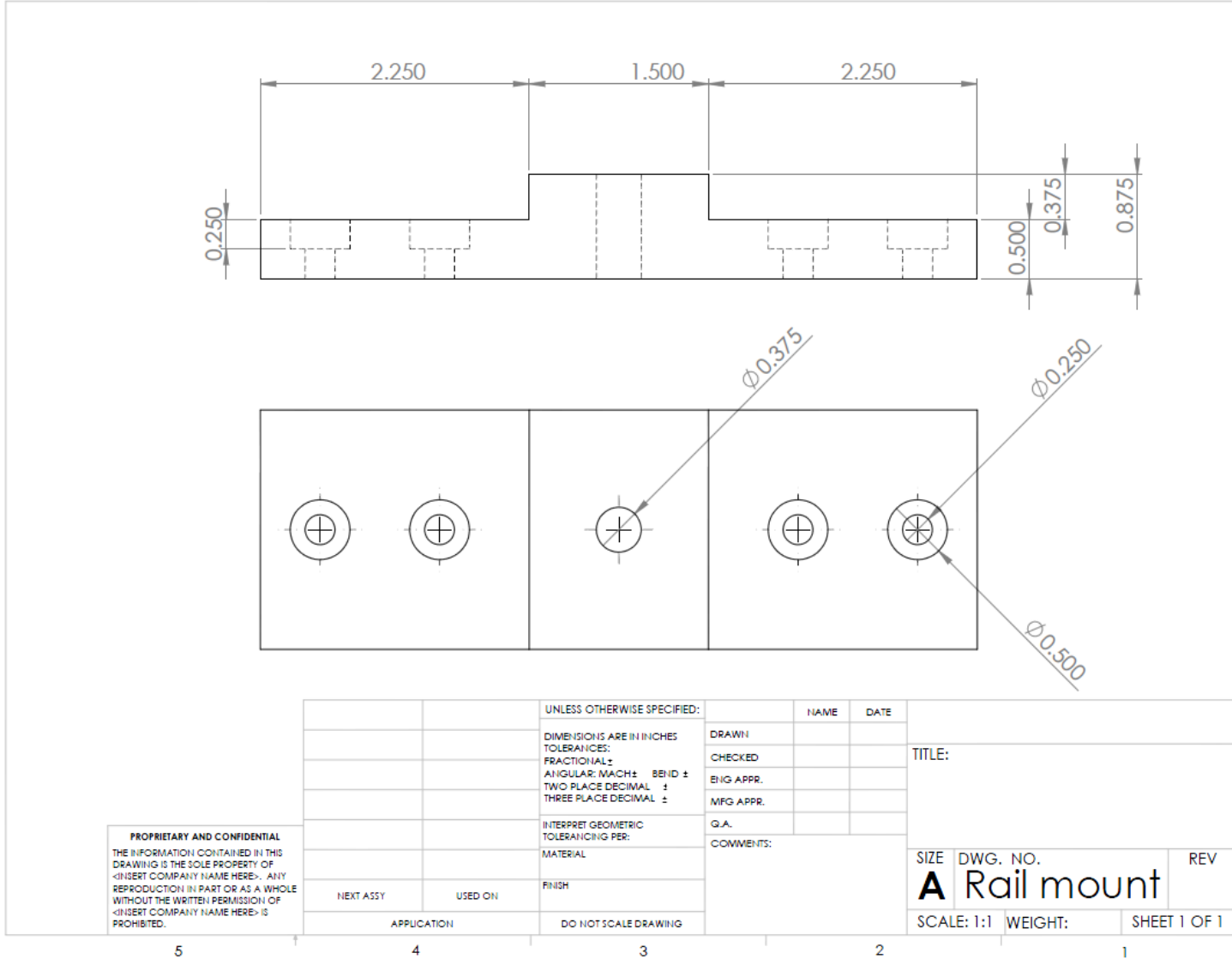
Flange Adaptor



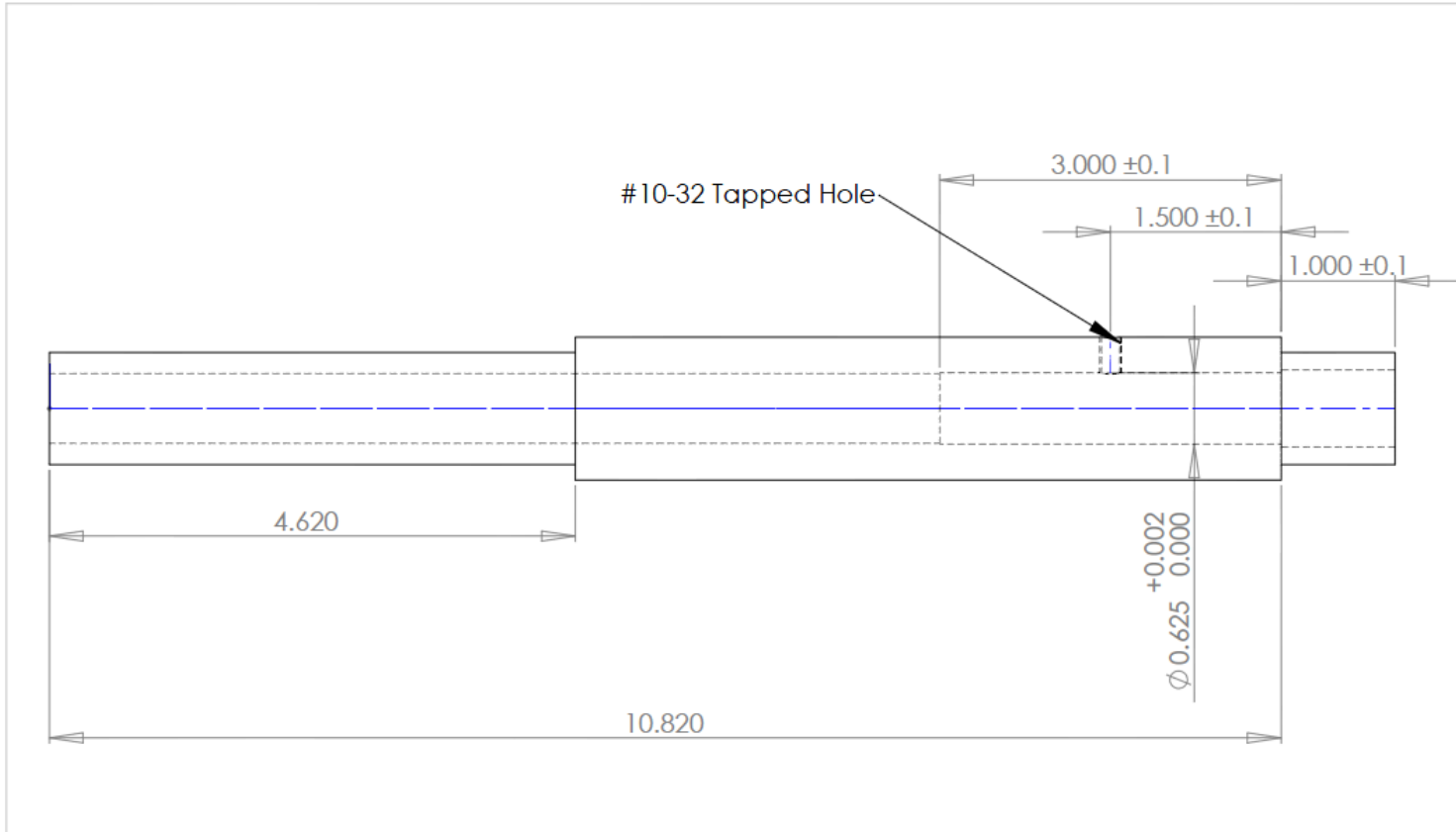
Spline Shaft



T-Block Rail Mount



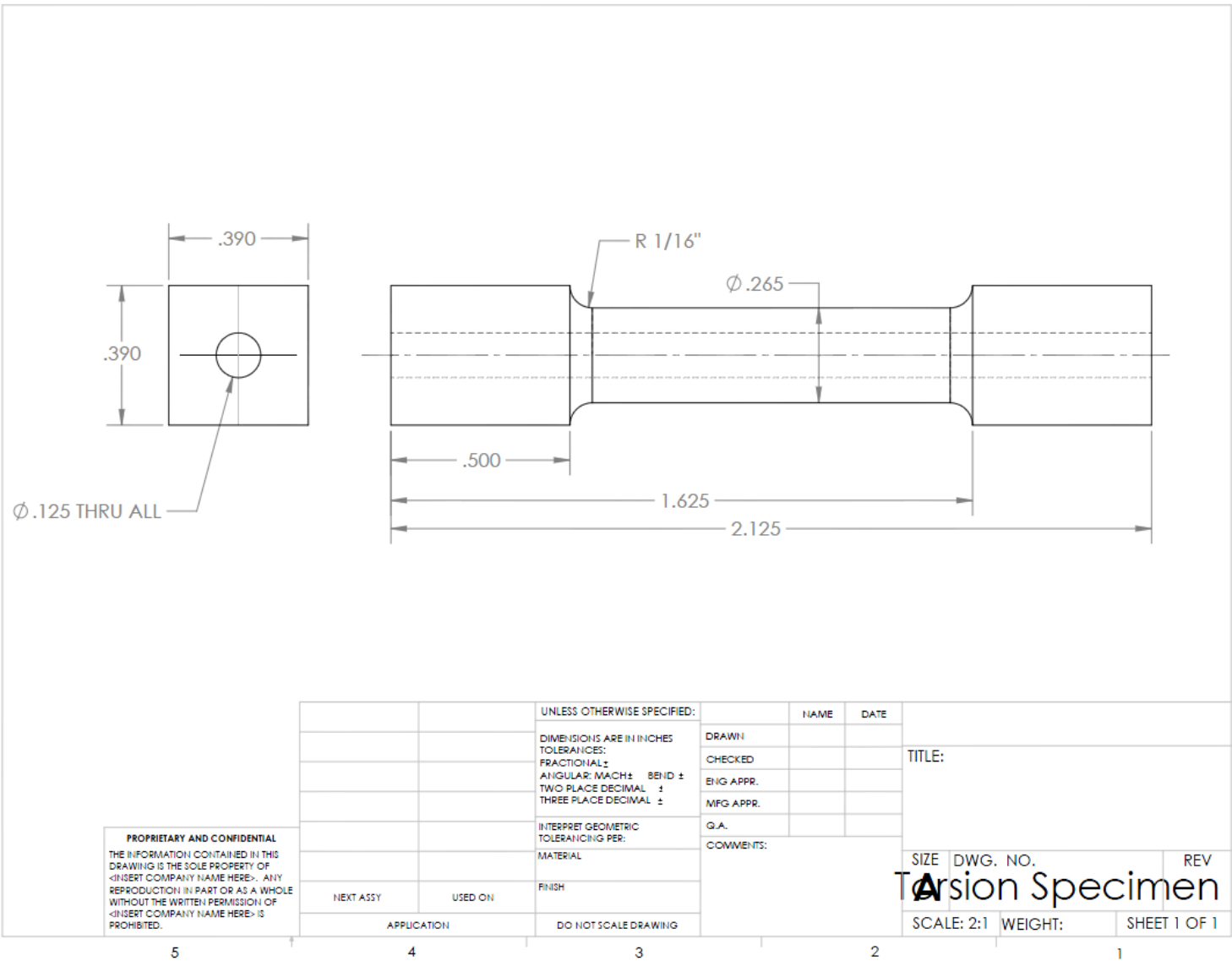
Spindle Shaft



PROPRIETARY AND CONFIDENTIAL
 THE INFORMATION CONTAINED IN THIS DRAWING IS THE SOLE PROPERTY OF <INSERT COMPANY NAME HERE>. ANY REPRODUCTION IN PART OR AS A WHOLE WITHOUT THE WRITTEN PERMISSION OF <INSERT COMPANY NAME HERE> IS PROHIBITED.

		UNLESS OTHERWISE SPECIFIED:		NAME	DATE		
		DIMENSIONS ARE IN INCHES		DRAWN		TITLE:	
		TOLERANCES:		CHECKED			
		FRACTIONAL ±		ENG APPR.			
		ANGULAR: MACH ± BEND ±		MFG APPR.			
		TWO PLACE DECIMAL ±		G.A.			
		THREE PLACE DECIMAL ±		COMMENTS:			
		INTERPRET GEOMETRIC TOLERANCING PER:					
		MATERIAL					
		FINISH					
NEXT ASSY	USED ON	APPLICATION		DO NOT SCALE DRAWING		SIZE DWG. NO.	REV
						A spindle shaft	
						SCALE: 1:5	WEIGHT:
						SHEET 1 OF 1	

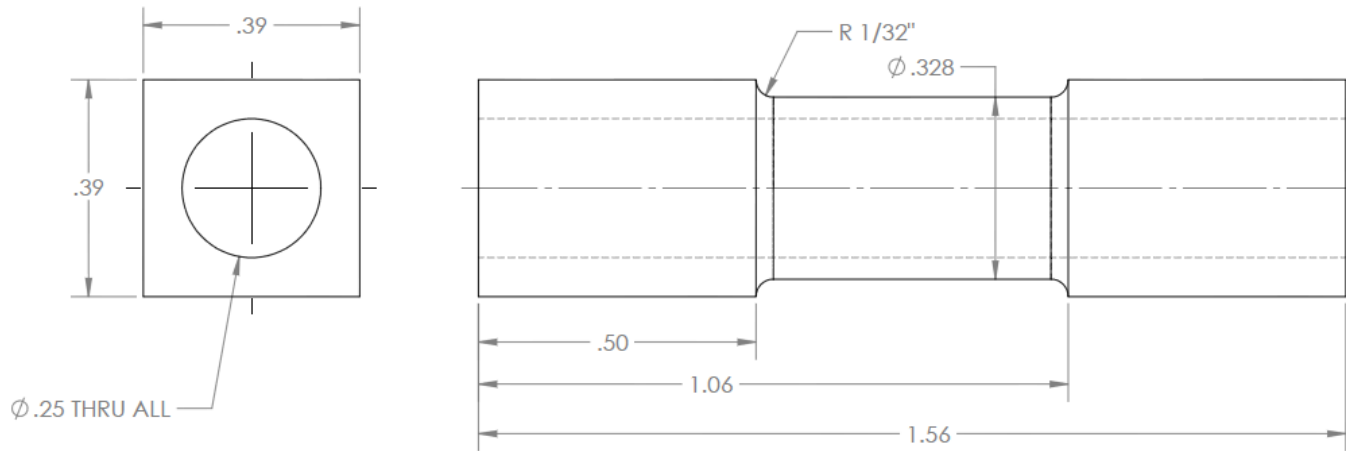
Torsion Specimen 1



PROPRIETARY AND CONFIDENTIAL
 THE INFORMATION CONTAINED IN THIS DRAWING IS THE SOLE PROPERTY OF <INSERT COMPANY NAME HERE>. ANY REPRODUCTION IN PART OR AS A WHOLE WITHOUT THE WRITTEN PERMISSION OF <INSERT COMPANY NAME HERE> IS PROHIBITED.

		UNLESS OTHERWISE SPECIFIED:	NAME	DATE	
		DIMENSIONS ARE IN INCHES	DRAWN		TITLE:
		TOLERANCES:	CHECKED		
		FRACTIONAL \pm	ENG APPR.		
		ANGULAR: MACH \pm BEND \pm	MFG APPR.		
		TWO PLACE DECIMAL \pm	G.A.		SIZE DWG. NO. REV
		THREE PLACE DECIMAL \pm	COMMENTS:		Torsion Specimen
		INTERPRET GEOMETRIC TOLERANCING PER:			SCALE: 2:1 WEIGHT: SHEET 1 OF 1
		MATERIAL			
NEXT ASSY	USED ON	FINISH			
APPLICATION		DO NOT SCALE DRAWING			

Torsion Specimen 2



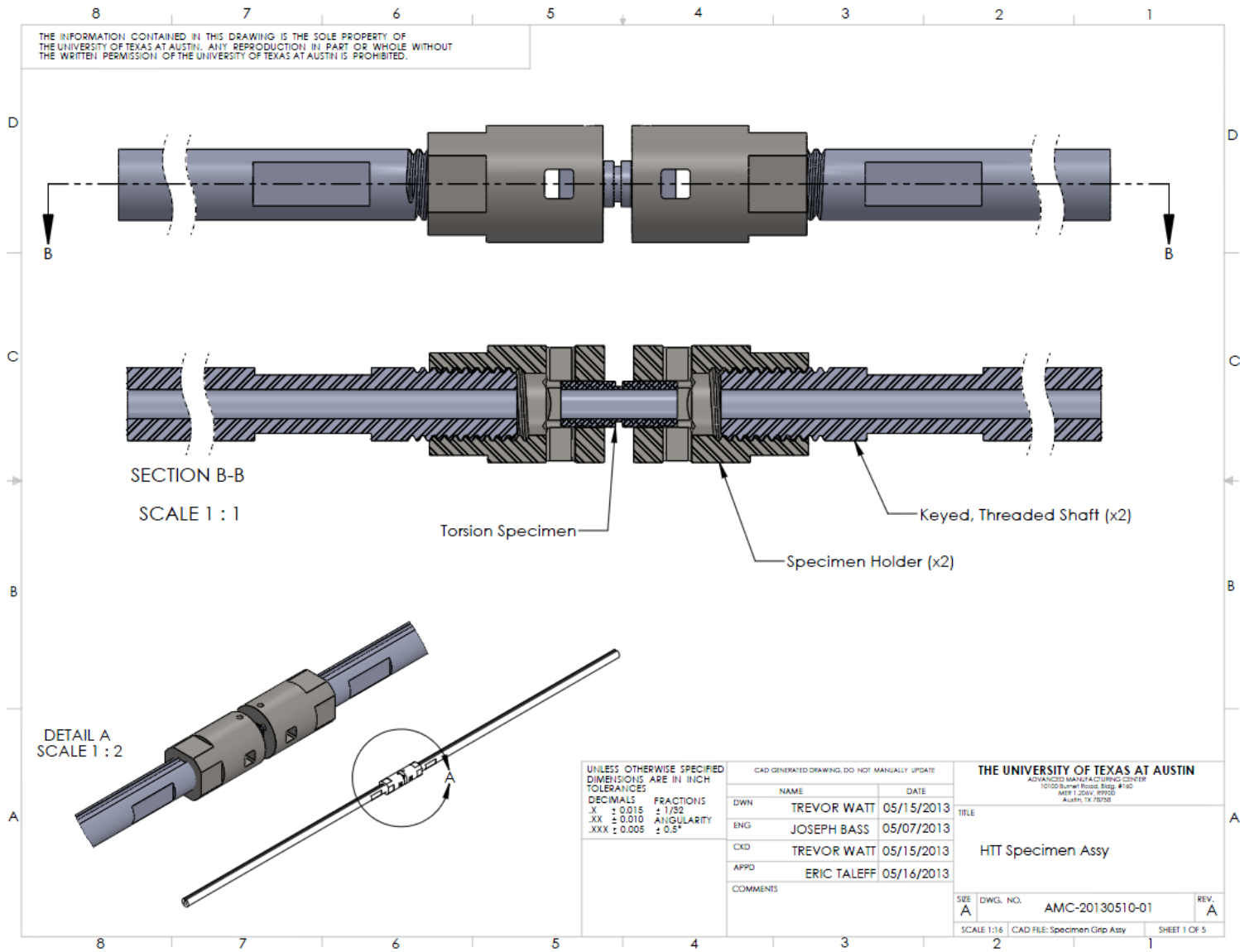
Ø .25 THRU ALL

PROPRIETARY AND CONFIDENTIAL
 THE INFORMATION CONTAINED IN THIS DRAWING IS THE SOLE PROPERTY OF <INSERT COMPANY NAME HERE>. ANY REPRODUCTION IN PART OR AS A WHOLE WITHOUT THE WRITTEN PERMISSION OF <INSERT COMPANY NAME HERE> IS PROHIBITED.

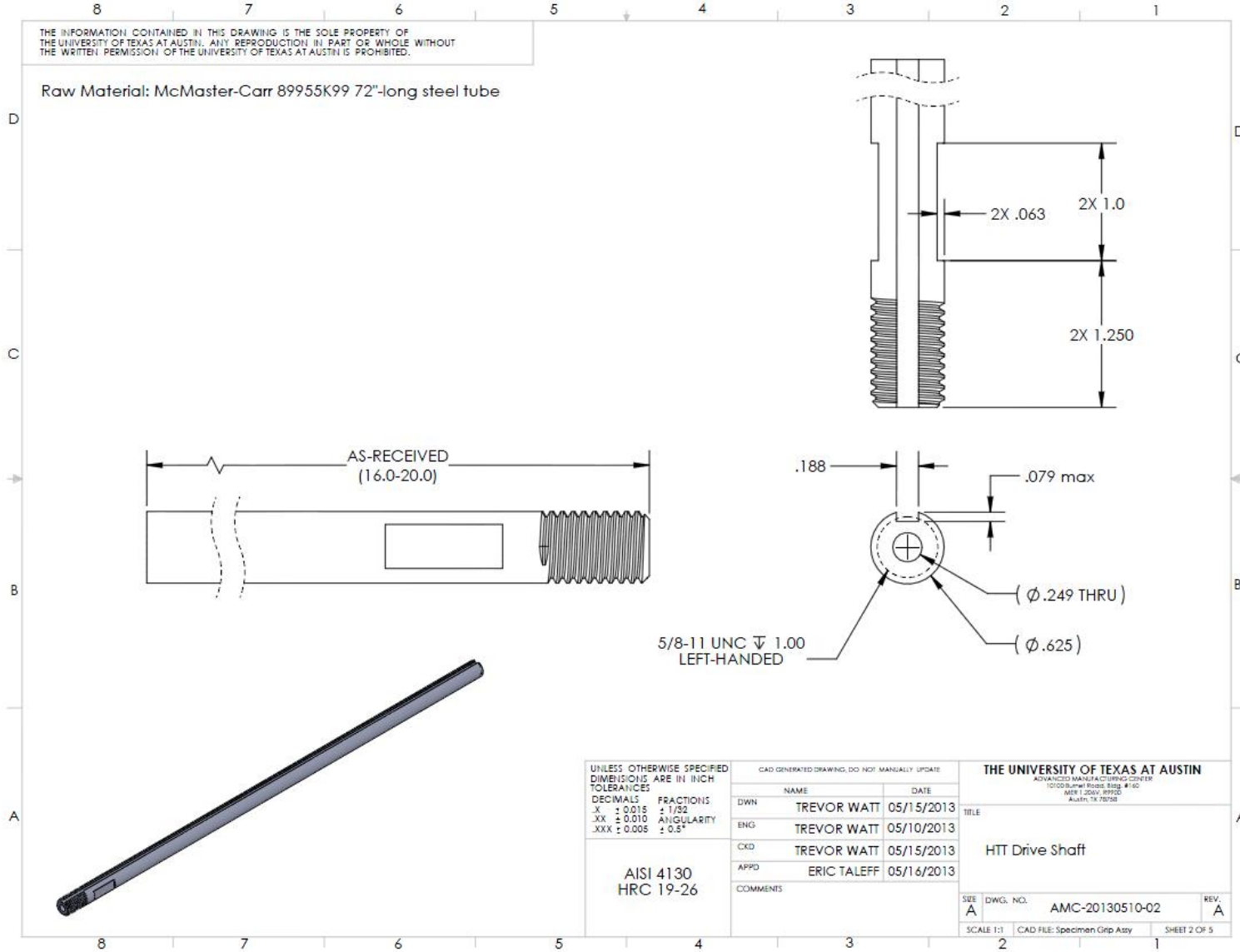
		UNLESS OTHERWISE SPECIFIED:		NAME	DATE	
		DIMENSIONS ARE IN INCHES	DRAWN			TITLE:
		TOLERANCES:	CHECKED			
		FRACTIONAL ±	ENG APPR.			
		ANGULAR: MACH ± BEND ±	MFG APPR.			
		TWO PLACE DECIMAL ±	Q.A.			
		THREE PLACE DECIMAL ±	COMMENTS:			
		INTERPRET GEOMETRIC TOLERANCING PER:				SIZE DWG. NO. REV
		MATERIAL				Torsion Specimen 2
		FINISH				SCALE: 2:1 WEIGHT: SHEET 1 OF 1
		APPLICATION				
		DO NOT SCALE DRAWING				
5	4	3	2	1		

Grip Assembly

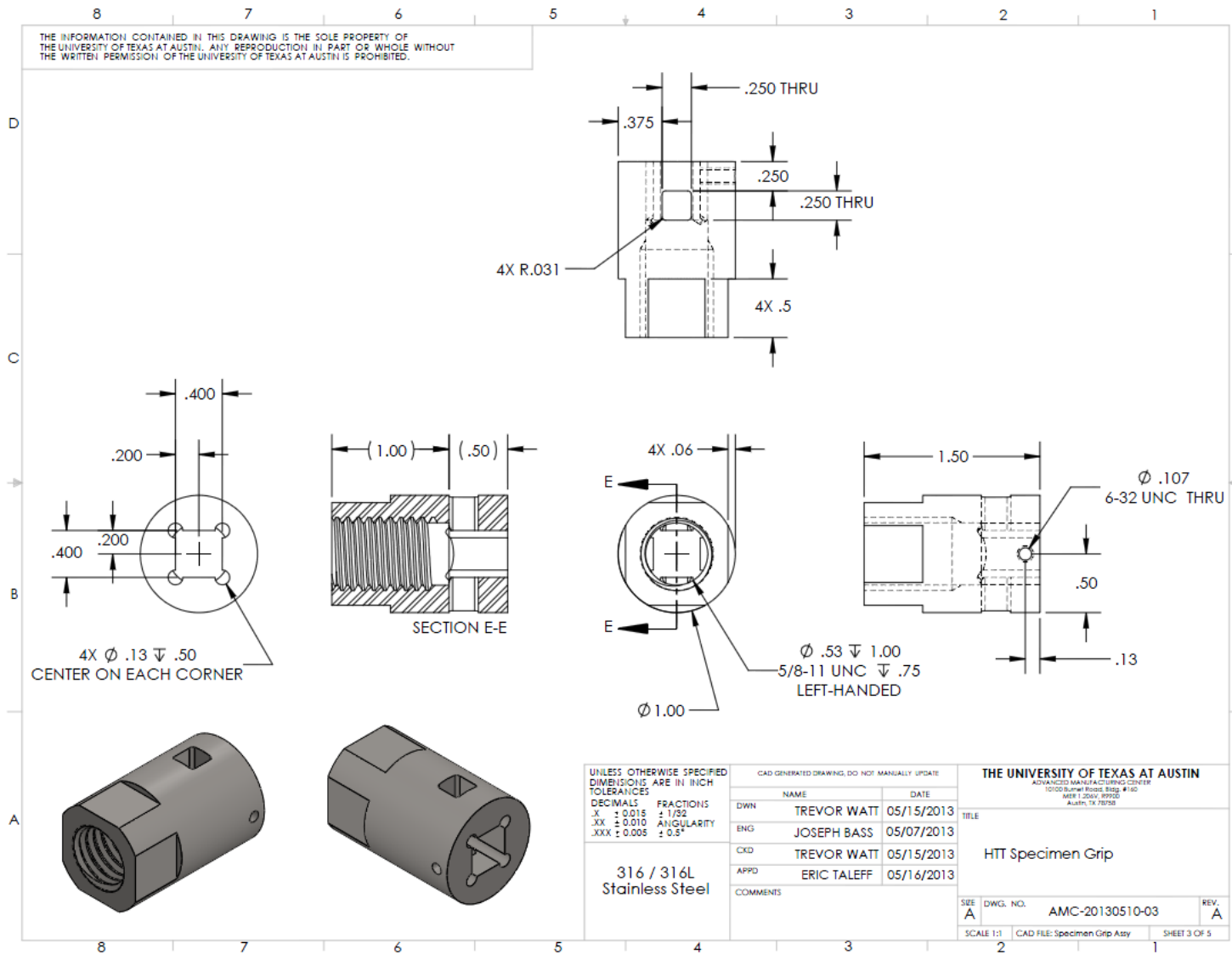
THE INFORMATION CONTAINED IN THIS DRAWING IS THE SOLE PROPERTY OF THE UNIVERSITY OF TEXAS AT AUSTIN. ANY REPRODUCTION IN PART OR WHOLE WITHOUT THE WRITTEN PERMISSION OF THE UNIVERSITY OF TEXAS AT AUSTIN IS PROHIBITED.



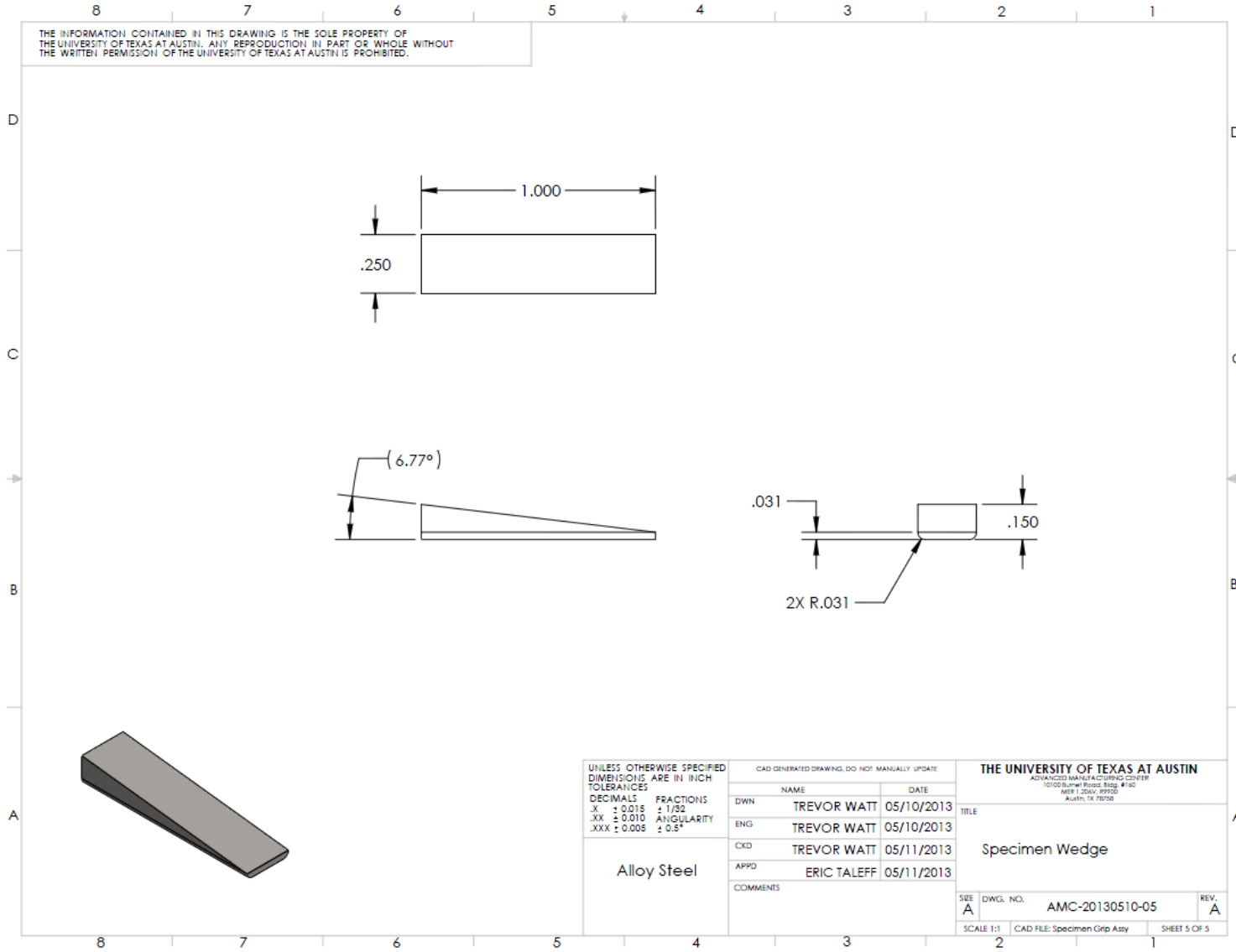
Drive Shaft



Specimen Grips



Specimen Wedge

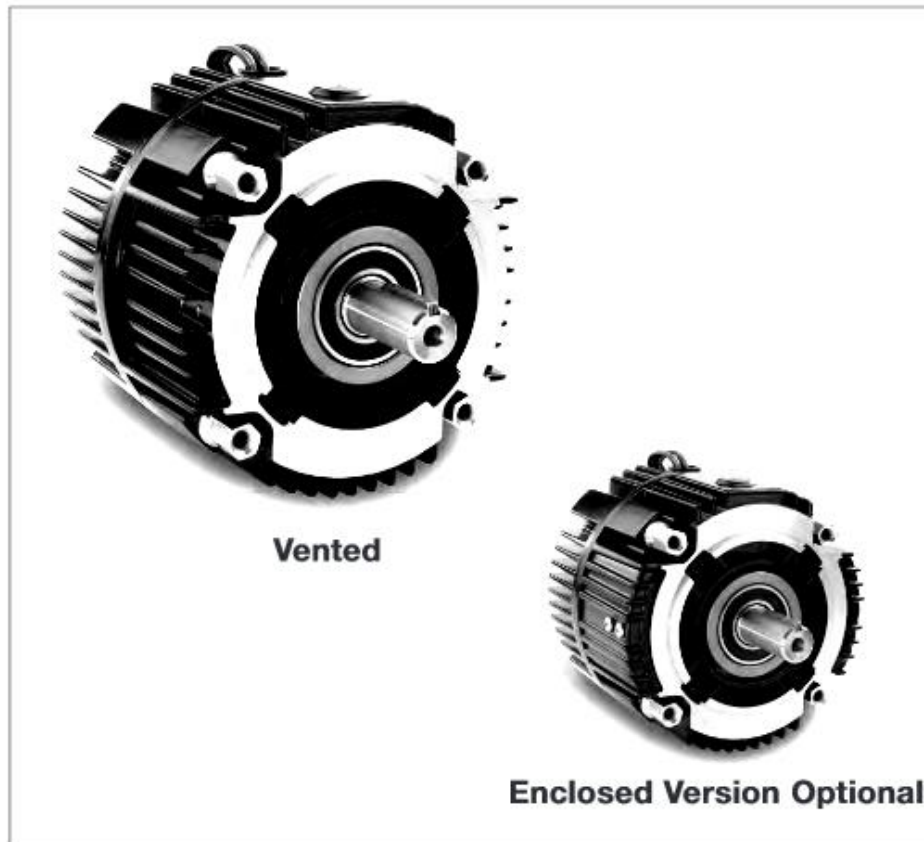


Appendix B: Warner Electric UM-100 Clutch/Brake

Gen 2
Clutch/Brake UniModule UM-50, UM-100, UM-180

P-273-4
819-0528

Installation Instructions




Warner
Electric
An Altra Industrial Motion Company

Contents

Enclosed UniModule Option	3
Mounting to a C-Face Motor	3
Mounting to a Reducer	4
Installing the Base Mount	5
Installing the Motor Mount Bracket ...	5
Mounting to other Power Transmission Components	6
Electrical Connections	6
Troubleshooting-Electrical	6
Troubleshooting-Mechanical	7
Warranty	BC

⚠ WARNING Failure to follow these instructions may result in product damage, equipment damage, and serious or fatal injury to personnel.

⚠ WARNING The equipment covered by this installation manual must be installed in accordance with these instructions. Failure to do so may damage the equipment and void the warranty.

Warner Electric UniModules are designed to National Electrical Manufacturers Association (NEMA) standards. They can be mounted to common NEMA C-Face motors and reducers as well as common power transmission drive components.





The 1020 and 1040 UniModules are designed to mount to the face of a C-Face motor as noted in Table 1.

UM Size	Corresponding NEMA Frame Sizes		Shaft Dia.	C-Face Pilot Dia.
	Old NEMA	New NEMA		
50	56 C	48 Y	5/8"	4-1/2"
100	56 C	48 Y	5/8"	4-1/2"
180	182 C	143 TC	7/8"	4-1/2"
	184 C	145 TC		

Table 1

The 2030 and 3040 UniModules are designed to mount using a base mounting kit. This allows the modules to be mounted as a separate drive unit driven from the prime mover by V-belts, chain and sprockets, couplings, timing belts and other standard power transmission components.

(For UniModule sizes 210 and 215 please refer to Warner Electric manual P-273-1)

For These UM Combinations	Use These Installation Steps:
 UniModule Clutch/Brake between C-Face Motor and Reducer - 1020 UniModule Clutch between Motor and Reducer - 1040	Mounting to a Motor Mounting to a Reducer Electrical Connections
 UniModule Clutch/Brake - 2030 UniModule Clutch - 3040	Mounting to other Power Transmission Components Electrical Connections
 Motor Mount Module Clutch/Brake on a C-Face Motor - 1020-M Motor Mount UniModule Clutch on a C-Face Motor - 1040-M	Mounting to a Motor Installing the Motor Mount Bracket Mounting to other Power Transmission Components Electrical Connections
 Base Mounted UniModule Clutch/Brake - 2030-B UniModule Clutch - 3040-B	Installing the Base Mount Mounting to other Power Transmission Components Electrical Connections

Install your specific UniModule combination according to the installation steps specified in the table. Use only those steps indicated for each combination.

Enclosed UniModule Option

Vented Warner Electric UniModules and base assemblies can be oriented as necessary to keep contaminants from entering the open housing vents.

If an Enclosed UniModule is required, an optional Cover Kit, Warner Electric part number 5370-101-076, can be purchased separately to enclose the open vents in the housing.

Each Cover Kit includes two (2) vent covers and four (4) screws needed to convert a vented UniModule to an enclosed design (non-washdown) as shown in Figure 1.



Figure 1

Note: When using this Cover Kit to enclose the module the vent covers should be assembled as the final step.

Mounting to a C-Face Motor

1. A hardened key is provided with the mounting hardware for UniModules. Insert this key onto the motor shaft (staking the key is necessary).
2. Align the keyway in the bore of the UniModule to the key in the motor shaft and slide the unit onto the motor shaft. The normal alignment of the module to the motor will be with the wire exit/conduit box in the upright (12 o'clock) position as shown in Figure 2.

⚠ WARNING Do not hammer or force the module into position. To do so may damage bearings or cause the friction faces to shift out of alignment.



Figure 2

⚠ CAUTION If anti-fretting lubricant is used on the motor shaft for future ease of removal, ensure that any excess is wiped off before unit assembly to avoid lubricant contaminating the clutch or brake friction faces.

3. Secure the UniModule to the motor with the four (4) long mounting tie-bolts provided. Tighten the four (4) bolts alternately to ensure even alignment of the module. Tighten them to 30-35 foot pounds.
4. Next secure the clutch rotor and fan assembly to the motor shaft by tightening the two (2) setscrew as follows:
 - a. There are two (2) access slots on either side of the UniModule. A long Allen wrench can be used to tighten the two setscrews (90° apart) which secure the clutch rotor and fan assembly to the motor shaft.

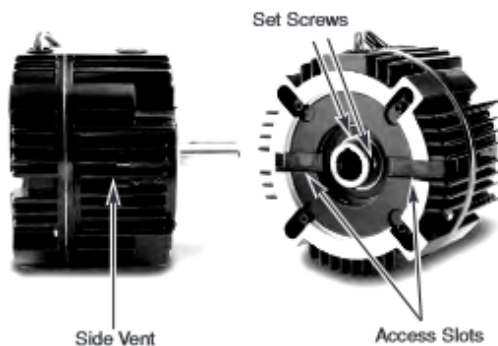


Figure 3a

- c. Using a torque wrench and long Allen socket, tighten the two (2) setscrews to: (Figure 3b)
 - Size 50: 80-85 inch pounds (Requires 5/32 inch Allen wrench)
 - Size 100 or 180: 40-45 inch pounds (Requires 1/8 inch Allen wrench)



Figure 3b

Mounting to a Reducer

1. Warner Electric UniModules are furnished with a hardened key pre-mounted on the output shaft.
2. Align the output shaft and key of the module with the corresponding bore and keyway of the reducer. Slide the assembly together as shown in Figure 4.



Figure 4

3. Bolt the module to the reducer flange.
The four (4) bolts that are required (3/8-16UNC2A) are typically provided with the reducer. Tighten to 18-22 foot pounds of torque.

Installing the Base Mount

Model 2030 and 3040 UniModules are designed to be base mounted as shown in Figure 5.

Optional Base Mount Kit,
Warner Electric part numbers:
UM-50/100.....5370-101-004
UM-180.....5370-101-002



Figure 5

1. The pilot diameters on each end of the UniModule will mate with the pilot diameters on the base.
2. Secure the base to the UniModule with the four (4) bolts provided. Tighten to 18 to 22 foot pounds.

Installing the Motor Mount Bracket

A Motor Mount Bracket can be installed on the output end of a 1020 and 1040 UniModule to provide a foot mounting for the complete assembly of a UniModule and C-face motor.

Optional Motor Mount Kit,
Warner Electric part numbers:
UM-50/100.....5370-101-078
UM-180.....5370-101-079

1. Mount the bracket to the face of the UniModule underneath the UniModule and motor as shown in Figure 6. A pilot diameter on the UniModule mates with a pilot diameter on the bracket.



Figure 6

2. Secure the motor bracket in place with four (4) short bolts and washers provided. Tighten to 18 to 22 foot pounds.

Mounting to other Power Transmission Components

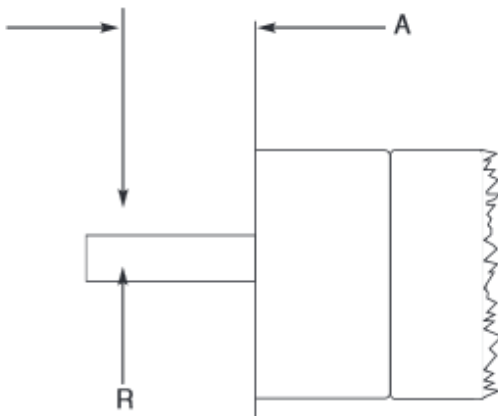
Couplings, pulleys, sprockets or similar power transmission components can be mounted to the input and output shafts of a UniModule.

⚠CAUTION When mounting a pulley or sprocket, ensure that the key is fully engaged within the device hub or bushing.

⚠CAUTION Confirm that the belt or chain tightness meets the maximum side load capability of the UniModule shown in Table 2.

Overhung Load Data (Shaft Side Load)

Overhung load data is provided in this manual for the design engineer concerned with a specific problem in this area. The maximum allowable overhung load which can be applied to the shaft of an UniModule may be determined by the use of the accompanying chart.



UniModule	Distance Load is Applied from Housing Face "A" Inches	Maximum Load Rating "R" Lbs.
UM-50	1" (Center of Shaft)	177
	2" (End of Shaft)	123
	3"	95
UM-100	1" (Center of Shaft)	192
	2" (End of Shaft)	134
	3"	104
UM-180	1" (Center of Shaft)	192
	2" (End of Shaft)	134
	3"	104

Table 2

Electrical Connections

⚠WARNING To avoid injury (or even death), always make certain all power is off before attempting to install or service this device or any electrical equipment.

Warner Electric UniModules are provided with a conduit hole threaded for a standard 1/2 inch conduit connection. Both the clutch and brake lead wires exit this opening. If a Conduit Box is desired, Warner Electric Conduit Box Kit, part number: 5370-101-042, can be purchased separately. The Conduit Box provides two conduit connection holes for standard 1/2 inch conduit connectors.

UniModule clutches and clutch/brakes operate on DC voltage. Warner Electric offers a complete line of electronic controls to meet the needs of almost any clutch or clutch/brake application. Each Warner Electric control will show the proper wiring connections for its use.

Troubleshooting - Electrical

A UniModule that is not functioning properly may be caused by other problems. It is best to check for these problems before replacing it.

A UniModule requires DC power to function. If power is not reaching the clutch or brake, they will not engage.

A good practice to follow is to check for power at the lead wires to the clutch or brake using a voltmeter.

- If power is present in the proper voltage and current (see Electrical Coil data), then skip ahead to the Mechanical Troubleshooting section.
- If power is not present, inspect the lead wires for breaks or cuts.
- If the wires are intact, the problem may be with the power supply or the switch.
- Using a voltmeter, check to see that proper DC voltage is leaving the power supply and that the switch is sending power to the clutch or brake.
- Finally, if there is no power leaving the switch or power supply, check the incoming AC power to ensure that it is reaching the power supply.

Electrical Coil Data

		Clutch	Brake	Clutch	Brake	Clutch	Brake
Voltage-D.C.		90	90	24	24	6	6
Resistance	UM-50	452	452	31.8	28.8	1.86	1.86
(OHMS)	UM-100/180	392	392	26.7	26.7	1.81	1.81
Current	UM-50	.199	.199	.755	.833	3.23	3.23
(Amperes)	UM-100/180	.230	.230	.896	.896	3.31	3.31
Power	UM-50	17.9	17.9	18.1	20.0	19.4	19.4
(WATTS)	UM-100/180	20.7	20.7	21.5	21.5	20	20
Coil Build Up	UM-50	52	53	52	53	52	53
Time (ms)	UM-100/180	72	75	72	75	72	70
Coil Decay	UM-50	6.2	5.0	6.2	5.0	6.5	5.0
Time (ms)	UM-100/180	12	10	12	10	12	10

Troubleshooting - Mechanical

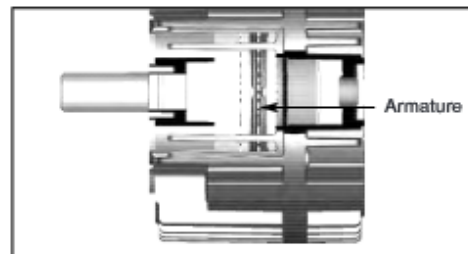
A likely mechanical cause for a clutch or brake not engaging when DC power is applied is that the airgap between the friction faces is too large. When power is applied to an electromagnetic clutch or brake, the unit magnetically clamps the friction faces together.

An airgap that is too large can keep the unit from clamping together. Sometimes this airgap, which is set at the factory, can shift during shipment or installation.

To reset the airgap, you will need to access the armatures. You will note that there are vents on both sides of the module.



When looking through one of these vents, you will see the fan on the clutch rotor. On the outer periphery of the fan there is a 1/2 by 1 inch window.



It is possible to look inside the module and see the armatures by looking through this window. When looking into the window you will be looking between the two armatures of the clutch or brake. (In a 1040 module there is only a single armature.)

If the armature for either the clutch or the brake is too far away from its mating surface, it is possible to move it back into adjustment using a flat head screwdriver.

This is a three step process.

1. Simply slide the screwdriver through the window. By twisting the screwdriver, it works as a wedge to apply pressure on the back of the armature pushing it toward its mating friction surface.
2. Rotate the output of the unit. The rotor and window should stay in place when you do this. Only the armatures will move. If you rotate the input of the unit, the rotor and access window will rotate as well.
3. Alternately repeat steps 1 & 2 to ensure that the airgap between the armature and its mating surface is about 1/32 inch and that the armature remains square to its mating surface. (If the armature is uneven, it may engage on just one side giving the appearance of engagement but failing to provide full torque.)

If there is a scraping or rubbing sound when the output shaft is rotated, this means that an armature is dragging and is too close to its mating surface. Simply repeat steps 1-3 above, but place the screwdriver between the face of the armature and its mating friction surface.

Note: If you have a Soft Start UniModule, you will see a compression spring between the two armatures. In this case, no airgap adjustment is needed.

Mechanical Data

	UM-50	UM-100/180
Static Torque - lb. ft.	16	30
Maximum Speed - rpm	3600	3600
Average Weight-lbs.		
1020	15.6	18.7
1040	14.0	16.6
2030	18.4	21.7
3040	16.8	19.5

Wt/s have been changed for GEN II

Inertia - WR - lb.ft.²

Configuration	50	100/180
1020 input	.021	.047
1020 output	.0195	.050
1040 input	.021	.047
1040 output	.0105	.027
2030 input	.021	.048
2030 output	.0195	.050
3040 input	.021	.048
3040 output	.0105	.027

Notes:

Visit Warner Electric's website at www.warnerelectric.com for dimensional drawings, weights, inertias, and a complete offering of our products including clutches, brakes and clutch/brake controls and service parts.

In addition, Warner Electric module products, controls, and service parts information can be found in our catalog P-1234-WE. Call 815-389-3771 to request any of our catalogs.

Appendix C: Omega TQ202 Torque Cell

REACTION TORQUE SENSORS

FLANGE-TO-SHAFT MOUNT LOW TORQUE RANGE

STANDARD AND METRIC MODELS

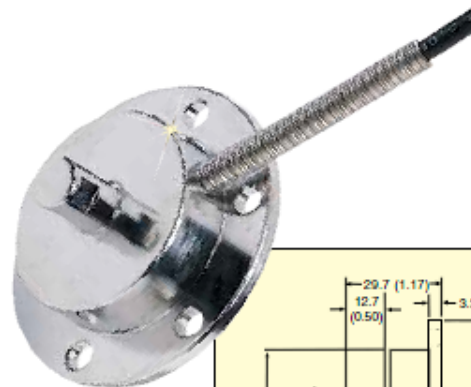
Reaction Torque
 0-25 oz-inch to 0-250 inch-lb
 0-0.18 N-m to 0-30 N-m

TQ202/TQM202 Series

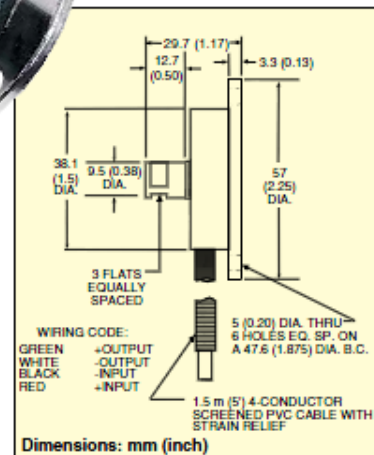


- ✓ All Stainless Steel Case for Long-Term Reliability in Industrial Environments
- ✓ High Accuracy
- ✓ Shielded Cable for Precise Low-Noise Measurements
- ✓ Heavy-Duty Mounting for Positive, Non-Slip Connection

OMEGA's TQ202/TQM202 Series torque sensors are small, high-accuracy flange- or surface-mount devices designed for measuring reaction torque forces up to 250 inch-lb. The shaft attachment has 3 equally spaced flat surfaces to ensure non-slip mounting without the use of a key. The all stainless steel construction ensures long life in industrial environments, as well as long-term accuracy.



TQ202-100Z, shown actual size.



SPECIFICATIONS

Output: 2 mV/V
Excitation: 10 Vdc, 15V max
Input Resistance: 360 Ω min
Output Resistance: 350 ±5 Ω
Accuracy: ±0.2% FSO (combined linearity, hysteresis and repeatability)
Zero Balance: ±2% FSO
Compensated Temp Range: 16 to 71°C (60 to 160°F)
Operating Temp Range: -54 to 107°C (-65 to 225°F)
Thermal Effects:
Zero: 0.005% FSO/°F
Span: 0.005% rdg/°F

Dimensions: mm (inch)

Safe Overload: 150% of capacity
Ultimate Overload: 300% of capacity
Construction: Stainless steel
Electrical: 1.5 m (5') 4-conductor shielded PVC cable with strain relief
Protection Class: IP65

To Order Visit omega.com/tq202 for Pricing and Details				
STANDARD RANGE	STANDARD MODEL NO.	METRIC RANGE	METRIC MODEL NO.	COMPATIBLE METERS
0 to 25 oz-inch	TQ202-25Z	0 to 0.175 N-m	TQM202-0.175	DP41-S, DP25B-S
0 to 30 oz-inch	TQ202-30Z	0 to 0.20 N-m	TQM202-0.2	DP41-S, DP25B-S
0 to 100 oz-inch	TQ202-100Z	0 to 0.70 N-m	TQM202-0.7	DP41-S, DP25B-S
0 to 120 oz-inch	TQ202-120Z	0 to 0.85 N-m	TQM202-0.85	DP41-S, DP25B-S
0 to 150 oz-inch	TQ202-150Z	0 to 1.0 N-m	TQM202-1	DP41-S, DP25B-S
0 to 200 oz-inch	TQ202-200Z	0 to 1.4 N-m	TQM202-1.4	DP41-S, DP25B-S
0 to 25 inch-lb	TQ202-25	0 to 2.8 N-m	TQM202-2.8	DP41-S, DP25B-S
0 to 50 inch-lb	TQ202-50	0 to 5.6 N-m	TQM202-5.6	DP41-S, DP25B-S
0 to 100 inch-lb	TQ202-100	0 to 11 N-m	TQM202-11	DP41-S, DP25B-S
0 to 250 inch-lb	TQ202-250	0 to 28 N-m	TQM202-28	DP41-S, DP25B-S

Comes complete with 5-point calibration.
Ordering Examples: TQ202-25Z, 25 oz-in range reaction torque sensor.
 TQ202-100, 100 in-lb range reaction torque sensor.

Appendix D: ElectroSensors TR400 Tachometer



Reliable Products
Trustworthy People

TR400 Tachometer

Tachometers, Counters & Displays

Features

- Displays rate or time-in-process
- Detects and converts 0.01 to 4,000 Hz signal input
- Optional relay outputs: 2 or 6
- Optional analog output: 4-20 mA or 0-10 V
- Completely field programmable
- Full diagnostic functions
- Single-channel or bidirectional (quadrature) decoding
- Front panel reverse direction indication
- 3 programmable inputs
- Built-in relay test function
- Optional explosion proof enclosure
- Optional NEMA 4X enclosure kit
- 115, 230 VAC (50-60 Hz) and 10-30 VDC power options



Description

The TR400 is a full logic control process ratemeter that can display any production rate or time in process easily and accurately. The ability to accurately detect and convert 0.01 to 4,000 Hz signal input makes the TR400 an inexpensive solution to many industrial applications. With the addition of optional relay outputs and/or 4-20 mA analog output, the TR400 becomes a complete process control and display system. The optional relay outputs can be programmed for under-speed or over-speed, and include adjustable delays at "power up" and output activation. The 4-20 mA output can be scaled to reflect any area of the monitored range, including operations requiring an inverse output.

Quadrature signal decoding gives the TR400 the ability to detect direction as well as speed for bidirectional applications. The relays and 4-20 mA outputs can be programmed in the reverse direction as well as the forward direction, or both directions.

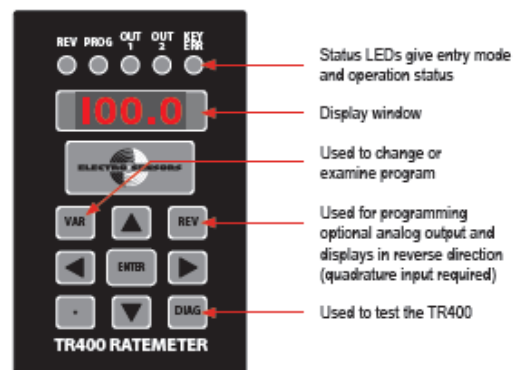
Options:

- Two or six programmable Form C relay contact outputs. Rated 250 VAC, 30 VDC at 5 amps resistive load
- Programmable 4-20 mA or 0-10 VDC output

Principle of Operation

A shaft-mounted pulser disc or pulser wrap generates an alternating magnetic field that is picked up by the sensing head. The sensor transmits the speed as a digital pulse frequency to the TR400 via a three-conductor shielded cable. The TR400 then compares this frequency signal to its programmed values to determine the appropriate display value and output states (if required).

When the TR400 is programmed to detect quadrature input signals, the front panel will indicate the reverse direction with the "REV" LED. All outputs are fully functional in both forward and reverse directions.





Reliable Products
Trustworthy People

TR400 Tachometer

Tachometers, Counters & Displays

Specifications

Input Power	
Voltage	115 VAC, 6 VA @ 50/60 Hz, 1/16 Amp, requires external fuse
Optional Voltages	230 VAC, 10-30 VDC
Sensor Input	Switch Selectable
NPN Open-Collector	2,200 Ohm pull up to 12 VDC, 2.5 Volt trigger level
PNP Open-Collector	2,200 Ohm pull down, 2.5 Volt trigger level
Logic Level	2.5 Volt trigger level
Magnetic Pick-up	150 mV peak-to-peak minimum signal, 50 mV trigger level
Sensor Supply	12 VDC unregulated, 100 mA max
External Control I/O	
Standard Inputs	3 programmable switch inputs
Setpoint Outputs (Relays)	2 or 6 programmable Form C relays on board, rated 250 VAC 5 Amp, 30 VDC 5 Amp resistive load
Optional Analog Output	1 programmable 4-20 mA or 0-10 VDC output, 12 bit DAC
Operational	
Accuracy	Display / Relays: 0.01% ± 1 Digit Analog: 0.1% of full scale
Input Frequency Range	0.01 Hz to 4,000 Hz
Response Time	Minimum 0.02 seconds
Control Range	Default 500 - 1, can be programmed from 9999 - 1
Modes of Operation	Speed, Time In Process, Single Channel, Quadrature
Setpoints	2 or 6 programmable as "over" or "under" and/or Forward and Reverse
Display Update Time	0.5 seconds min, 8 seconds max
Mechanical	
Enclosure	ABS Plastic 94V-0
Keypad	Polycarbonate Tactile Switch Pad, Chemical Resistant, and Splash Proof
Display	4-Digit, 0.3" Height, 7-Segment Displays, 5-Status LEDs
Operating Temperature	0° C to +50° C (+32° F to +122° F)
Dimensions	3.10" w x 4.85" h x 6.25" l
Panel Cutout	2.61" w x 4.31" h

Specifications subject to change without notice.

ES400 Rev F © 2013 Electro-Sensors, Inc. All rights reserved.

Ordering

Input Power	# of Relays	Analog Output	Part Number
115 VAC	-	-	800-078701
115 VAC	2	-	800-078705
115 VAC	-	4-20 mA	800-078703
115 VAC	2	4-20 mA	800-078707
115 VAC	-	0-10 V	800-078713
115 VAC	2	0-10 V	800-078717
115 VAC	6	4-20 mA	800-078800
230 VAC	-	-	800-078702
230 VAC	2	-	800-078706
230 VAC	-	4-20 mA	800-078704
230 VAC	2	4-20 mA	800-078708
230 VAC	-	0-10 V	800-078714
230 VAC	2	0-10 V	800-078718
230 VAC	6	4-20 mA	800-078801
10-30 VDC	-	-	800-078719
10-30 VDC	2	-	800-078721
10-30 VDC	-	4-20 mA	800-078720
10-30 VDC	2	4-20 mA	800-078722
10-30 VDC	-	0-10 V	800-078723
10-30 VDC	2	0-10 V	800-078724
10-30 VDC	6	4-20 mA	800-078802

Options	
Explosion Proof Enclosure	305-001400
NEMA 4X Enclosure Kit	725-003600
Relay Kit	725-000007
Faceplate Kit	725-000009

Customization

If one of our standard products does not meet your specifications, please call one of our applications specialists. Many of our products can be customized to fit specific needs.

Additional Information

See the TR400 Installation and Operating Manual for complete details, specifications, and programming instructions.



Appendix E: Encoder Products 25T Encoder

Model 25T Thru-Bore, or Model 25H Hollow Bore (Blind)



Features

- 2.5" Opto-ASIC Encoder with a Low Profile (2.0")
- Standard Bore Sizes Ranging from 0.625" to 1.125"
- Metric Bore Sizes Ranging from 6 mm to 28 mm
- Single Replacement Solution For 2.0" to 3.5" Encoders
- Resolutions to 10,000 CPR; Frequencies to 1 MHz
- Versatile Flexible Mounting Options
- RoHS Compliant



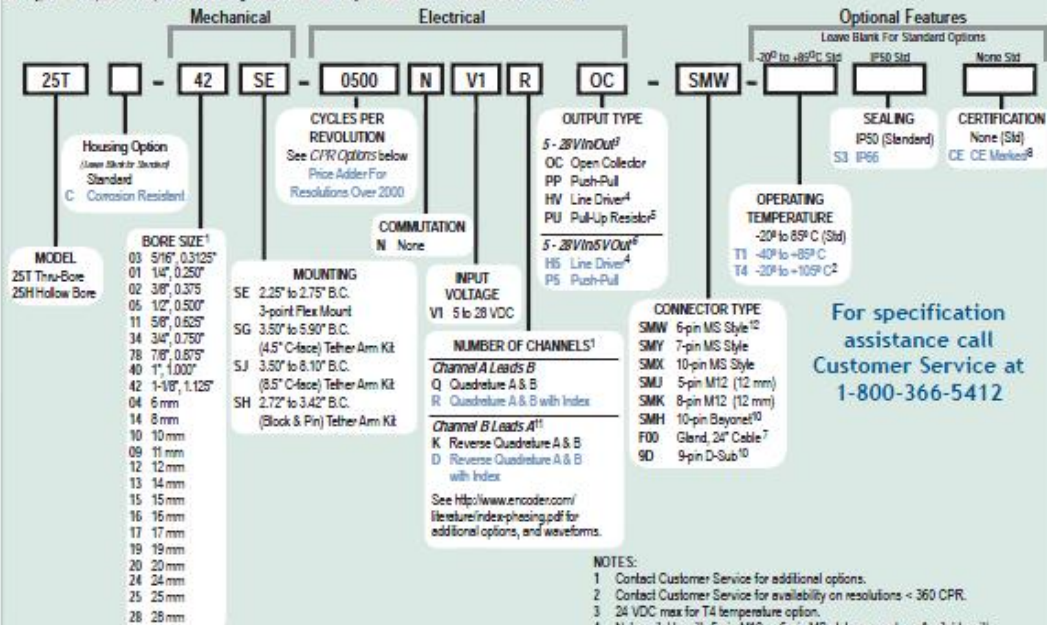
Introducing the next generation of high performance encoders - the Model 25T. As contemporary as its appearance, the Model 25T features the largest thru-bore available in a 2.5" encoder, mounting directly on shafts as large as 1.125" or 28 mm. With resolutions of up to 10,000 CPR, and Frequencies of up to 1MHz this industrial strength encoder is perfect for fast revving motors. The 25T features the next generation of EPC's proprietary Opto-ASIC sensor which provides superior accuracy and precision counts. The injection molded housing, made from EPC's custom blend of nylon composites, is grooved with "cooling fins" and can take the extreme heat of the motion control industry. With sealing available of up to IP66 and many new rugged flexible mounting options, the Model 25T can perform in demanding industrial environments. This revolutionary new 2.5" encoder truly is unlike any other.

Common Applications

Motor-Mounted Feedback and Vector Control, Specialty Machines, Robotics, Web Process Control, Paper and Printing, High Power Motors

Model 25T/H Ordering Guide

Blue type indicates price adder options. Not all configuration combinations may be available. Contact Customer Service for details.



Model 25T/H CPR Options

0001	0002	0003	0005	0008	0010	0011	0012
0024	0025	0030	0032	0050	0060	0064	0070
0080	0100	0105	0115	0120	0125	0150	0180
0192	0200	0240	0250	0256	0300	0336	0360
0500	0512	0600	0625	1000	1024	1200	1250
2000	2048	2500	4096	5000	10,000		

Contact Customer Service for other disk resolutions.

NOTES:

- 1 Contact Customer Service for additional options.
- 2 Contact Customer Service for availability on resolutions < 360 CPR.
- 3 24 VDC max for T4 temperature option.
- 4 Not available with 5-pin M12 or 6-pin MS style connectors. Available with 7-pin MS style connector without index Z.
- 5 With Input Voltage above 16 VDC, operating temperature is limited to 85° C max.
- 6 Standard operating temperature only.
- 7 For non-standard English cable lengths enter "F" plus cable length expressed in feet. Example: F05 = 5 feet of cable.
- 8 Please refer to Technical Bulletin TB100: *When to Choose the CE Option* at www.encoder.com. Contact Customer Service for availability.
- 9 Not available with Pull-Up Output Type.
- 10 Not available with corrosion resistant option.
- 11 Reverse Quadrature not available with PU output type.
- 12 Not available with CE option.

For specification assistance call
Customer Service at
1-800-366-5412

Model 25T Thru-Bore, or Model 25H Hollow Bore (Blind)



Model 25T/H Specifications

Electrical

Input Voltage.....4.75 to 28 VDC max for temperatures up to 85° C
4.75 to 24 VDC max for temperatures between 85° and 105° C

Input Current.....100 mA max with no output load

Output Format.....Incremental- Two square waves in quadrature with channel A leading B for clockwise shaft rotation, as viewed from the mounting face.
See *Waveform Diagram*.

Output Types.....Open Collector- 20 mA max per channel
Pull Up - Open Collector with 2.2K ohm resistor; 20 mA max per channel
Push-Pull- 20 mA max per channel
Line Driver- 20 mA max per channel (Meets RS 422 at 5 VDC supply)
Once per revolution.

Index.....361 to 10,000 CPR; Gated to output A
1 to 360 CPR; Ungated
See *Waveform Diagram*.

Max Frequency.....250 kHz for 1 to 2500 CPR
500 kHz for 2501 to 5000 CPR
1 MHz for 5001 to 10,000 CPR

CE Testing.....Emissions tested per EN61000-6-3:2001 as applicable. Immunity tested per EN61000-6-2:2005 as applicable

Min. Edge Sep......45" electrical min, .63" electrical or better typical

Rise Time.....Less than 1 microsecond

Accuracy.....Within 0.1° mechanical from one cycle to any other cycle, or 6 arc minutes.

Mechanical

Max Shaft Speed.....6000 RPM, 8000 RPM intermittent
4000 RPM for IP66 seal option

Bore Size......0250" through 1.125"
6 mm through 28 mm

Bore Tolerance.....-.00007/+0.0005"

User Shaft Tolerances
Radial Runout......0005" max
Axial Endplay......0050" max

Starting Torque.....IP50 sealing: 1.0 oz-in typical
IP66 sealing: 4.0 oz-in typical
Note: Add 1.0 oz-in typical for -20° C operation

Moment of Inertia.....7.6 x 10⁻⁴ oz-in-sec²

Max Acceleration.....1x10⁵ rad/sec²

Electrical Conn.....5-, 7-, or 10-pin MS Style, 5- or 8-pin M12 (12 mm), 10-pin Bayonet or gland with 24 inches of cable (foil and braid shield, 24 AWG conductors), 9-pin D-Sub

Housing.....Proprietary nylon composite

Mounting.....2.25" to 2.75" B.C. 3-point flex mount
3.50" to 5.90" B.C. (4.5" C-face) tether arm kit, 3.50" to 8.10" B.C. (8.5" C-face) tether arm kit and 2.72" to 3.42" B.C. (Block & Pin) tether arm kit. See mechanical drawing for dimensions

Weight.....8 oz typical

Environmental

Operating Temp.....-20° to +85° C for standard models
-20° to +105° C for high temperature option
-40° to +85° C for low temperature option

Storage Temp.....-20° to +85° C

Humidity.....98% RH non-condensing

Vibration.....20 g @ 5 to 2000 Hz

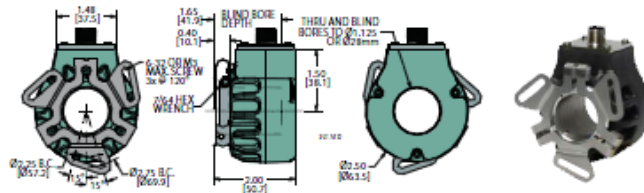
Shock.....80 g @ 11 ms duration

Sealing.....IP50, IP66 with shaft seals at both ends

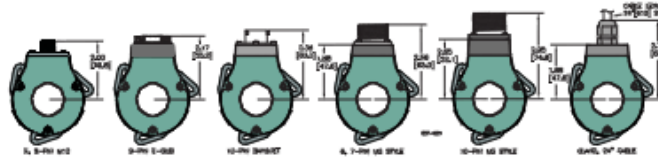


Protect your encoder with the 56C Cover.

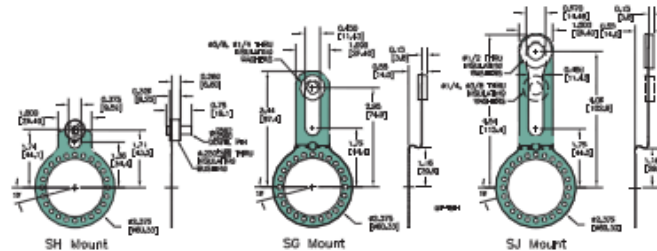
Model 25T/H



Model 25T/H Connector Options

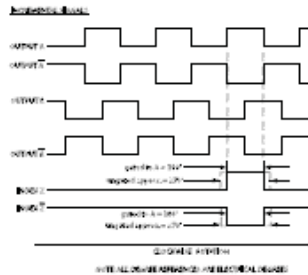


Model 25T/H Mounting Options



All dimensions are in inches with a tolerance of $\pm 0.005"$ or $\pm 0.01"$ unless otherwise specified

Waveform Diagram



Wiring Table

Function	Gland Cable Wire Color	5-pin M12 ¹	5-pin M12 ²	8-pin MS	8-pin MS (V1)	7-pin MS (OC, PS)	9-pin MS (OC, PS)	9-pin D-sub (OC, PS)	10-pin (OC, PS)
Com	Black	3	7	F	F	F	A, F	9	F
+VDC	White	1	2	D	D	D	B	1	D
A	Brown	4	1	A	A	A	D	2	A
A'	Yellow	---	3	H	C	---	---	3	H
B	Red	2	4	E	B	B	E	4	B
B'	Green	---	5	I	E	---	---	5	J
Z	Orange	5	6	C	---	C	C	6	C
Z'	Blue	---	8	J	---	---	---	7	K
Case	---	---	---	G	G	G	---	8	G
Shield	Bar ³	---	---	---	---	---	---	---	---

¹CE Option: Cable shield (bare wire) is connected to internal case
²CE Option: Read Technical Bulletin TB111

Appendix F: Thermal Analysis on Hollow Shaft

```

function = 1D_conduction

T_inf = 298;
T_b = 773;
h = 15;
k = 42.7;
L = 0.305;
OD = 0.01587;
ID = 0.00635;
Ac = (3.14159/4)*(OD^2 - ID^2);
P = 3.14159*OD;
m = sqrt((h*P)/(k*Ac));
x = 0;

hold on

while x <= L

a = cosh(m*(L-x));
b = (h/(m*k))*sinh(m*(L-x));
c = cosh(m*L);
d = (h/(m*k))*sinh(m*L);

T = ((a+b)/(c+d))*(T_b-T_inf)+T_inf - 273;

x = x*39.37;

plot(x,T,'-rs','LineWidth',1)

x = x/39.37;
x = x + .01;

end

end

```

Bibliography

- [1] *U.S. Energy Information Administration*. U.S. Department of Energy, 26 Dec. 2013. Web. 21 Jan. 2014. <<http://www.eia.gov/totalenergy/data/monthly/index.cfm#petroleum>>.
- [2] U.S. Department of Energy. "70m for materials to reduce car weight." *Materials News* June 2005: n. pag. Print.
- [3] *The Aluminum Association*. Innov8iv Design, 2008. Web. 21 Jan. 2014. <<http://www.aluminum.org/Content/NavigationMenu/TheIndustry/TransportationMarket/AutoTruck/default.htm>>.
- [4] Totten, George E., Kiyoshi Funatani, and Lin Xie. *Handbook of Metallurgical Process Design*. New York: Marcel Dekker, 2004. Print.
- [5] Humphreys, F. J., and M. Hatherly. *Recrystallization and Related Annealing Phenomena*. 2nd ed. Amsterdam: Elsevier, 2004. Print.
- [6] McQueen, H. J. *Hot Deformation and Processing of Aluminum Alloys*. Boca Raton: CRC, 2011. Print.
- [7] Bressan, Jose Divo, and Ricardo Kirchhof Unfer. "Construction and validation tests of a torsion test machine." *Journal of Materials Processing Technology* 179 (2006): 23-29. Print.
- [8] Agarwal, Sumit, Paul E. Krajewski, and Clyde L. Briant. "Texture Development and Dynamic Recrystallization in AA5083 During Superplastic Forming at Various Strain Rates." *TMS (The Minerals, Metals & Materials Society)* (2004): n. pag. Print.
- [9] Carpenter, H.C. H., and C.F. Elam. "The Production of Single Crystals of Aluminum and their Tensile Properties." *Proc. R. Soc. Lond* 100.329 (1921): n. pag. Print.
- [10] Chang, Jung-Kuei, et al. "Abnormal Grain Growth and Recrystallization in Al-Mg Alloy AA5182 Following Hot Deformation." *ASM International* 41A (2010): n. pag. Print.
- [11] "ROCKWELL 12' Newer Style Variable Wood Lathe." *Ozark Woodworker*. N.p., n.d. Web. 11 Feb. 2014. <http://www.ozarkwoodworker.com/ROCKWELL-12-Newer-Style-Variable-Wood-Lathe-Manual_p_591.html>.

- [12] *Torsion Testing and Assess Bulk Workability: Specimen Design*. Materials Park: ASM International, 2005. Print. Vol. 14 of *ASM Handbook*.
- [13] Jadon, Vijay Kumar, and Suresh Verma. *Analysis and Design of Machine Elements*. New Delhi: I.K. International Pub., 2010. Print.
- [14] "Warner Electric Clutch." *MSC Industrial Supplies*. N.p., n.d. Web. 12 Feb. 2014. <<http://www.mscdirect.com/product>>.
- [15] "TQ202." *Omega*. N.p., n.d. Web. 11 Feb. 2014. <http://www.omegaeng.cz/ppt/pptsc_eng.asp?ref=TQ202>.
- [16] "TR400." *Electro Sensors*. N.p., n.d. Web. 12 Feb. 2014. <<http://www.electro-sensors.com/products/tachometers-counters-displays/tr400/>>.
- [17] "Pulser Discs." *Electro Sensors*. N.p., n.d. Web. 12 Feb. 2014. <<http://www.electro-sensors.com/products/pulse-generators/pulser-discs/>>.
- [18] "Model 25T." *Encoder Products Company*. N.p., n.d. Web. 12 Feb. 2014. <<http://www.encoder.com/model25th.html>>.
- [19] *Chamber IR Model E4 Infrared Heating System*. N.p.: Research Inc., n.d. Print.
- [20] Incropera, Frank P. *Fundamentals of Heat and Mass Transfer*. 6th ed. Hoboken: John Wiley, 2007. Print.
- [21] Fulop S. *et al.*, *Journal of Testing and Evaluation* 5 (1977). Print.
- [22] "Alloy Digest." *Aluminum 5083*. Upper Montclair, New Jersey: Engineering Alloys Digest, Inc., 1978. N. pag. *ASM International*. Web. 9 Feb. 2014.
- [23] Ueki, Masanori. "Evaluation of the hot workability of 5083 alloy by the torsion test, using tubular specimens." *Journal of Mechanical Working Technology* 11.3 (1985): 355-64. Print.
- [24] Bray, J. W. "Properties and Selection: Nonferrous Alloys and Special- Purpose Materials." *Aluminum Mill and Engineered Wrought Products*. N.p.: ASM International, 1990. 29-61. Print. Vol. 2 of *ASM Handbook*.
- [25] Taleff, Eric M., and Jun Qiao. "The Effects of Ternary Alloying Additions on Warm and Hot Deformation in Al-Mg Alloys." *Light Metals 2001: Metaux Legers* (2001): 77-88. Print.

[26] *gimp* 2.8. N.p., 23 Jan. 2014. Web. 16 Feb. 2014. <<http://www.gimp.org/>>.

[27] "Combination Linear Drive Ball Bearing." *McMaster-Carr*. N.p., n.d. Web. 18 Feb. 2014. <<http://www.mcmaster.com/#61145k36/=rlfttv>>.